Design, Synthesis and Self-assembly of β-Cyclodextrin Based Materials for Drug Delivery and Photoinduced Electron Transfer Applications

THESIS SUBMITTED TO **AcSIR** FOR THE AWARD OF THE DEGREE OF

DOCTOR OF PHILOSOPHY IN CHEMISTRY

UNDER THE FACULTY OF SCIENCE

By

Nagaraj Nayak

Enrolment No: 10CC12J39013

UNDER THE GUIDANCE OF

Dr. K. R. Gopidas

PHOTOSCIENCES AND PHOTONICS

CHEMICAL SCIENCES AND TECHNOLOGY DIVISION

CSIR-NATIONAL INSTITUTE FOR INTERDISCIPLINARY SCIENCE AND TECHNOLOGY (CSIR-NIIST)

THIRUVANANTHAPURAM - 695 019, KERALA

January 2017

DECLARATION

I hereby declare that the matter embodied in the Ph. D. thesis entitled: **"Design, Synthesis and Self-assembly of β-Cyclodextrin Based Materials for Drug Delivery and Photoinduced Electron Transfer Applications"** is the result of an independent work carried out by me at the Photosciences and Photonics, Chemical Sciences and Technology Division of the CSIR-National Institute for Interdisciplinary Science and Technology (CSIR-NIIST), Thiruvananthapuram, under the supervision of Dr. K. R. Gopidas and the same has not been submitted elsewhere for other degree or diploma.

In keeping with the general practice of reporting scientific observations, research material obtained from other investigations has been duly cited and acknowledged in the thesis.

Nagaraj Nayak

Thiruvananthapuram

January 2017

सीएसआईआर- राष्ट्रीय अंतर्विषयी विज्ञान तथा प्रौद्योगिकी संस्थान
CSIR-NATIONAL INSTITUTE FOR INTERDISCIPLINARY SCIENCE & TECHNOLOGY
इंडस्ट्रियल इस्टेट पी.ओ., तिरुवनंतपुरम - 695 019, केरल, भारत
Industrial Estate P.O., Thiruvananthapuram - 695 019, Kerala, INDIA.

डॉ. के.आर. गोपिदास, एफ.ए.एससी
Dr. K. R. Gopidas F.A.Sc.
मुख्य वैज्ञानिक
Chief Scientist
रसायन विज्ञान तथा प्रौद्योगिकी प्रभाग
Chemical Sciences and Technology Division

January 31, 2017

CERTIFICATE

This is to certify that the work incorporated in this Ph. D. thesis entitled: **"Design, Synthesis and Self-assembly of β-Cyclodextrin Based Materials for Drug Delivery and Photoinduced Electron Transfer Applications"** has been carried out by Mr. Nagaraj Nayak under my supervision at the Photosciences and Photonics, Chemical Sciences and Technology Division of the CSIR-National Institute for Interdisciplinary Science and Technology (CSIR-NIIST), Thiruvananthapuram and the same has not been submitted elsewhere for a degree.

Dr. K. R. Gopidas

(Thesis Supervisor)

टेलीफोन /Telephone: 91-471-2515390(O), 9446520537(M)
फ़ैक्स /Fax : +91-471-2491712, ई-मेल /E-mail: gopidaskr@niist.res.in, gopidaskr@gmail.com

ACKNOWLEDGEMENTS

I have great pleasure in placing on record my deep sense of gratitude to Dr. K. R. Gopidas, my thesis supervisor, for suggesting the research problem and for his guidance, support and encouragement throughout my research career which lead to the successful completion of this work.

I would like to express my sincere thanks to Professor M. V. George for being a real motivation and his support during the tenure of this work.

I wish to thank Dr. A. Ajayaghosh and Dr. Suresh Das, present and former Directors of the CSIR-National Institute for Interdisciplinary Science and Technology, Thiruvananthapuram, for providing me the necessary facilities for carrying out this work.

Dr. D. Ramaiah, Dr. Joshy Joseph, Dr. N. Unni, Dr. K. Yoosaf, Dr. C. Vijayakumar, Dr. B. P. Deb and Dr. V. Karunakaran, Scientists of the Photosciences and Photonics, Chemical Sciences and Technology Division, are greatly acknowledged for the scientific discussions. Also, I would like to thank Dr. Luxmi Verma, Dr. Mangalam S. Nair and Dr. S. Ananthakumar for their help in successful completion of my course work.

I would like to thank Dr. K. Retheesh, Dr. A. M. Rakhi, Dr. Tony George Thomas, Mr. M. V. Vinayak, Ms. K. Sreedevi, Mr. T. M. Lakshmykanth, Mr. S. P. Prakash and Mr. K. Sumesh Babu for their valuable suggestions, advice and constructive critics. Also, I wish to thank Mr. M. Yoosuf, Ms. K. J. Athira and Mrs. K. B. Daisymol for their care and support.

I sincerely thank Mr. P. Robert and Mr. M. Kiran for TEM data, Mr. J. S. Kiran for artwork, Mrs. Saumini, Mr. Saran for NMR analysis, Mrs. Viji and Ms. Athira for HRMS data.

I am also indebted and grateful to all my friends at NIIST, especially Mr. K. V. Sandeep, for the good wishes and moral support he has given me over the years.

I fervently express my gratitude to my parents and sister who are the circle of my strength. Very special thanks to Mrs. P. Sudha for her patience, understanding and her ability to make me laugh in any situation.

Finally, I take this opportunity to sincerely thank Council of Scientific and Industrial Research (CSIR), Government of India for financial assistance.

Nagaraj Nayak

CONTENTS

PREFACE

This thesis focuses on the design and study of self-assembled functional materials of β-Cyclodextrin (β-CD) for applications in drug delivery and artificial photosynthesis. CDs are cyclic oligosaccharides having hydrophobic cavities capable of encapsulating suitably-sized organic molecules from aqueous solutions. Commercially available CDs, namely α–, β- and γ-CDs have, respectively, 6, 7, or 8 D-glucopyranose units linked by α-(1,4) linkages. These are shaped like truncated cones with the primary hydroxyl groups arranged around the narrow rim of the cone and the secondary hydroxyl groups assembled on the wider rim. Almost all applications of CDs deal with the formation of host-guest complexes. The cavity size of β-CD matches with several organic guests such as adamantane and the complexes formed in this case exhibited the highest stability constant in the CD family. In almost all of such complexes, the guest is expected to enter the CD cavity through the wider rim. Recently our group has reported a novel binding mode of β-CD with *N*-alkyl pyromellitic diimide derivatives (PMDI), which was named as 'rim-binding'. In this mode of binding, the PMDI core remains just outside of the smaller rim of the CD while the *N*-alkyl group enters into the cavity through the smaller rim. In the present thesis, we have employed both inclusion and rim-binding modes of binding for the fabrication of self-assembled functional materials.

The thesis is divided into four chapters. The **first chapter** is a review of the literature on CD with more emphasis on β-CD complexes. A brief section on 'rim-binding' interaction of β-CD is also given in this chapter. In addition, a detailed literature review on CD based functional materials such as vesicles, polymers and hydrogels for various applications is also presented in this chapter.

In **Chapter 2** of this thesis, we have reported the synthesis and characterization of a molecule AD-AD having adamantane groups at both ends. AD-AD interacted with two equivalents of β-CD to give the bis-inclusion complex β-CD⊂AD-AD⊃β-CD, which was well characterized by ^{1}H NMR titration, 2D NMR and ITC experiments. A careful examination of ^{1}H NMR titration spectra revealed that the bis-inclusion complex is undergoing a secondary inter-complex interaction in the aqueous medium. We recognized that the secondary interaction resulted in the unexpected formation of supramolecular vesicles, which were also thoroughly characterized by AFM, TEM, SEM, DLS and Confocal Microscopy studies. Further, we have demonstrated that the vesicles formed can be loaded with the hydrophilic anti-cancer drug doxorubicin. Finally, the loaded drug could be stimuli released into the medium upon the addition of a competitive inclusion binder such as adamantane carboxylate.

In the **third Chapter** we describe the reorganization of the β-CD⊂AD-AD⊃β-CD vesicles reported in Chapter 2 in the presence of a bis-pyromellitic diimide derivative PI-PI, into ultra-long supramolecular fibers. The same fibrous structures are also formed when AD-AD, PI-PI and β-CD are dissolved in water in 1:1:2 ratio. Using TEM, AFM and time-dependent ICD measurements of the three-component system and the constituent two-component systems (β-CD/AD-AD/PI-PI and β-CD/AD-AD), we could identify the intermediate stages involved in the fiber formation. We also identified the involvement of two social self-sorting and two narcissistic self-sorting processes in the self-assembly. In a mixture consisting of all the three components, initially a bis-inclusion complex of β-CD and AD-AD is formed through a social self-sorting process. The bis-inclusion complex undergoes a narcissistic self-assembly to give vesicles which were same as those described in Chapter 2. Vesicle formation is followed by rim-binding interaction which led to

joining of the vesicles to give long fibrous structures. The rim-binding motif is effectively exploited herein to perform the functions of vesicle recognition and vesicle joining.

Our studies in Chapter 3 revealed that in a mixture composed of β-CD, AD-AD and PI-PI (2:1:1), fibrous structures which incorporated all the three components are formed. Few recent reports have shown that when donors and acceptors are incorporated in fibrous structures photoinduced electron transfer (PET) led to long-lived charge separated states. The PI-PI moiety is comprised of two pyromellitic diimide (PMDI) units and PMDI is known to be a good electron acceptor in PET reactions. We have designed a bis-adamantane derivative AD-AN-AD, which also incorporated the electron donor anthracene (AN). In **Chapter 4** we report the self-assembly of AD-AN-AD/β-CD and AD-AN-AD/β-CD/PI-PI systems, which were studied by ^{1}H NMR titration, ITC and UV-visible spectroscopic methods. We also report details of PET processes taking place in the self-assembled AD-AN-AD/β-CD/PI-PI system. We observed efficient PET taking place in the three component nano-fibrous system upon excitation of the anthracene chromophore. The PET process was studied by steady state fluorescence quenching, nanosecond laser flash photolysis and EPR techniques. The PMDI $^{\bullet-}$ formed in PET process was found to be long-lived. We attributed this to the protection of the anionic species within the supramolecular polymeric environment. Generation of long-lived CS states in aqueous medium is an extremely important area of research because of its important applications in solar water splitting to produce molecular hydrogen.

……

Note: *The abbreviations of various compounds given here correspond to those given under the respective chapters.*

LIST OF FIGURES

LIST OF SCHEMES

LIST OF ABBREVIATIONS

1. A **–** Acceptor

2. Å **–** Angstrom

3. AD – Adamantane

4. AN **–** Anthracene

5. ADC – Adamantane carboxylate

6. AD-AD – Bis-adamantane derivative of 1,4-bis(4-pyridyl)ethane

7. AD-AN-AD – Bis-adamantane derivative of anthracene

8. AFM – Atomic force microscopy

9. B_0 – Magnetic field strength

10. BET – Back electron transfer

11. CD – Cyclodextrin

12. CDs – Cyclodextrins

13. CCD – Charge-coupled device

14. CS – Charge separated

15. CV – Cyclic voltammetry

16. CB – Cucurbituril

17. CLSM – Confocal laser scanning microscope

18. D – Donor

19. D* – Excited donor

20. D_2O – Deuterated water

21. DLS – Dynamic light scattering

22. Dox – Doxorubicin

23. $\Delta\delta$ – Change in chemical shift value

24. ΔS – Entropy change

25. ΔH – Enthalpy change

26. d_{cc} – Centre to centre distance

27. ε – Extinction co-efficient

28. ET – Electron transfer

29. E_{ox} – Oxidation potential

30. E_{red} – Reduction potential

31. E_s– Singlet state energy

32. E_t– Triplet state energy

33. ESI – Electrospray ionization

34. EPR – Electron paramagnetic resonance

35. et al. – et alii/alia

36. eV – Electron volt

37. FTIR – Fourier transform infrared spectroscopy

38. Φ_{cs} – Quantum yield of charge separated state

39. Φ_{em} – Quantum yield of emission

40. ΔG_{ET} – Free energy change in ET process

41. HRMS – High Resolution Mass Spectrometry

42. HRTEM – High resolution transmission electron microscopy

43. ICD – Induced circular dichroism

44. ISC – Inter system crossing

45. ITC – Isothermal titration calorimetry

46. K_a – Association constant

47. k_{ET} – Rate of forward electron transfer

48. MALDI Tof – Matrix-assisted laser desorption/ionization Time of flight

49. mg – Milligram

50. MHz – Megahertz

51. mL – Millilitre

52. mM – millimolar

53. μs – Micro second

54. Nd – Neodymium

55. NHE – Normal hydrogen electrode

56. NMR – Nuclear magnetic resonance

57. NOE – Nuclear overhauser effect

58. NOESY - Nuclear overhauser effect spectroscopy

59. ns – nanosecond

60. OD – Optical density

61. PI –PI – Bis-PMDI derivative of 1,4-bis(4-pyridyl)ethane

62. PET – Photoinduced electron transfer

63. PMDI – Pyromellitic Diimide

64. ppm – Parts per million

65. rt – Room temperature

66. SA – Supramolecular amphiphile

67. ROESY – Rotating-frame overhauser effect spectroscopy

68. SEM – Scanning electron microscope

69. TCSPC – Time-correlated single photon counting

70. tert – tertiary

71. TEM – Transmission electron microscopy

72. τ_{cs} – CS state lifetime

73. UV – Ultraviolet

74. λ_{ex} – Excitation wavelength

75. Vis – Visible

76. WAXS – Wide angle X-ray scattering

77. YAG – Yittrium aluminium garnet

Chapter 1

Cyclodextrin Based Supramolecular Systems: An Overview

1.1. Introduction

The early development of supramolecular chemistry was primarily because of three people namely Lehn, Cram, and Pedersen. These three professors won the Nobel Prize in chemistry on account of their leading discoveries in the host-guest systems in the year 1987. From then, the idea of supramolecular chemistry has attracted several researchers ranging from chemists to biologists including material scientists. Prof. Jean-Marie Lehn defined supramolecular chemistry as "chemistry beyond the molecule" bearing on the organized entities of higher complexity that result from the association of two or more chemical species held together by intermolecular forces.[1] In general, the intermolecular forces are non-covalent interactions such as hydrogen-bonding interaction, π–π stacking interaction, electrostatic interaction, van der Waals force, hydrophobic/hydrophilic interaction etc. used to construct the complex systems from simple molecules.[2,3] These non-covalent interactions present several advantages over covalent interactions. The non-covalent linkages are relatively weak and dynamic in nature and hence the supramolecular materials are reversible, responsive to external stimuli and have self-repairing ability allowing convenient dissociation and reconstruction of the supramolecular systems at a low energy cost.

Under the theme of 'supramolecular chemistry', the supramolecular association of molecules through host-guest interaction is a well-studied area in the last few decades. Apart from simple host molecules such as crown ethers,[4] there are few more molecular containers namely calixarenes,[5] cucurbiturils,[6] pillararenes,[7] cyclodextrins (CDs)[8,9] etc. In

the present thesis we limit our studies on CD based host-guest systems resulting in self-assembled functional materials. In their detailed review, Uekama and Szejtli identified CDs as the most important among all potential hosts listed above due to following reasons.[9]

1. CDs are synthetic substances obtained from the enzymatic (cyclodextrin glucanotransferase) degradation of commonly known polysaccharide, starch and hence they are easily available at affordable costs.
2. They have well-defined and rigid chemical structure, yielding many potential sites for chemical modification or conjugation.
3. Availability of cyclodextrins of different cavity size.
4. Low toxicity, low pharmacological activity and certain water solubility make CDs as extremely important candidate for materials of biological importance.

1.2. Structure and properties of cyclodextrins

In the early 1890's, a French chemist and pharmacist namely Antoine Villier, during experiments on the degradation of carbohydrates under the action of ferments accidently found the formation of white substance which was later proved as CDs.[10,11] Although they have been discovered in 19th century, CDs got real attention during 1980s when they found useful in pharmaceutical and food industries. Sometimes regarded as semi-natural compounds, CDs are commonly composed of five or more α-D-glucopyranoside units in a ring linked by α-1,4-glycosidic bonds. The three commonly used CDs contain six, seven and eight glucopyranoside units and they are named α-cyclodextrin (α-CD), β-cyclodextrin (β-CD), or γ-cyclodextrin (γ-CD)[8] respectively which are schematically represented in Figure 1.1. These three major CDs are crystalline, homogeneous and non-hygroscopic. The CD ring is frequently characterized as doughnut-

shaped truncated cone with a hollow cavity which is hydrophobic in nature. Because of this cone type of structure, CDs have two openings on either side of the cone with unequal radius as shown in Figure 1.1. The side which is composed of **C-2** and **C-3** carbon atoms of glucose units with their 2° hydroxyl groups is called secondary rim or wider rim. On the other hand the rim composed of 1° hydroxyl groups attached to **C-6** carbon of the glucose monomer is called primary rim or narrow rim. The remaining carbon atoms of glucose monomer namely **C-1**, **C-4**, **C-5** and **C-6** along with the anomeric oxygen constitutes the body of the cone lying in between smaller and wider rims. The hydrogen atoms attached to **C-3**, **C-5** and **C-6** of glucose units are facing inwards into the cavity of the CDs. Along with this, the non-bonding pair of electrons on the glycosidic oxygen atom also facing towards inside of the cavity producing a high electron density and which is leading to Lewis base character. These two arrangements make the interior cavity of CDs hydrophobic. When compared to the monomer, these oligosaccharides are not very soluble in water but generally solubility increases with temperature.[8] The lower aqueous solubility is explained as follows: The hydroxyl group on the **C-2** carbon of one glucose unit is involved in intermolecular hydrogen bonding with the hydroxyl group on the **C-3** carbon of the neighbouring glucose unit.

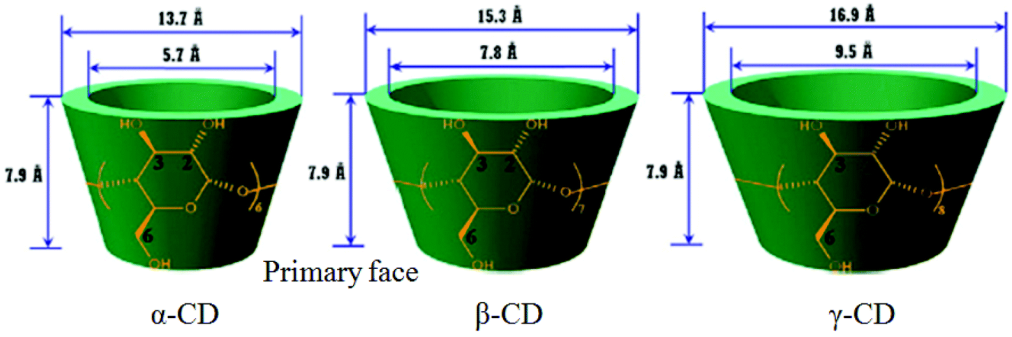

Figure 1.1. Schematic representation of CDs with their dimensions.

This secondary interaction makes CDs a rigid structure with high lattice energy which decreases aqueous solubility. Interestingly β-CD with seven glucose units found to

be least soluble (22.8mg/g of water at 30° C) when compared to α-CD (165 mg/g of water at 30° C) and γ-CD (320 mg/g of water at 30° C). The reason for this is the secondary hydrogen bonding belt is complete in the case of β-CD and has more rigid structure compared to α-CD and γ-CD which they have incomplete hydrogen bonding belt. The hydrogen bonding could be destroyed by alkylation of hydroxyl groups in the CDs which increases the aqueous solubility enormously.[11]

X-ray diffraction studies provided detailed structural information of these host molecules. CDs crystallize from water as hydrates and particularly β-CD crystallizes from water with 11 water molecules per CD. In the solid state or aqueous medium, CD cavity cannot be regarded as an empty space because the energy required for maintaining the empty space will be very high. As a result, even in solid state the CDs accommodate water as guest molecules and for β-CD the number of water molecules will be on average 6-7 molecules per CD. The X-ray studies further confirmed in the case of β-CD that the **O-2** to **O-3** distances is in the range of 270-300 pm. The seven glycosidic oxygen atoms are arranged nearly in a regular heptagon with the radius measuring to nearly 500 pm. The cavity volume of β-CD is estimated to be 0.262 nm^3 (in 1 g, 0.14 ml).[11] The height of all the three CDs found to be same at 7.8 A° (Table 1.1), whereas the size of the primary and secondary sides of the CDs increases as number of monomers increases. The molecular dimensions and structural parameters of three common CDs (α-CD, β-CD and γ-CD) are listed in Table 1.1.

Melting points of CDs is not defined generally as they begin to decompose above 200 °C. Studies have indicated that CDs have significantly high dipole moment (13 Debye for α-CD).[11] Similarly, dielectric constants of CDs have been estimated by monitoring the changes in emission properties of pyrene-3-carboxaldehyde as guest and for β-CD this value found to be 48 units. Both α-CD and β-CD give characteristic peaks on a cyclic

voltammogram which confirms the adsorption and desorption properties of CDs. The glycosidic bond in CDs is fairly stable in alkaline medium but gets cleaved into linear chain oligosaccharides with strong acids. Further, they are more resistant to acid catalyzed hydrolysis and enzyme-catalyzed degradation compared to linear sugars. CDs found to be non-toxic if daily dose is not more than 3% of the diet.[11] The orally administered CD is metabolized in the colon which is in contrast with starch metabolism in the small intestine. β-CD is hardly hydrolyzed at all in human blood.[11]

Property	α-CD	β-CD	γ-CD
No. of glucose units	6	7	8
Empirical formula (anhydrous)	$C_{36}H_{60}O_{30}$	$C_{42}H_{70}O_{35}$	$C_{48}H_{80}O_{40}$
Molecular weight	972.85	1134.99	1297.14
Maximum internal diameter (A°)	5.7	7.8	9.5
Diameter of outer periphery (A°)	13.7	15.3	16.9
Height of torus (A°)	7.8	7.8	7.8
Cavity volume (nm^3)	0.174	0.262	0.427

Table 1.1. Some structural parameters of CDs.

1.3. Host-guest complexes of cyclodextrins

CD inclusion complexes are the first example of the supramolecular complex formed by single host molecule.[11] As described above, CDs can be considered as empty containers of molecular size. When the cavity of CDs is filled with the molecule/s of another substance, the formed moiety is called 'inclusion complex'.[12] Generally, this complex formation takes place by the entry of guest into the cavity of CD through the wider rim. Interestingly, there will not be any covalent bonding between the host and guest and they are held together by purely physical forces. As a result of this, the association-dissociation equilibrium in solution is one of the basic characteristic features of inclusion complexes. The guest can be included totally or partly into the cavity of CDs and practically almost all the applications of CDs include this complexation process. The

prominent forces which hold guest inside the host are hydrophobic (the magnitude of this interaction is determined by average hydrophobic area of the guest), van der Walls and possible hydrogen bonding interactions of guest with the host. Majority of the inclusion complexes are studied in aqueous medium and the process of inclusion is driven by both entropy as well as enthalpy. Despite extensive research in the past four decades, it is not fully understood why inclusion complex forms at all. Nevertheless, the following points could be derived from the literature.[11,13]

1. It is understood that the cavity of CD contains water molecules when dissolved in aqueous medium. This energetically unfavoured polar – apolar interaction between included water molecules and CD cavity can be transformed into energetically favoured apolar-apolar interactions between included guest and CD cavity, and polar-polar interaction between included water and bulk water molecules (Figure 1.2).
2. In few cases it is found that the strain in the CD ring releases upon complexation which favours the complex formation.
3. van der Wall's interactions between CD cavity and bulky guest molecule will be more compared to the same interaction between CD cavity and included water molecules.

Water molecules inside the cavity of CD are regarded as high energy water which is shown in Figure 1.2, because the water molecules in the cavity cannot participate in regular tetrahedral hydrogen bonding as observed in bulk water. Most importantly, for stable complex formation the polarity and geometry of the guest are the crucial factors. Highly hydrophilic molecules are not suitable as guest molecules regardless of their geometry. It is interesting to note that in the case of guest molecule with charges, the geometry is adopted by guest molecule in such a way that the charged group is solvated

and hydrophobic part is inside the cavity. CDs are known to form complexes with inorganic salts, Halogens and Hydrogen halides, gases like CO_2, Xe, SO_2, hydrocarbons, metals and even with bulky fullerenes. In the present thesis, we limit our study using only organic guest molecules.

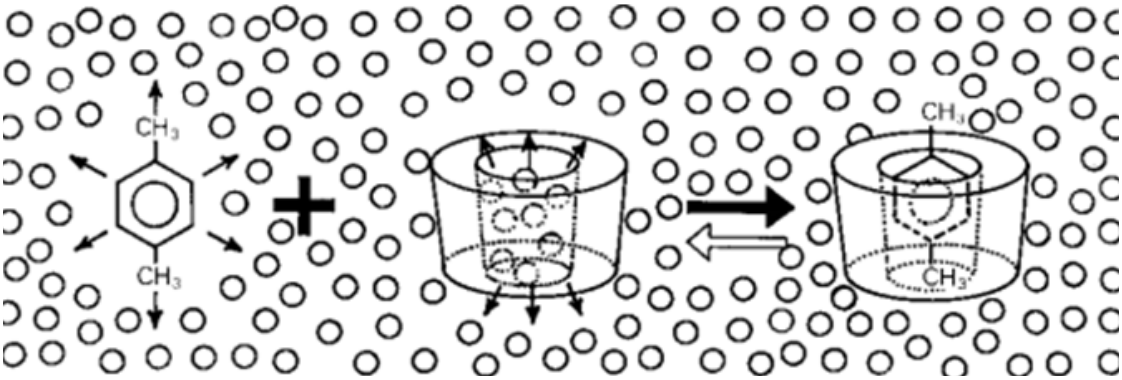

Figure 1.2. Schematic representation of the CD inclusion complex formation. The guest is p-xylene and circles represent water molecules. "Reprinted with permission from (Szejtli, J. *Chem. Rev.* **1998,** *98,* 1743). Copyright 1998, American Chemical Society."

The last few decades have witnessed large domain of CD inclusion complexes. After reviewing this literature, particularly for β-CD we understand that adamantane moiety is the best guest molecule which fits well into the β-CD cavity.[14] This pair is known to form inclusion complexes with highest association constant (of the order of 10^4) known till date in the CD family. A schematic representation of complex formation between β-CD and adamantane is shown in Figure 1.3.

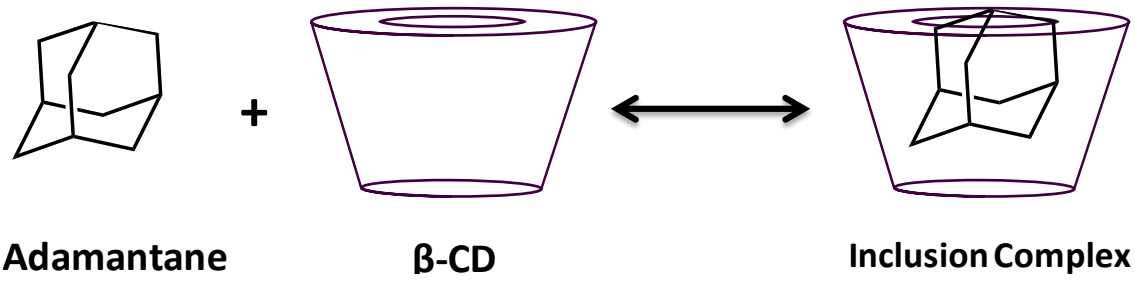

Figure 1.3. Scheme showing inclusion complex formation between adamantane and β-CD.

The free energy change for this pair usually lies near -30 kJ/mol. This is because the adamantane molecule is highly hydrophobic and the shape of the molecule is made for the cavity of β-CD. As a result of this, the hydrophobic interactions and van der Waals interactions are very high and the complex formation results in the displacement of all the water molecules from the CD cavity.

The high affinity between β-CD and adamantane pair has been utilized by several researchers for the fabrication of functional materials. For instance, Harada and co-workers have prepared supramolecular polymers with molecular weight above one lakh Dalton units by making use of this interaction.[15] They synthesized a β-CD dimer linked by PEG (M_n = 600) and a ditopic adamantane molecule linked again by PEG. When the two molecules mixed in water in the 1:1 ratio, they observed the formation of ultra long supramolecular polymers which is shown in Figure 1.4. The adamantane moiety was bound to the cavity of β-CD with the association constant of 1.2×10^4 / M and this is the reason for the formation of supramolecular polymers which could be compared to conventional polymers.

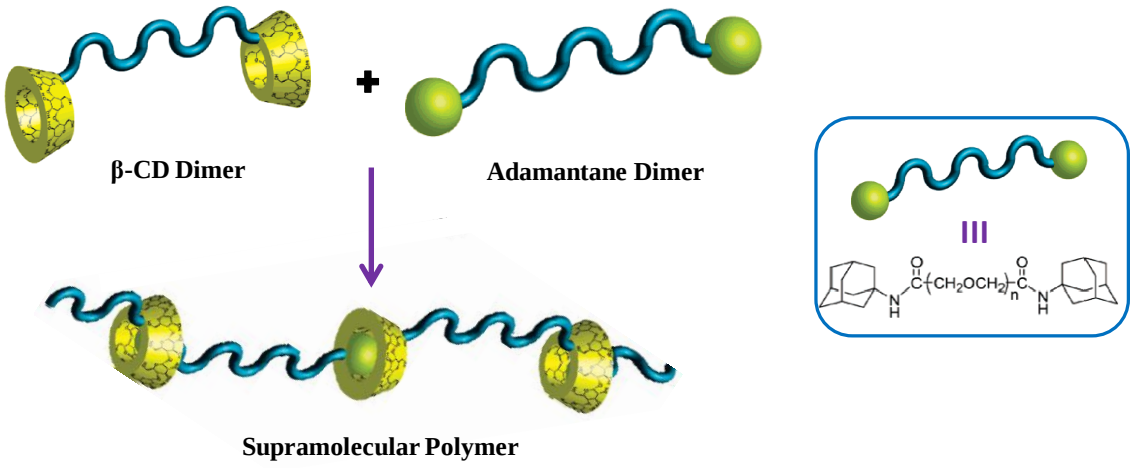

Figure 1.4. Scheme showing supramolecular polymer formation by the iterative interaction between adamantane guest and β-CD host molecules.

Similarly, our group for the last two decades have been involved in the complex formation studies between native β-CD as well as functionalised β-CD with small organic molecules for the application of photoinduced electron transfer (PET) reactions. For example we have functionalised β-CD in its narrow rim by electron rich molecules like pyrene and anthracene. These hydrocarbons are insoluble in water but upon attaching to CDs, they were made soluble in water. We also studied efficient PET after encapsulating electron deficient molecules such as pyromellitic dimide (PMDI) into the cavity of functionalised β-CD as shown in Figure 1.5. The rate of electron transfer was found to be similar with the donor and acceptors attached by covalent bonds.[16,17]

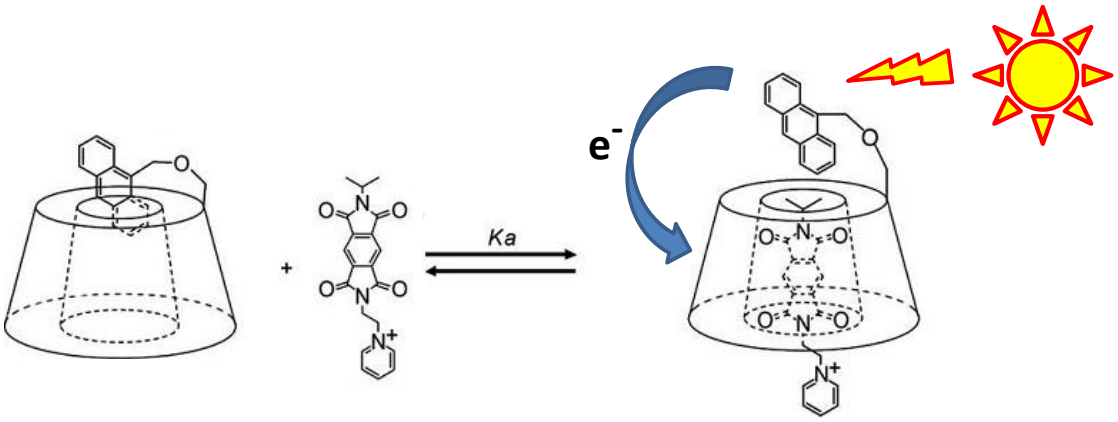

Figure 1.5. Scheme showing encapsulation of PMDI into the cavity of β-CD and efficient PET from anthracene to PMDI molecule.

Similar to β-CD, the α-CD with relatively smaller size forms stable complexes with mono- or disubstituted phenyl compounds. The α-CD cavity dimensions and phenyl ring dimensions are comparable and hence in the complex of them, the phenyl ring will be in contact with CD cavity which results in better van der Waals interactions.[13] Similar to β-CD and adamantane pair, the complexes with α-CD and benzoic acid is probably the most widely studied pair. The benzoic acid can enter into the cavity of α-CD by one of the two ways as shown in Figure 1.6. By using advanced NMR techniques, it is finally arrived at

a conclusion that the acid group enters first followed by the aromatic moiety as shown in B.[18]

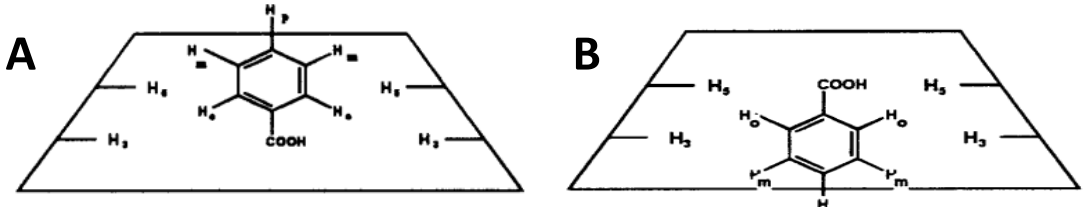

Figure 1.6. Scheme showing two different modes of entry of benzoic acid into α-CD cavity.

In the case of para disubstituted phenyl compounds, if one of the groups is relatively polar compared to another, it is observed that the non polar part is deeply inserted into the cavity the polar group protrudes outside through secondary side of the ring. For example, in the case of 4-hydroxybenzoic acid system, the carboxy group is inserted into the cavity with aromatic core and the hydroxy group protrudes from the secondary hydroxyl end of the cavity.[18] Harada and co-workers proposed that cinnamamide group is the ideal guest for α-CD and by using this interaction they have prepared several functional materials. For example the 3-cinnamoylaminohexanamide α-CD when dissolved in water formed intermolecular supramolecular complex as shown in Figure 1.7. In proton NMR titration experiments, the aromatic protons of the cinnamamide group showed an upfield shift with an increase in the concentration showed that this group is included in the cavity of CD.

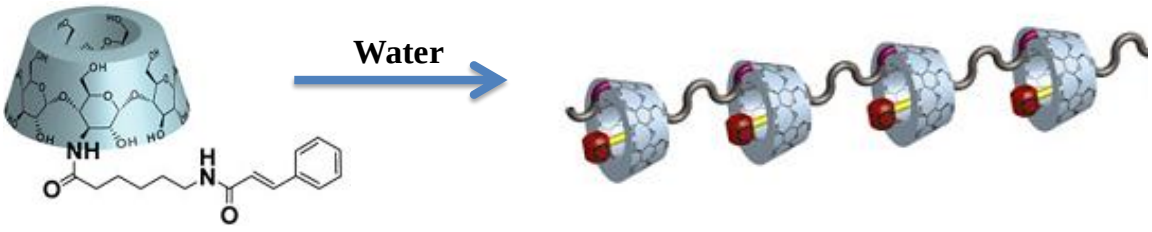

Figure 1.7. Intermolecular supramolecular complex formation by functionalised α-CD.

The γ-CD complexes are not very popular as the other two CD complexes because of their very large cavity size and collapsed cylinder structure. When guests suitable for α-CD or β-CD are used with γ-CD, the complex formed will be of 2:1 stoichiometry with two guests included into γ-CD cavity. Mittal and co-workers successfully prepared complex of Buckminster Fullerene (C_{60}) with γ-CD[19] which enhanced the solubility of C_{60} in water several folds (0.1 m mol) which is insoluble otherwise. As the cavity of γ-CD can accommodate more than one guest, this property has been utilized by Luo and co-workers for synthesising series of chemical compounds with superior yields. For instance, they have reported that γ-CD complexed with two molecules of 2-substituted naphthalene, which on irradiation gives substituted cubane-like photodimers with only one configuration.[20] In the absence of γ-CD, the irradiation always results in mixture of products which are difficult to separate.

It is widely accepted in the CD scientific community that the host-guest complex formation takes place by the entry of guest into CD cavity through wider rim. In contrast to this belief, in a series of publications we reported that β-CD could form noninclusion type complexes with certain N-alkyl derivatives of pyromellitic diimide (PMDI).[21-23] In this type of complex formation, we proposed that the PMDI core just remains outside near the smaller rim while the N-alkyl group enters into the cavity through smaller rim and we have named this novel interaction as 'rim binding' which is shown in Figure 1.8a. Interestingly, the PMDI derivatives formed true inclusion complexes with β-CD when the smaller rim is covalently functionalised to block the entrance by relatively bulky groups like Anthracene[21] (Figure 1.8c). Further, the stability of rim bound complex was dependent on the type of N-substituent on PMDI. We found that *tert*-butyl group fits well inside the β-CD cavity as its dimensions match with the dimensions of narrow cavity. Hence the complex of *tert*-butyl PMDI with β-CD was the strongest of all the complexes

we studied. Other substituents like n-butyl, isopropyl and n-hexyl formed complexes with less association constant. This accidental observation was confirmed by variety of techniques like UV−visible spectroscopy, induced circular dichroism (ICD), cyclic voltammetry (CV), isothermal titration calorimetry (ITC), MALDI-TOF mass spectrometry and ^{1}H NMR titration spectroscopies. Recently the structure of rim-binding complex was firmly confirmed by advanced NMR experiments like 2D-ROESY and COSY techniques also.[23]

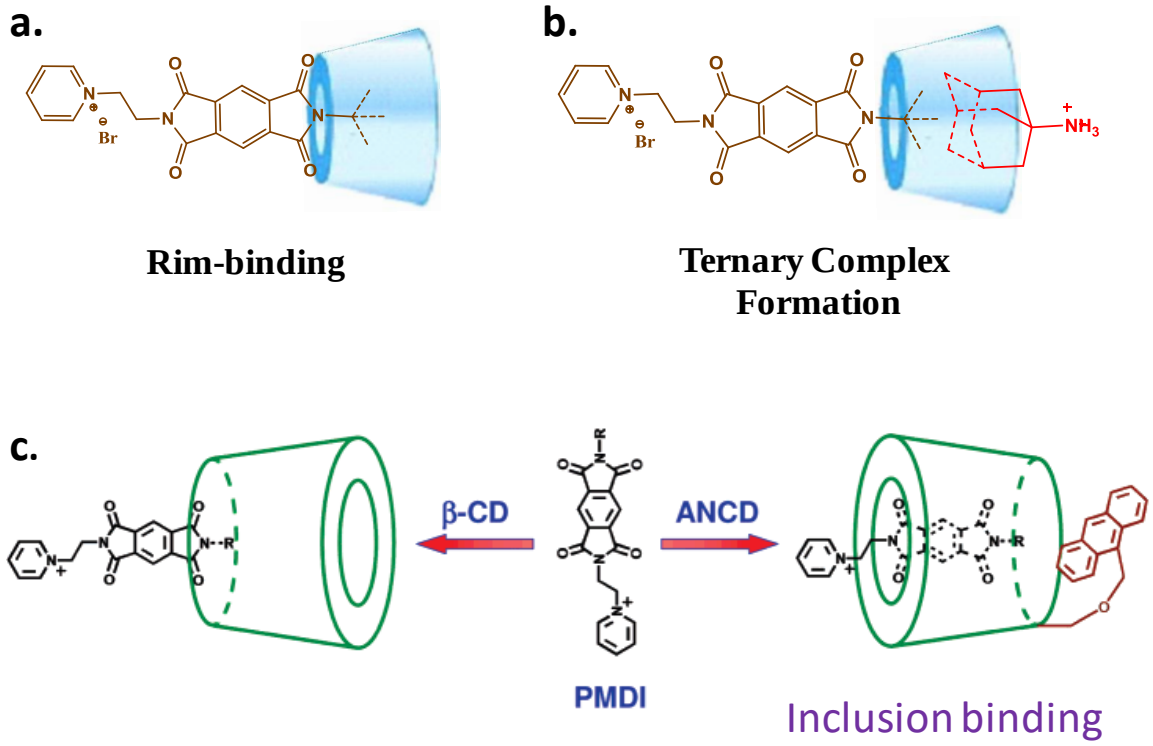

Figure 1.8. a) The rim binding interaction of PMDI derivative with β-CD. b) The ternary complex formation of β-CD with PMDI and adamantane derivative. c) Formation of true inclusion complex by β-CD with PMDI when primary rim is blocked with bulky substituents.

In a ROESY experiment of the rim-binding complex of N-alkyl PMDI@β-CD, the PMDI aromatic proton did not show any cross peaks with any of the β-CD interior protons, indicating that the PMDI moiety is not residing inside the cavity. The N-alkyl

protons, on the other hand, exhibited cross peaks with the H-3 and H-5 protons of β-CD indicating that these groups are placed inside the cavity. It is proved earlier that the adamantane moiety even though forms complex with β-CD with highest association constant, it occupies only 66 % of the cavity.[23] Hence even after complexation with adamantane group, the β-CD still has 34% of the space unoccupied. We have estimated that the *tert*-butyl group will occupy less than 34% of the cavity of β-CD from narrow side. We utilized this idea to encapsulate the adamantane moiety from wider rim and *tert*-butyl group from narrow rim simultaneously as shown in Figure 1.8b. We proved this ternary structure by ROESY experiment wherein we observed a cross peak between adamantyl protons and *tert*-butyl protons.

This property of β-CD viz. the ability to form ternary complexes was effectively utilized by our group for the fabrication of supramolecular hydrogels.[22] A ditopic molecule with adamantane at one end and *tert*-butyl PMDI group at the other end of 1,4-bis(4-pyridyl)ethane has been synthesized and made water soluble by quarternizing pyridine nitrogen. When this molecule was mixed with one equivalent of native β-CD, we observed the formation of ultra long supramolecular polymers as shown in Figure 1.9. We proposed that the polymer formation was by repetitive interaction of adamantane and *tert*-butyl groups with β-CD respectively by inclusion and rim-binding modes. The interactions were proved by ITC and ICD techniques and polymers were characterized by AFM and TEM experiments. Most importantly the formed nanofibers could trap water molecules even at a concentration of 10^{-6} M which led to the formation of supramolecular hydrogels which were characterized by frequency sweep as well as temperature dependent Rheology experiments. In this work we also proved that the β-CD molecule can be used to connect two molecules without creating actual covalent bond between them and by using only secondary interactions.

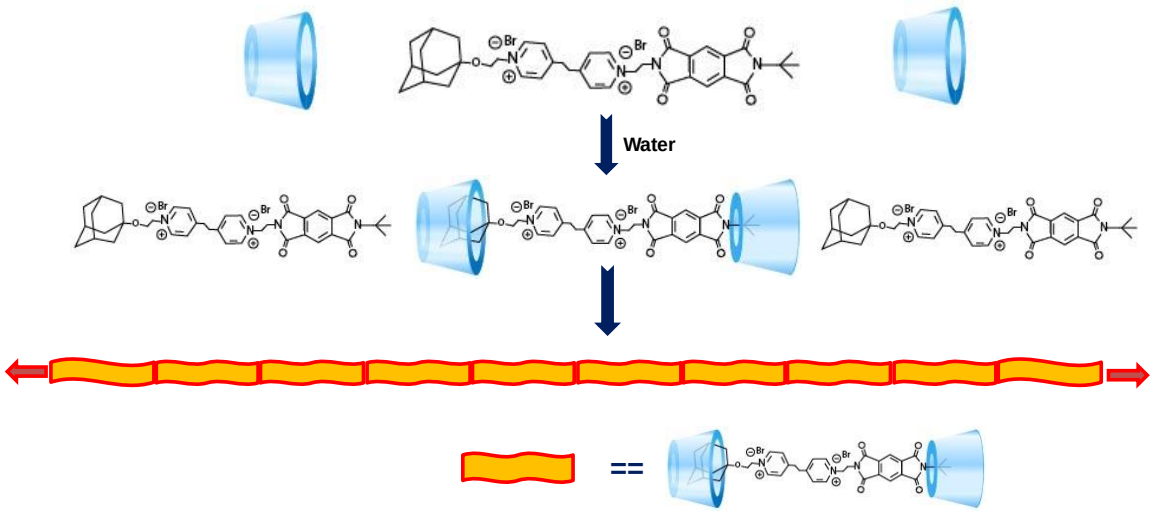

Figure 1.9. Pictorial representation of supramolecular polymer formation by β-CD with a ditopic molecule bearing adamantane and t-Bu-PMDI groups. "Reprinted with permission from (Krishnan R. et al., J. *Phys.Chem. Lett.* **2011,** *17, 2094*). Copyright 2011, American Chemical Society."

1.4. Cyclodextrin based self-assembled functional materials

The fabrication of supramolecular materials with uniform size ranging between one to few hundred nanometer window has become an active research topic, because of their absolute applications in the field of controllable drug transport, energy and electron transfer, template synthesis, sensors, imaging etc. The self-assembled materials can adjust their aggregated nanostructures in response to external stimuli such as pH, light, temperature, competitive molecules, redox etc. Cyclodextrin based self-assembled materials are particularly utilized in the field of bio-materials because of their water solubility and nontoxicity.[24] There are several kinds of smart materials of cyclodextrins at the nano scale have been reported which includes vesicles, micelles, supramolecular polymers, rotaxanes, catanenes, nanoparticles and hydrogels to mention a few.[25]

1.4. 1. Cyclodextrin based supramolecular vesicles and micelles

Both vesicles and micelles in general are self-assembled nanomaterials one or more layers of amphiphilic molecule. A typical amphiphile consists of a polar head group and non polar tail.[26] However the number of heads and tails in a given amphiphile can vary which results in different classes of amphiphiles as shown in Figure 1.10.

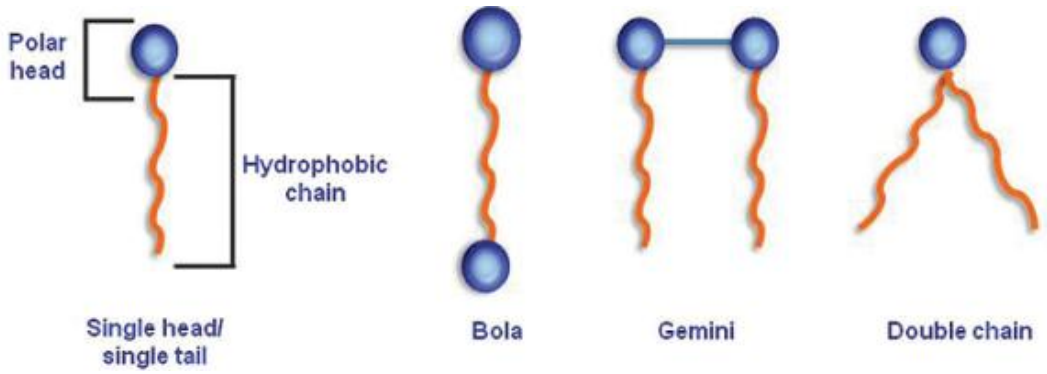

Figure 1.10. The schematic representation of different class of conventional amphiphiles.

For example, if an amphiphile consists of two polar head groups separated by long nonpolar group in between is called a bola amphiphile.[26] Two surfactant molecules covalently linked at their polar head groups are called Gemini amphiphiles. Double chain amphiphiles contain a polar head group connected to two long chains and are widely used for DNA delivery applications (Figure 1.10).

Recent advances in the field of supramolecular chemistry have yielded new class of amphiphiles namely 'supramolecular amphiphiles' or 'super-amphiphiles' (SA)[27,28] which are schematically illustrated in Figure 1.11. In contrast to conventional amphiphiles, SAs are formed by secondary interactions by combining the idea of conventional amphiphiles and supramolecular chemistry. SAs always contain two or more components held together by non-covalent forces. SAs allow tuning of their amphiphilicity by external stimuli which leads to assembly or disassembly of

nanostructures based on the requirements. Required functional groups can be attached to supramolecular amphiphiles by using various non-covalent interactions, which avoids the tedious covalent synthesis. The self-aggregation of amphiphilic molecules is a well studied area and has yielded a rich variety of assemblies which in turn depend on the molecular structure of the amphiphile and on experimental conditions. Among the large domain of assemblies, micelles and vesicles are the two main and commonly observed assemblies in aqueous medium (Figure 1.11).

Micelles are small volume of self-assembled nano-materials whose size can vary between 20 – 200 nm.[26] They contain a polar head group exposed to bulk of water and non polar tail concentrated at the center. Micelles of different shapes are reported in the literature but most commonly observed micelles are spherical in shape. Vesicles are generally spherical or ellipsoidal in shape and are composed of amphiphile bilayer structures with an internal cavity containing the aqueous solution.[28] If vesicles contain only one bilayer which encloses water, they are called unilamellar vesicles. If the number of bi-layers is two, then they are named as bilamellar vesicles. While for multi-lamellar vesicles, the number of bilayers can go to any number but water exists in both the center and interlayer. The vesicles of conventional amphiphiles can be stable for months but those formed by SAs are generally not stable so long because of weak interactions within SA. But less stability leads to more opportunities to construct smart materials as they will have quick response to external stimuli. In biological term vesicles are referred as liposomes as they are formed by natural phospholipids. Vesicles are pervasive building blocks in biological systems which function as media for storage, transport and delivery of molecules and materials within and between cells.[29] Nevertheless, vesicles can be synthesized by amphiphiles in laboratory. Based on the purpose of synthesis and synthetic procedure, their sizes can range from few nanometers to several micrometers. It is

important to note that both micelles and vesicles are dynamic structures similar to other self-assembled nano-structures and they will be always in equilibrium with their non-assembled monomers.

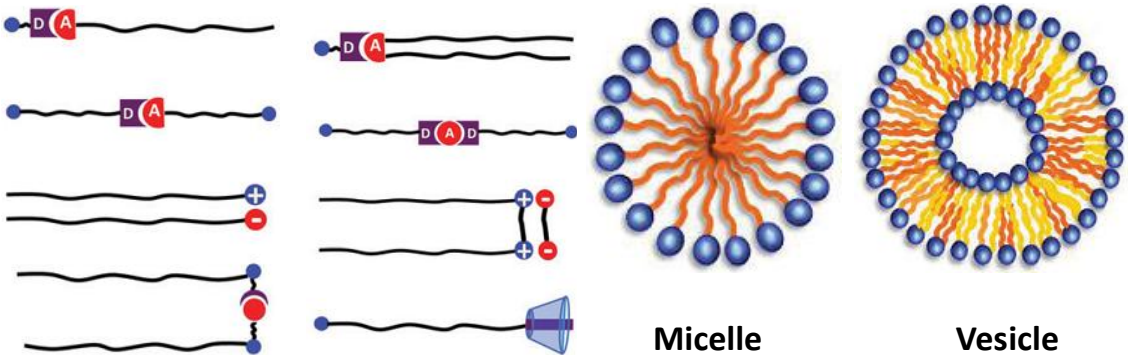

Figure 1.11. Cartoon showing different topologies of SAs with schematic representation of micelle and vesicles.

CDs offer a very good platform for the fabrication of these materials because of their hydrophilic nature. CDs are proved to be nontoxic and are biocompatible. Hence the CD based vesicles would have potential uses as drug/gene delivery agents.[30] Most importantly, the well-documented ability of the CDs to form inclusion complexes with a very wide range of guest molecules in aqueous solution has been widely exploited. The vesicles of CDs are usually prepared by constructing a supramolecular amphiphile of CD, as hydrophobic modification of CD is synthetically challenging process.[31] Following the self-assembly of SA, vesicles are prepared by combining multiple components through non-covalent interactions.

The first capable construction of vesicles by using a CD based SA was reported by Chen et al. in the year 2007.[32] The supramolecular complex of 1-naphthylammonium chloride (NA), sodium bis(2-ethyl 1-hexyl)sulfosuccinate (AOT) was prepared in aqueous medium in the presence of natural β-CD. In the complex, the compound NA found to be included into the cavity of β-CD while the other side of NA is found to be interacting

with the amphiphile AOT by cation-anion interactions as shown in Figure 1.12. Vesicles are formed after sonicating the mixture and were characterized by various spectroscopic techniques. Although the stability of these vesicles found to be unsatisfactory, the finding undoubtedly started a new era of functional materials prepared by SAs.

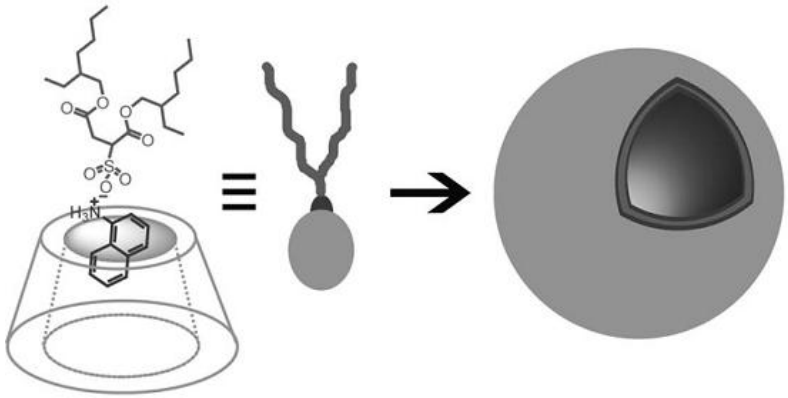

Figure 1.12. Schematic representation of the vesicle formation between native β-CD, AOT and NA.

Tao and co-workers have prepared a SA by using N-alkylamino-1-anthraquinone as a guest with β-CD and this SA further self-assembled into fluorescent vesicles.[33] They also observed that upon addition of acetic acid, the vesicles found to be disappeared. Interestingly, the vesicles were reformed when the pH is adjusted back to 7.0 by adding a base. When acid is neutralized, the ammonium reverts to amine and amphiphilic nature of complex is reverted. This is the first example of pH-responsive vesicles based on SA. The process is schematically shown in Figure 1.13.

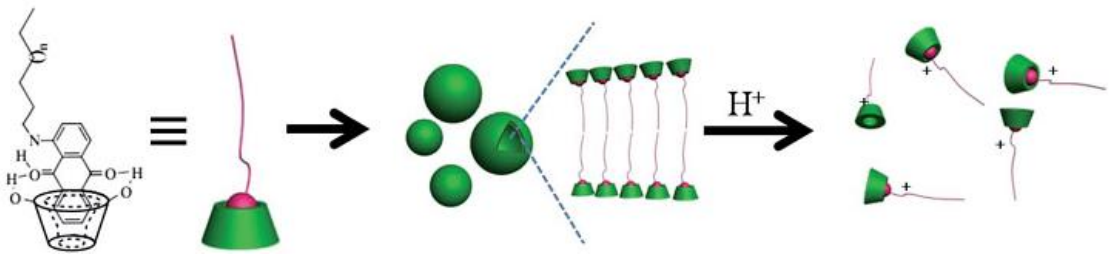

Figure 1.13. Scheme showing vesicle formation by SA of anthraquinone derivative and β-CD.

Among the numerous stimuli, light is always considered as a clean and instant energy which can act remotely, cleanly, and rapidly. Azobenzene, because of its combined properties of photoinduced *cis-trans* isomerisation and being recognized by CDs particularly in its *trans* form has attracted several researchers to construct photo-responsive materials. Wang's group in the year 2007, first reported photoresponsive vesicles by using a SA based on α-CD.[34] In a smart design they have used conventional amphiphile with long alkyl chain ending with azobenzene unit at one end and pyridinium moiety at other end (AzoC10) as shown in Figure 1.14. This typical surfactant molecule could self-assemble in aqueous medium forming stable vesicles. But when α-CD is added to the vesicles solution, the stable *trans* form of azobenzene gets included into the CD cavity which leads to the dis-assembly of vesicles. Interestingly, photo-irradiation of the aqueous mixture with UV light (365nm) for 500 seconds resulted in the reassembly of the vesicles. This is because the *trans* form of azobenzene gets converted to *cis* upon irradiation which will not form inclusion complexation with CD. Hence the original surfactant molecule excludes out from the CD cavity self-assembles to give back the vesicles. This could be an important observation because visible light which is safe compared to UV, is used for disassembling the vesicles which can find applications in bio-medical field.

Recently, Zhou et al. reported a photoresponsive vesicles based on supramolecular Janus hyperbranched polymer on the basis of β-cyclodextrin/azobenzene host−guest molecular recognition.[35] They have used hydrophilic hyperbranched polyglycerol connected to β-cyclodextrin at one end and hyperbranched poly(3-ethyl-3-oxetanemethanol) with an apex of an azobenzene group which is graphically shown in Figure 1.15.

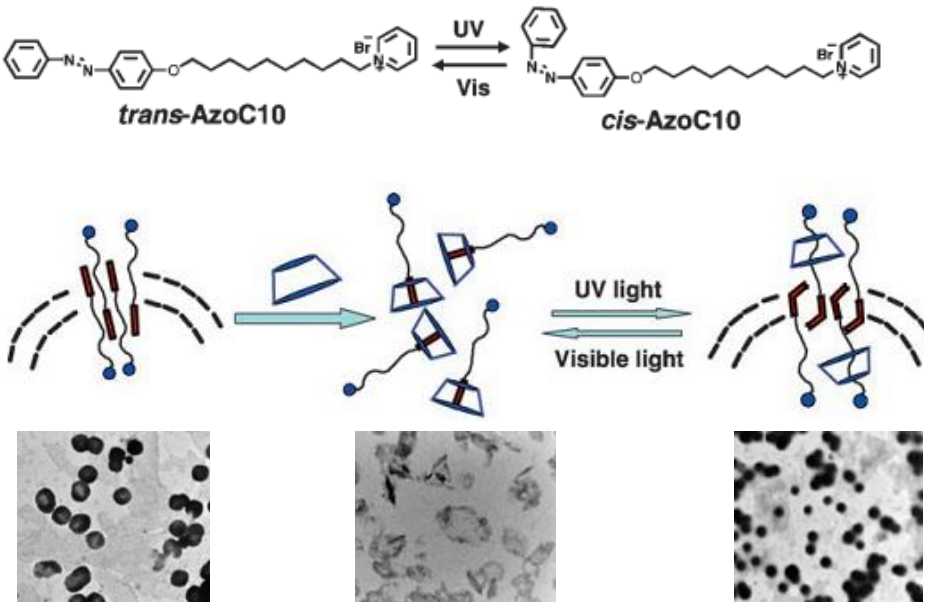

Figure 1.14. *Cis-trans* isomerisation enabled reversible self-assembly and dis-assembly of Azo-C10 and corresponding TEM images.

The host-guest complexation between the two molecules results the formation of a Janus particle.[35] The so formed Janus hyperbranched monomer self -assembled into supramolecular unilamellar vesicles and the assembly - disassembly process could be triggered several times by UV/visible light irradiation. The finding was very interesting because it demonstrates that the photo-responsive property can also be introduced into the polymer SA vesicles.

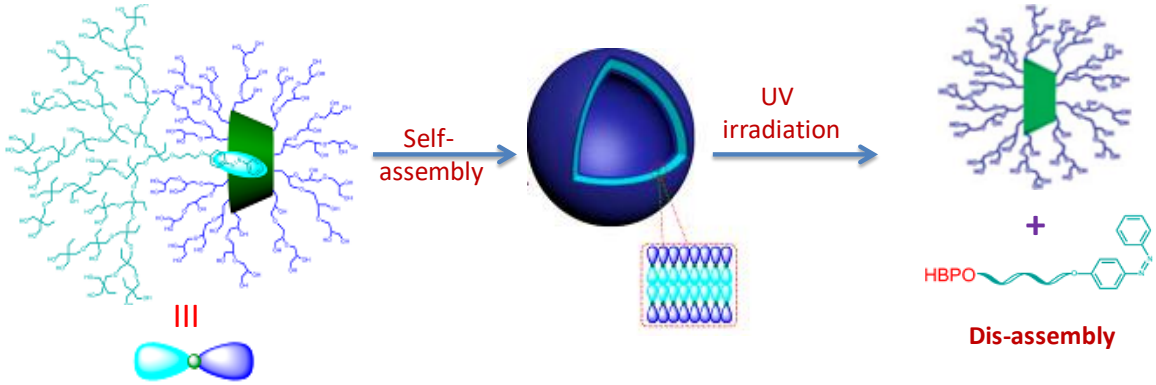

Figure 1.15. Schematic of self-assembly disassembly process of hyperbranched polymer resulting in the formation of supramolecular vesicles triggered by light.

Construction of voltage-responsive supramolecular self-assemblies is considered significantly attractive because similar to light, they can be easily controlled remotely and do not contaminate the system.[36] Moreover oxidation reduction processes are very common in the biological system. In the field of voltage responsive systems viologen and ferrocenes (Fc) are common guest molecules and β-CDs and calixarenes are frequently used hosts. Fc prefer the cavity of β-CD to form host-guest system where as the oxidized form of ferrocenes (Fc^{+}) readily comes out from the cavity and this process can be precisely controlled by redox potentials. Yuan's group fabricated a voltage-responsive supramolecular amphiphile based on β-CD ended polystyrene (PS-CD) and polyethylene oxide containing Fc (PEO-Fc) with uncharged ferrocenes which is shown in Figure 1.16.[37]

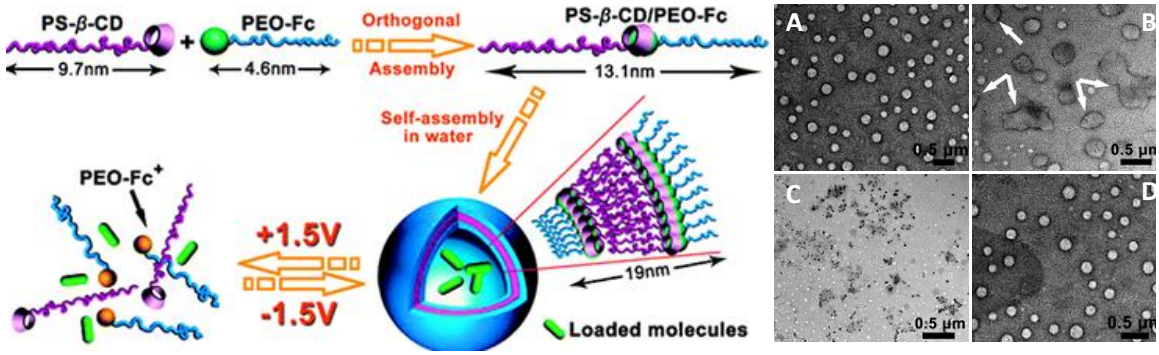

Figure 1.16. Cartoon representation of the formation of SA by host-guest complexation of PS-β-CD/PEO-Fc, and its reversible self-assembly and disassembly in response to voltage. (Right) TEM images of supramolecular vesicles (A), After applying voltage of +1.5 V for 2 h (B), after 5 h 9 (C), and -1.5 V after 5 h.

Upon host-guest complexation, the formed SA self-assembled into supramolecular vesicles as evident from the TEM images and the formed vesicles were stable for more than 3 months. The distinct contrast difference between particle skin and inner cavity is characteristic feature of a vesicle.[38] Interestingly, the wall of vesicle began to disrupt when a positive voltage of +1.5V was applied for 2 h. After 5 h, the vesicles were

transformed into irregular aggregates. The aggregates could be transformed back into vesicles by the application of negative potential and the cycle could be repeated several times. The group used these vesicles for loading of active molecules and release by applied voltage.

SAs always prepared by complexing more than one component and hence the molar ratio between them plays an important role on the properties of the vesicles prepared. SAs particularly if prepared based on host-guest interactions, any one of the component is in excess will change hydrophilic-hydrophobic balance and may lead to disassembly of nanostructures. Making use of this idea several researchers have prepared smart systems by using SAs.

For example, recently, Zhou and co-workers have synthesized a linear hyperbranched supramolecular amphiphile by the use of an adamantane containing long alkyl chain and a β-CD modified with hyperbranched polyglycerol as shown in Figure 1.17.[39] The high affinity of adamantane moiety for the β-CD cavity has been utilized by authors to construct the SA. The association constant for the adamantane β-CD complexation was found to be 1.7×10^3 M^{-1}, which was lower than the typical K_a value ($\sim 10^4$) between β-CD and adamantane group and the reason for this may be the steric hindrance of the hyperbranched chains on β-CD. Because of the amphiphilic nature, the SA self-assembled into supramolecular vesicles with diameters ranging between 60 – 600 nm. It is known that β-CD can also complex with hydrophobic alkyl chains but with lower association constant than that with adamantane moiety. So upon addition of more equivalents of β-CD, the excess β-CD gets threaded on alkyl chain attached to adamantane which makes whole complex hydrophilic (Figure 1.17). Hence as expected the vesicles were spontaneously disassembled and the process is not reversible.

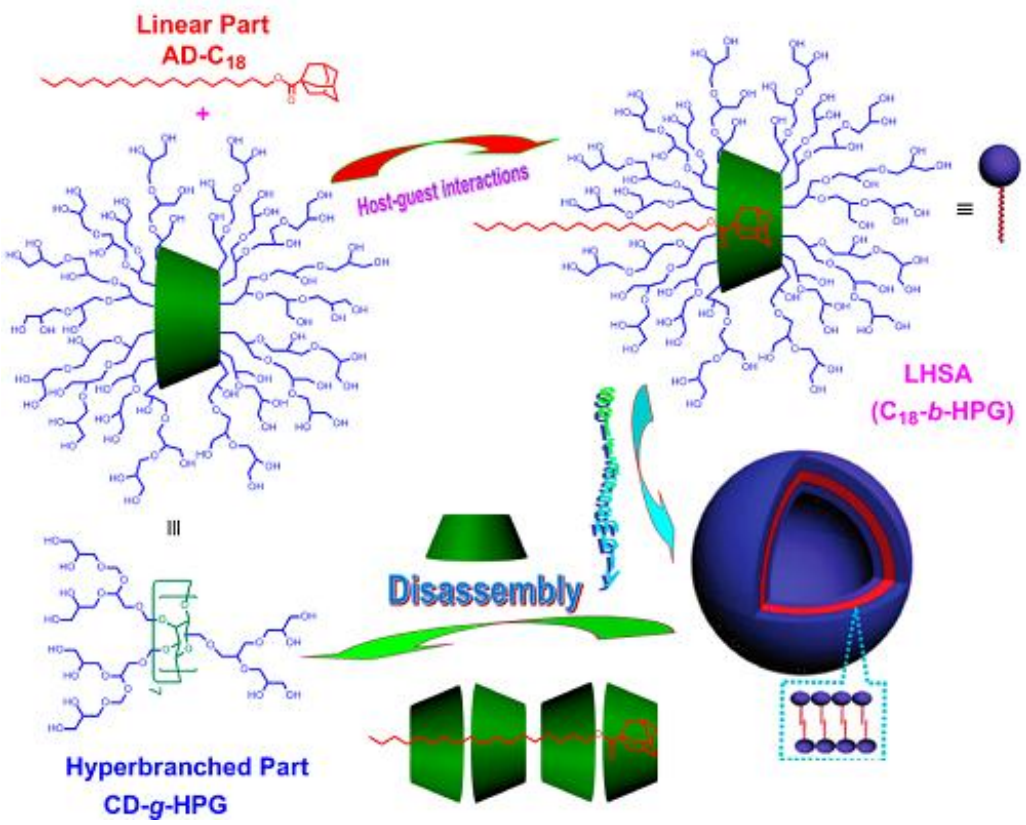

Figure 1.17. Scheme showing preparation, self-assembly and disassembly of vesicles prepared by supramolecular amphiphile of modified β-CD and long alkyl chain connected adamantane molecules.

One of the important applications of vesicles in living system is delivery of bioactive molecules within and in between cells.[29] Synthetic vesicles can also be used to perform similar functions. Usually the drug/gene delivery vehicles will be prepared and characterized first and bioactive molecule will be loaded into it and used for applications. But Hao and co-workers have utilized a novel strategy for the preparation of supramolecular vesicles for drug delivery. They have used hydrophobic functional material itself as guest to β-CD which is hydrophilic and thus formed SA self-assembled into vesicles. For example they have used paclitaxel, which is well-known anticancer drug as hydrophobic part to amine modified β-CD and this complexation resulted in the formation of SA (Figure 1.18).[40] The so formed SA self -assembled into supramolecular

vesicles in which the hydrophobic part was drug. Further, when these vesicles meet copper ions disassembly takes place leading to the release of drug. It is interesting to note that the cavity of these vesicles also is empty and it can be further used to load active molecules. Hence authors propose that the single nanostructure can be used to deliver two bio-active molecules simultaneously.

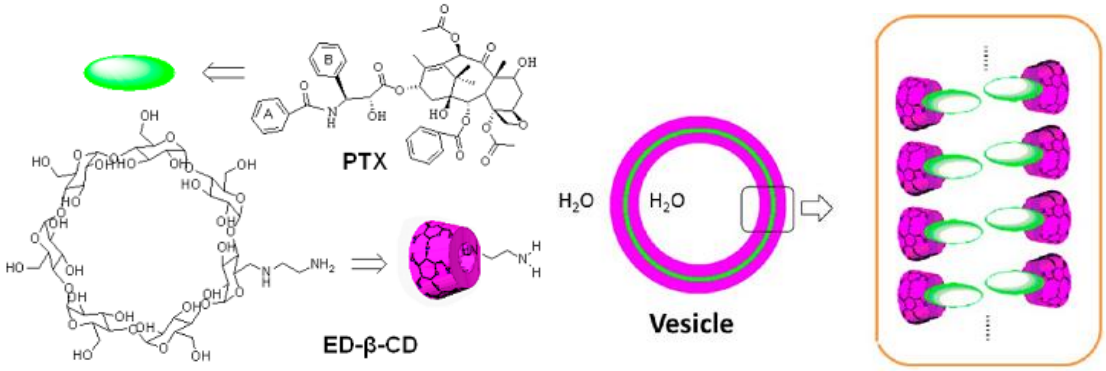

Figure 1.18. Vesicle formation by the combination of CD and paclitaxel, an anticancer drug.

1.4.2. CD based supramolecular polymers and hydrogels

The combination of two areas of science namely conventional polymers and supramolecular chemistry has delivered a new area called supramolecular polymers, caught considerable interest in recent years. Similar to classical polymers they are also formed by the repetitive interaction between their monomers but a major difference is that the monomer units are held together by weak secondary interactions. Even though the field of the synthetic supramolecular polymers caught attention in recent days, the natural supramolecular polymers such as double helix DNA, microtubules, and microfilaments play important role in maintaining the life and are known for centuries.The covalent polymers are chemically quite robust and mechanically difficult to process. On the other hand, owing to the weak interactions between the monomer units, the supramolecular polymers have several advantages such as easy processing, recyclability, self-healing,

stimuli responsiveness etc. Generally supramolecular polymers are not useful in the fields which they require mechanical strength and chemical stability but find several applications in the field of optoelectronic materials, self-healing materials, biomedical applications etc. The supramolecular polymers in almost all organic solvents have been reported but those synthesized in water most important because virtually all biological processes takes place in aqueous medium. The non-covalent interactions in water are specific and it is reported that the selective binding between avidin and its guest biotin has highest association constant (10^{15} M^{-1}) reported till date. Hydrophobic and π-π interactions are the prominent non-covalent interactions useful in aqueous medium along with other interactions such as H-bonding and van der Walls forces. The π-π interaction has limitation in water because increase in pi surface area for stronger interactions results in poor aqueous solubility hence the researchers are more leaned towards hydrophobic interactions. As a result of this most commonly used molecules to construct supramolecular polymers in aqueous medium are CDs and cucurbiturils.

The major finding on supramolecular polymers by using CDs comes from the group of Harada.[41,42] As discussed earlier, adamantane group binds with β-CD with highest association constant while α-CD shows similar preferences with para substituted benzenes. Based on this idea, Harada and co-workers have functionalised β-CD with a guest compatible to α-CD and vice versa i. e. they have functionalised β-CD with ^{t}Boc-cinnamoyl group (6-*p*-^{t}BocCiNH- β-CD) which is suitable guest for α-CD. Similarly another molecule, α-CD was functionalised with adamantane group which is suitable guest for β-CD. When these two monomers were mixed in aqueous medium in 1:1 ratio they observed the formation of supramolecular polymers[43] with alternating α-CD and β-CD and the schematic representation of the process is shown in Figure 1.19.

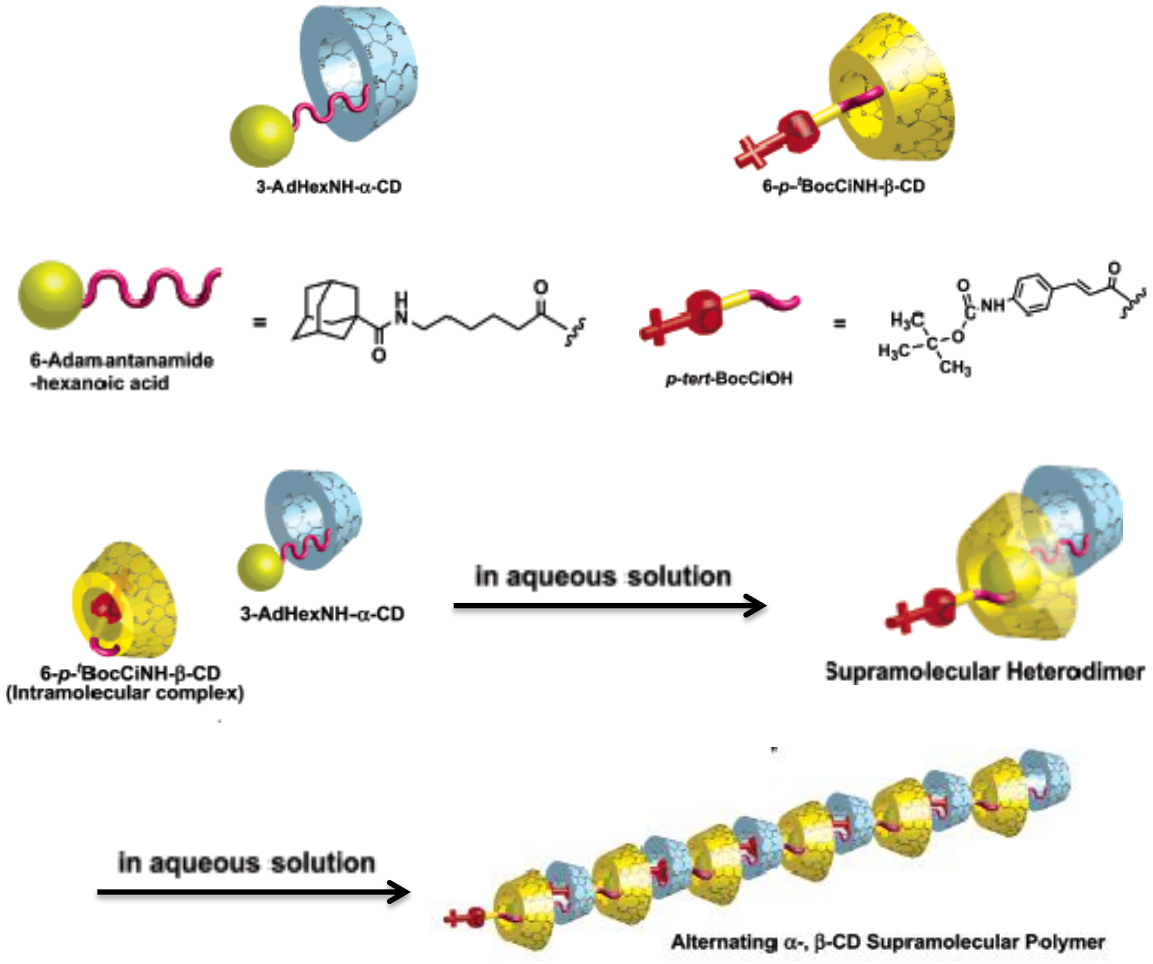

Figure 1.19. Schematic representation of molecular structure of 6-*p*-^{t}BocCiNH-β-CD and 3-Ad-HexNH-α-CD and mechanism of their supramolecular polymerisation.

Careful control experiments showed that, in the case of the molecule 6-*p*-^{t}BocCiNH- β-CD ^{t}Boc-cinnamoyl group enters into the cavity of β-CD to form intramolecular complex. Such complex formation is not possible with second molecule as the attached adamantane group is too bulky for the cavity of α-CD. When the two molecules are mixed in 1:1 ratio, the adamantane group pushes out ^{t}Boc-cinnamoyl group from the cavity of β-CD and enters into it. As a result the intramolecular complex breaks and intermolecular complex formation begins which ultimately leads to the formation of alternating supramolecular polymers.

Harada and co-workers have prepared photoresponsive supramolecular polymers by the use of stilbene as photoactive moiety.[44] Stilbene molecule in the *trans* state can be converted to *cis* by the irradiation of UV (365nm) light and *cis* could be converted back to trans by irradiating 254 nm light. Authors have prepared a β-CD dimer bridged in the center by stilbene and a bis-adamantane molecule linked by a pyridinium moiety which is shown in Figure 1.20. When these two molecules were mixed with host in its *trans* state, only discrete nanostructures (dimers) of 30 nm were observed. In contrast, the use of host in its *cis* form with bis-adamantane derivative yielded supramolecular polymer with overall length of 350 nm (Figure 1.20).

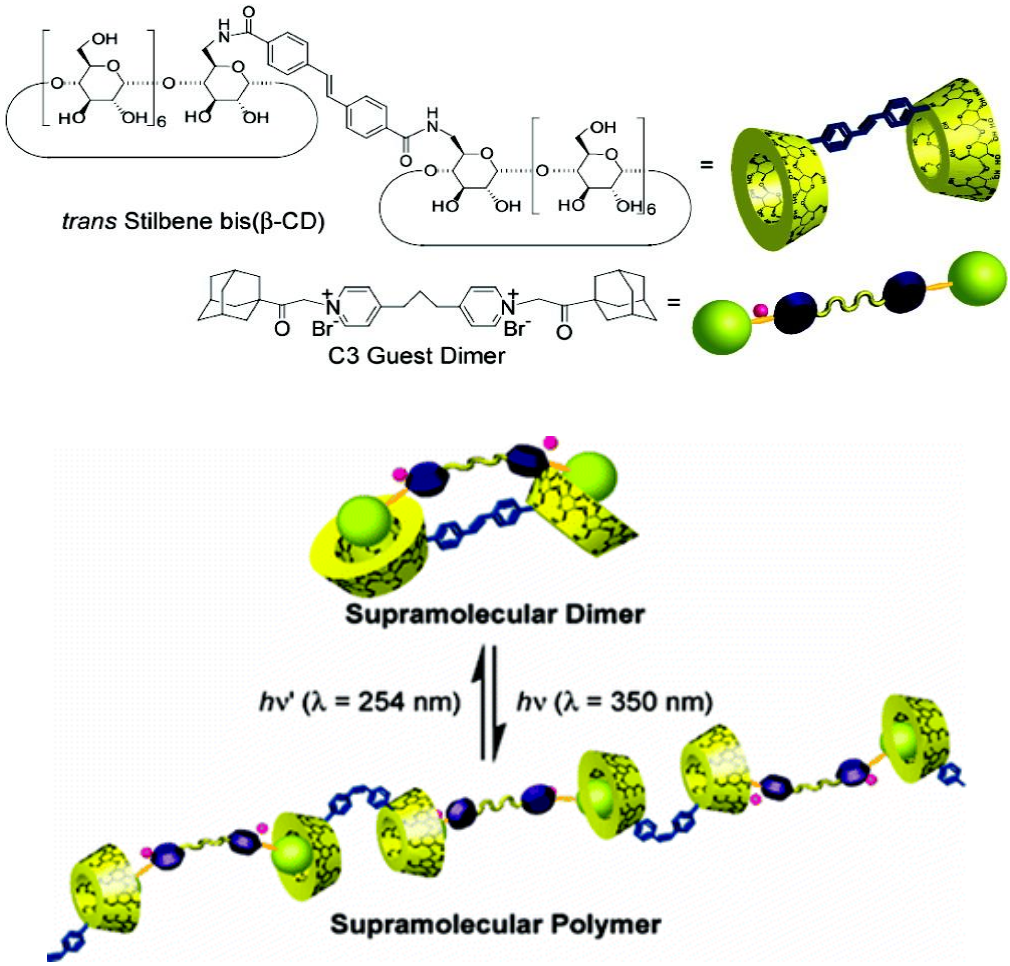

Figure 1.20. Scheme showing chemical structures of β-CD dimer bridged by stilbene, adamantane dimer linked by pyridine molecules and summary of supramolecular polymerisation process controlled by light.

Further the ITC data showed that the *trans* isomer binds to bis-adamantane molecule with higher association constant than *cis* isomer (about 3 times higher association constant). This is because of the co-operative effect resulted by the complexation of ditopic guest by both CD residues of the host dimer to give a 1:1 complex. In the case of *cis* isomer, the ditopic guest is complexed by two CDs belonging to two dimers which result in the formation of linear structures.

In some cases the polymerisation process continues to get larger supramolecular polymers with higher molecular weight. Some of the so formed high molecular weight supramolecular polymers have peculiar property of immobilizing the solvent molecules by trapping them in their three dimensional structures. This results a superior class of materials namely 'gels'.[45] Particularly, if the trapped solvent is water then the gel is known as 'hydrogel' and they find applications mainly in medical field ranging from tissue engineering to regenerative medicine.[30,46,47]

CDs because of their bio-compatibility have been extensively used for the preparation of supramolecular hydrogels.[48] There are several reports in the literature which makes use of CD based small molecules for the preparation of hydrogels. For example, Harada and co-workers have observed that when trinitrophenyl group was attached to aminocinnamoyl β-CD, the compound formed supramolecular polymers of high molecular weight.[49] In the 2D-NMR ROESY experiment, the protons of trinitrophenyl group showed strong cross peaks with inner protons of β-CD (C_5 and C_6 protons) which clearly shows that the trinitrophenyl group is included in the β-CD cavity. Further, at higher concentrations of 20 mM of monomer, the supramolecular polymers spontaneously transformed into orange colored hydrogels with critical gelation concentration of 2.9 weight % as shown in Figure 1.21. The authors suggested that the hydrogen bonding interaction between hydroxyl groups of CDs after the formation of

supramolecular polymer is responsible for the formation of hydrogels. Finally the gel to sol conversation could be easily achieved by the addition of competitive binder to β-CD. This is the first example for CD based stimuli-responsive supramolecular hydrogel without a polymeric back bone.

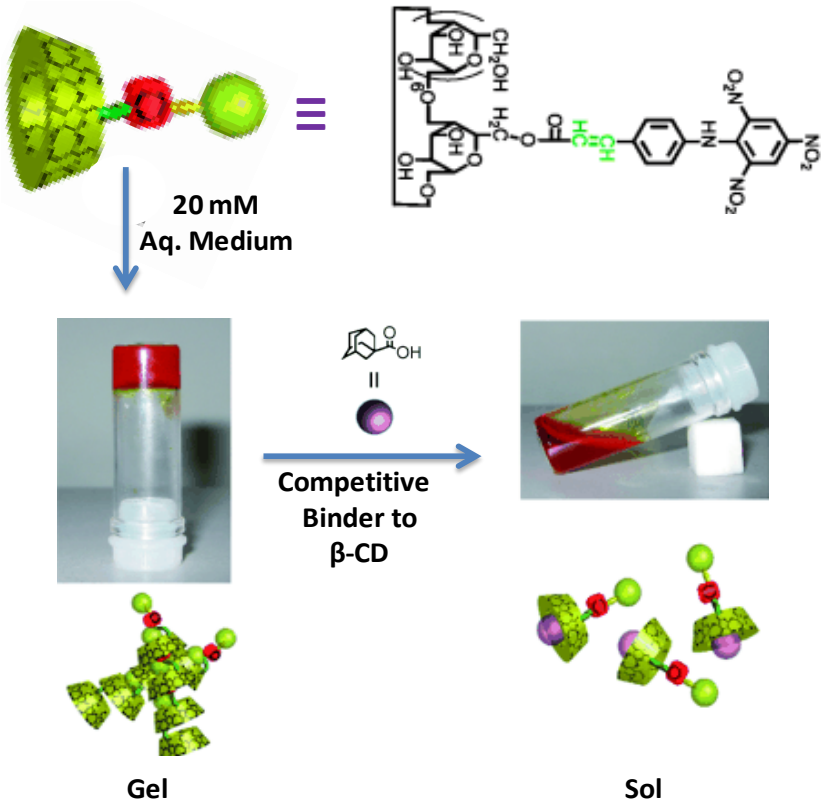

Figure 1.21. Chemical structure of modified β-CD with trinitrophenyl group, its spontaneous hydrogel formation and stimuli-responsive disaggregation to sol.

CD based host-guest recognition was effectively used in the literature for the directed assembly of macroscopic molecules into larger aggregates. In a series of publications by Harada's group, the macroscopic discrimination of molecules could be visually recorded which otherwise occurs in microscopic scale. For example they have observed self-assembly in the visually recordable level which arises because of microscopic recognition of suitable counterparts in the pool of guests by CD hosts.[50] They have synthesized two acrylamide-based hydrogels with pendent adamantane group (guest gel) and β-CD (host gel). When a piece of β-CD gel was brought closer to another piece

of adamantane bearing gel, both the pieces adhered firmly and a new piece of gel is formed which is showed schematically in Figure 1.22. The reason for the sticking of gel pieces is attributed to the host-guest recognition between adamantane and β-CD in their respective gels. The united gel piece only could be detached at a temperature above 90 °C because of high association constant between adamantane/β-CD pair and the process of attachment-detachment is reversible.

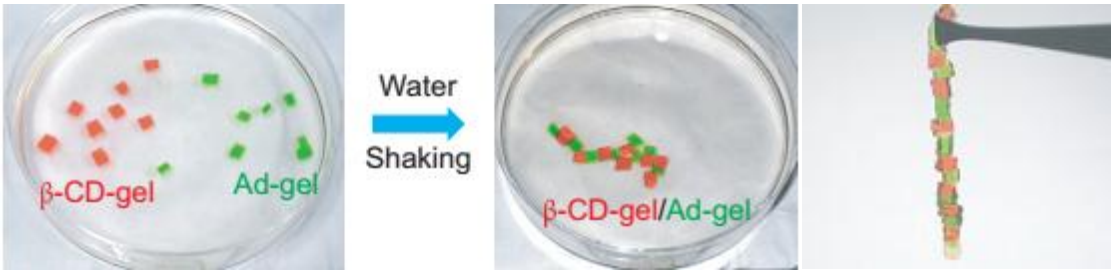

Figure 1.22. Visualization of macroscopic molecular host-guest recognition process by two acrylamide gels with β-CD (red) and adamantane (green) groups. The gels are stained to differentiate the two gels upon sticking. "Reprinted with permission from (Harada, A. and co-workers *Nat. Chem.* **2011,** *3,* 34). Copyright 2010, Nature Publishing Group."

Along with above two gels, another set of acrylamide based hydrogels with α-CD (host gel), t-butyl and n-butyl groups (guest gels) were also prepared. Very interestingly, in aqueous solution when two host gel pieces were mixed with two guest gel pieces (t-butyl and n-butyl gels), the guest gels clearly identified the hosts where in they can form complexes with highest association constant. Macroscopically one can visualize that the pieces of α-CD gel sticked to pieces of n-butyl gel, and only pieces of β-CD gel sticked to pieces of t-butyl gel as observed in Figure 1.23. The narrow n-butyl group fits well in the α-CD cavity, and the heavy t-butyl group fits well in the larger β-CD cavity. Further, by the use of azobenzene and ferrocenes as photoactive and redox active molecules respectively linked to acrylamide gels, they have showed above macroscopic recognition process could be controlled by light and voltage.[51]

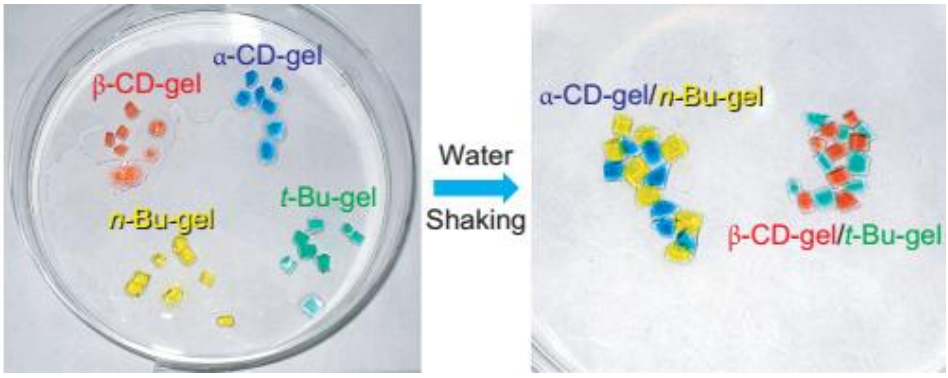

Figure 1.23. Scheme showing recognition events occurring between four different gel molecules mixed simultaneously in water initiated by host-guest recognition. The four hydrogels are stained with different color for easy identification upon gel adhesion. "Reprinted with permission from (Harada, A. and co-workers *Nat. Chem.* **2011,** *3,* 34). Copyright 2010, Nature Publishing Group."

1.5. Origin of the proposal

For the past several years our research group was involved in the study of host-guest complexes based on native as well as functionalised β-CD for applications in photoinduced electron transfer reactions. In the course of these studies, we observed an anomalous behavior of N-alkyl pyromellitic diimide derivatives (PMDI) towards the β-CD cavity for complex formation. We observed that when the narrow rim of β-CD is blocked by covalent modification using bulky groups such as anthracene, these PMDI derivatives actually formed inclusion complexes of PMDI. With unmodified β-CD the same PMDI derivatives preferred to stay outside the cavity near the narrow rim with only the N-alkyl group entering into the cavity through narrow rim (Figure 1.24). We named this peculiar mode of association of N-alky PMDI derivatives with native β-CD as 'rim-binding'. After detailed investigation, we concluded that the rim binding is independent to the alkyl substituents with the *tert*-butyl derivative exhibiting the highest association constant. Further, we also established that a β-CD could simultaneously hold an

adamantane derivative in the inclusion binding mode and N-*tert*-butyl PMDI in the rim binding mode form ternary complexes. Subsequently, we designed a ditopic molecule with PMDI on one end and adamantane moiety at the other which in the presence of β-CD formed long fibers through iterative inclusion and rim-binding interactions.

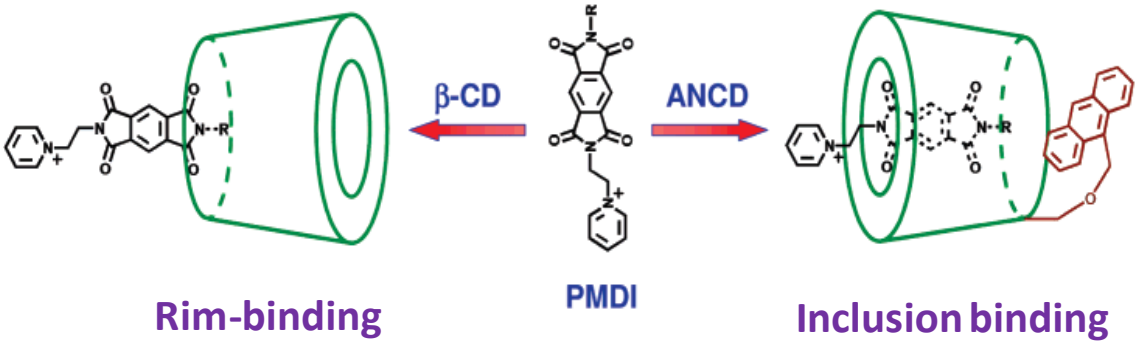

Figure 1.24. Two different modes of association of PMDI derivatives with β-CD.

In the present thesis, we have attempted formation of long fibers using a three component system. For this, we have designed two novel molecules that contained 1, 2-Bis(4-pyridyl)ethane moiety in the middle flanked by two adamantyl (AD-AD) and two *tert*-butyl PMDI (PI-PI) end groups. We expect the ditopic AD-AD and PI-PI to form three component linear supramolecular fibers upon reaction with β-CD by repetitive inclusion and rim-binding interactions. During the investigations, to our surprise we noted that the AD-AD reacted with β-CD to form β-CD⊂AD-AD⊃β-CD bis-inclusion complex which spontaneously self- assembled into supramolecular vesicles. The vesicles, because of their empty cavity, have attracted the attention of several researchers for encapsulation of active materials such as drugs and their on demand delivery. The literature reports several hundreds of novel vesicles every year but only few will reach clinical trial stage. Hence there is a huge demand for novel vesicles. **Chapter 2** of this thesis describes in detail the formation, characterization and application of β-CD⊂AD-AD⊃β-CD supramolecular vesicles as anticancer drug carrier.

In the **3rd chapter** we have shown that the rim-binding motif can be effectively exploited to perform the functions of vesicle recognition, adhesion and fusion leading to formation of supramolecular fibers. In an aqueous three component mixture of AD-AD, PI-PI and β-CD, we initially observed the formation of supramolecular vesicles which are later joined by rim-binding interactions by PI-PI to form fibers. By the careful investigation of mechanism of this morphological transformation, we could identify two social self-sorting and two narcissistic self-sorting processes in the self-assembly. In this chapter we also prove that the rim-binding interaction can take place not only with PMDI derivatives having pyridine end group (as we observed earlier) but also with a ditopic PMDI derivative PI-PI.

It is believed that at least a part of earth's energy crisis could be solved if solar energy can be made to split water into hydrogen and oxygen. One of the most important pathways for solar water splitting is photoinduced electron transfer leading to long-lived charge separated states. The nature produces long-lived (1 s) charge separated species by arranging the electron donors and acceptors in definite order by wrapping them in a protein matrix. In the **4th chapter** of this thesis we attempted to mimic this by arranging donors and acceptors by supramolecular interactions and embedding them in a supramolecular polymer. The capacity of β-CD to simultaneously hold adamantane and *tert*-butyl PMDI is exploited in this process. A novel ditopic anthracene derivative with two adamantane units at the two ends (AD-AN-AD) was used instead of AD-AD, as anthracene is good electron donor for PMDI. AD-AN-AD formed a supramolecular polymer in the presence of two equivalents of β-CD in aqueous medium. The nanosecond laser excitation in the presence of PI-PI generated charge separated species which survived for microseconds. The microsecond stability of PMDI radical anion which is otherwise unstable in water could only be attributed to wrapping of it in supramolecular

polymers. We also propose that the definite ordering of donor and acceptors by the aid of rim-binding interactions helped to place them in a fixed distance which facilitated electron transfer process.

1.6. References

(1) Lehn, J. M.: Supramolecular chemistry. *Science* **1993**, *260*, 1762.

(2) Whitesides, G. M.; Grzybowski, B.: Self-assembly at all scales. *Science* **2002**, *295*, 2418.

(3) Jean-Marie, L.: Supramolecular polymer chemistry? Scope and perspectives. *Polym. Int.* **2002**, *51, 894*.

(4) Krakowiak, K. E.; Bradshaw, J. S.; Zamecka-Krakowiak, D. J.: Synthesis of aza-crown ethers. *Chem. Rev.* **1989**, *89*, 929.

(5) Tanaka, Y.; Miyachi, M.; Kobuke, Y.: Selective vesicle formation from calixarenes by self-assembly. *Angew. Chem. Int. Ed.* **1999**, *38*, 504.

(6) Assaf, K. I.; Nau, W. M.: Cucurbiturils: From synthesis to high-affinity binding and catalysis. *Chem. Soc. Rev.* **2015**, *44*, 394.

(7) Ogoshi, T.; Kanai, S.; Fujinami, S.; Yamagishi, T.; Nakamoto, Y.: Para-bridged symmetrical pillar[5]arenes: Their lewis acid catalyzed synthesis and host–guest property. *J. Am. Chem. Soc.* **2008**, *130*, 5022.

(8) Crini, G.: Review: A history of cyclodextrins. *Chem. Rev.* **2014**, *114*, 10940.

(9) Szejtli, J.: Introduction and general overview of cyclodextrin chemistry. *Chem. Rev.* **1998**, *98*, 1743.

(10) Villiers, A.: Proceedings of the académie des sciences *Bull. Soc. Chim. Paris* **1891**, *45*,, 468.

(11) Szejtli, J.; Atwood, J. L.; Lehn, J. M.: Comprehensive supramolecular chemistry. *Volume 3*, Pergamon: New York, **1996**.

(12) Chen, G.; Jiang, M.: Cyclodextrin-based inclusion complexation bridging supramolecular chemistry and macromolecular self-assembly. *Chem. Soc. Rev.* **2011**, *40*, 2254.

(13) Rekharsky, M. V.; Inoue, Y.: Complexation thermodynamics of cyclodextrins. *Chem. Rev.* **1998**, *98*, 1875.

(14) Carrazana, J.; Jover, A.; Meijide, F.; Soto, V. H.; Vazquez Tato, J.: Complexation of adamantyl compounds by β-cyclodextrin and mono-aminoderivatives. *J. Phys. Chem. B* **2005**, *109*, 9719.

(15) Hasegawa, Y.; Miyauchi, M.; Takashima, Y.; Yamaguchi, H.; Harada, A.: Supramolecular polymers formed from β-cyclodextrins dimer linked by poly(ethylene glycol) and guest dimers. *Macromolecules* **2005**, *38*, 3724.

(16) Balan, B.; Gopidas, K. R.: Photoinduced electron transfer in α-cyclodextrin based supramolecular dyads: A free-energy dependence study. *Chem. Eur. J.* **2006**, *12*, 6701.

(17) Balan, B.; Gopidas, K. R.: An anthracene-appended β-cyclodextrin based dyad: Study of self-assembly and photoinduced electron transfer processes. *Chem. Eur. J.* **2007**, *13*, 5173.

(18) Schneider, H. J.; Hacket, F.; Rüdiger, V.; Ikeda, H.: Nmr studies of cyclodextrins and cyclodextrin complexes. *Chem. Rev.* **1998**, *98*, 1755.

(19) Priyadarsini, K. I.; Mohan, H.; Tyagi, A. K.; Mittal, J. P.: Inclusion complex of γ-cyclodextrin - C_{60}: Formation, characterization and photophysical properties in aqueous solutions. *J. Phys. Chem.* **1994**, *98*, 4756.

(20) Luo, L.; Liao, G.-H.; Wu, X.-L.; Lei, L.; Tung, C.-H.; Wu, L.-Z.: γ-cyclodextrin-directed enantioselective photocyclodimerization of methyl 3-methoxyl-2-naphthoate. *J. Org. Chem.* **2009**, *74*, 3506.

(21) Balan, B.; Sivadas, D. L.; Gopidas, K. R.: Interaction of pyromellitic diimide derivatives with β-cyclodextrin and anthracene-appended β-cyclodextrin: Rim-binding vs inclusion complexation. *Org. Lett.* **2007**, *9*, 2709.

(22) Krishnan, R.; Gopidas, K. R.: β-cyclodextrin as an end-to-end connector. *J. Phys. Chem. Lett.* **2011**, *2*, 2094.

(23) Krishnan, R.; Rakhi, A. M.; Gopidas, K. R.: Study of β-cyclodextrin–pyromellitic diimide complexation. Conformational analysis of binary and ternary complex structures by induced circular dichroism and 2D nmr spectroscopies. *J. Phys. Chem. C* **2012**, *116*, 25004.

(24) Hedges, A. R.: Industrial applications of cyclodextrins. *Chem. Rev.* **1998**, *98*, 2035.

(25) Ortiz Mellet, C.; Garcia Fernandez, J. M.; Benito, J. M.: Cyclodextrin-based gene delivery systems. *Chem. Soc. Rev.* **2011**, *40*, 1586.

(26) Jürgen-Hinrich, F.; Tianyu, W.: Bolaamphiphiles. *Chem. Rev.* **2004**, *104*.

(27) Xing, P.; Sun, T.; Hao, A.: Vesicles from supramolecular amphiphiles. *RSC Advances* **2013**, *3*, 24776.

(28) Sorrenti, A.; Illa, O.; Ortuno, R. M.: Amphiphiles in aqueous solution: Well beyond a soap bubble. *Chem. Soc. Rev.* **2013**, *42*, 8200.

(29) McMahon, H.; Gallop, J.: Membrane curvature and mechanisms of dynamic cell membrane remodelling. *Nature* **2005**, *438*, 590.

(30) Zhang, J.; Ma, P. X.: Cyclodextrin-based supramolecular systems for drug delivery: Recent progress and future perspective. *Adv. Drug Deliv. Rev.* **2013**, *65*, 1215.

(31) Khan, A. R.; Forgo, P.; Stine, K. J.; D'Souza, V. T.: Methods for selective modifications of cyclodextrins. *Chem. Rev.* **1998**, *98*, 1977.

(32) Jing, B.; Chen, X.; Wang, X.; Yang, C.; Xie, Y.; Qiu, H.: Self-assembly vesicles made from a cyclodextrin supramolecular complex. *Chem. Eur. J.* **2007**, *13*, 9137.

(33) Sun, T.; Li, Y.; Zhang, H.; Li, J.; Xin, F.; Kong, L.; Hao, A.: pH-reversible vesicles based on the "supramolecular amphiphilies" formed by cyclodextrin and anthraquinone derivate. *Colloids Surf. A* **2011**, *375*, 87.

(34) Wang, Y.; Ma, N.; Wang, Z.; Zhang, X.: Photocontrolled reversible supramolecular assemblies of an azobenzene-containing surfactant with α-cyclodextrin. *Angew. Chem. Int. Ed.* **2007**, *46*, 2823.

(35) Liu, Y.; Yu, C.; Jin, H.; Jiang, B.; Zhu, X.; Zhou, Y.; Lu, Z.; Yan, D.: A supramolecular janus hyperbranched polymer and its photoresponsive self-assembly of vesicles with narrow size distribution. *J. Am. Chem. Soc.* **2013**, *135*, 4765.

(36) Napoli, A.; Valentini, M.; Tirelli, N.; Muller, M.; Hubbell, J. A.: Oxidation-responsive polymeric vesicles. *Nat. Mater.* **2004**, *3*, 183.

(37) Yan, Q.; Yuan, J.; Cai, Z.; Xin, Y.; Kang, Y.; Yin, Y.: Voltage-responsive vesicles based on orthogonal assembly of two homopolymers. *J. Am. Chem. Soc.* **2010**, *132*, 9268.

(38) Jiang, W.; Zhou, Y.; Yan, D.: Hyperbranched polymer vesicles: From self-assembly, characterization, mechanisms and properties to applications. *Chem. Soc. Rev.* **2015**, *44*, 3874.

(39) Tao, W.; Liu, Y.; Jiang, B.; Yu, S.; Huang, W.; Zhou, Y.; Yan, D.: A linear-hyperbranched supramolecular amphiphile and its self-assembly into vesicles with great ductility. *J. Am. Chem. Soc.* **2012**, *134*, 762.

(40) Sun, T.; Yan, H.; Liu, G.; Hao, J.; Su, J.; Li, S.; Xing, P.; Hao, A.: Strategy of directly employing paclitaxel to construct vesicles. *J. Phys. Chem. B* **2012**, *116*, 14628.

(41) Harada, A.: Cyclodextrin-based molecular machines. *Acc. Chem. Res.* **2001**, *34*, 456.

(42) Harada, A.; Takashima, Y.; Yamaguchi, H.: Cyclodextrin-based supramolecular polymers. *Chem. Soc. Rev.* **2009**, *38*, 875.

(43) Miyauchi, M.; Harada, A.: Construction of supramolecular polymers with alternating α-, β-cyclodextrin units using conformational change induced by competitive guests. *J. Am. Chem. Soc.* **2004**, *126*, 11418.

(44) Kuad, P.; Miyawaki, A.; Takashima, Y.; Yamaguchi, H.; Harada, A.: External stimulus-responsive supramolecular structures formed by a stilbene cyclodextrin dimer. *J. Am. Chem. Soc.* **2007**, *129*, 12630.

(45) Buerkle, L.; Rowan, S.: Supramolecular gels formed from multi-component low molecular weight species. *Chem. Soc. Rev.* **2012**, *41*, 6089.

(46) Doring, A.; Birnbaum, W.; Kuckling, D.: Responsive hydrogels-structurally and dimensionally optimized smart frameworks for applications in catalysis, micro-system technology and material science. *Chem. Soc. Rev.* **2013**, *42*, 7391.

(47) Li, J.; Mooney, D. J.: Designing hydrogels for controlled drug delivery. *Nature Rev. Materials* **2016**, *1*, 16071.

(48) Du, X.; Zhou, J.; Shi, J.; Xu, B.: Supramolecular hydrogelators and hydrogels: From soft matter to molecular bio-materials. *Chem. Rev.* **2015**, *115*, 13165.

(49) Deng, W.; Yamaguchi, H.; Takashima, Y.; Harada, A.: A chemical-responsive supramolecular hydrogel from modified cyclodextrins. *Angew. Chem. Int. Ed.* **2007**, *46*, 5144.

(50) Harada, A.; Kobayashi, R.; Takashima, Y.; Hashidzume, A.; Yamaguchi, H.: Macroscopic self-assembly through molecular recognition. *Nat. Chem.* **2011**, *3*, 34.

(51) Yamaguchi, H.; Kobayashi, Y.; Kobayashi, R.; Takashima, Y.; Hashidzume, A.; Harada, A.: Photo-switchable gel assembly based on molecular recognition. *Nat. Commun.* **2012**, *3*, 603.

Chapter 2

Self-assembly of a Hydrophilic β-Cyclodextrin Inclusion Complex into Vesicles Capable of Drug Encapsulation and Release

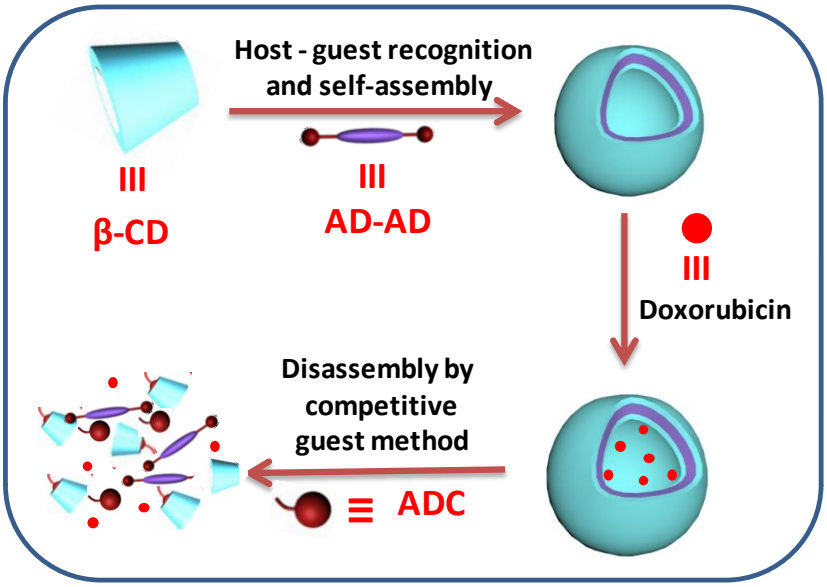

2.1. Abstract

In this chapter, the formation of a hydrophilic β-cyclodextrin (β-CD) host-guest supramolecular complex, its spontaneous self-assembly into stable supramolecular vesicles and the application of these vesicles for the encapsulation and stimuli-responsive release of anticancer drug are described. The very high affinity of adamantane derivatives for inclusion in the β-CD cavity has been utilized for the preparation of a supramolecular complex by host–guest recognition. Accordingly, we synthesized an adamantane derivative of 1,4-bis(4-pyridyl)ethane (AD-AD) with two adamantane groups at the two ends which interacted with two equivalents of β-CD to give the bis-inclusion complex β-CD⊂AD-AD⊃β-CD. The complex formed was well characterized by ^{1}H NMR, 2D NMR and ITC experiments. By the careful examination of ^{1}H NMR titration spectra,

we found that along with host-guest interaction the complex is undergoing secondary inter-complex interactions. This secondary interaction led to the unexpected formation of supramolecular vesicles which were thoroughly characterized by AFM, TEM, SEM, DLS and Confocal Microscopy. Further, we have also shown that the nano-structures formed have the characteristics of the vesicle by effective loading of the hydrophilic anti-cancer drug doxorubicin. Finally, the loaded drug could be stimuli-released into the medium upon the addition of a competitive inclusion binder such as adamantane carboxylate.

2.2. Introduction

The present century has witnessed a large number of human mortalities because of cancer and in the top ten causes of death cancer remains in the second position.[1] With the advance of science and technology, many treatment options for cancer are available which include surgery, chemotherapy, radiation therapy, hormonal therapy etc. Normally the treatment includes the combinations of above methods and the treatment may or may not be curative. Chemotherapy, which is sometimes abbreviated as 'chemo' is the most commonly employed treatment method for almost all types of cancer. In this method one or more cytotoxic drugs (chemotherapeutic agents) are administered to patients and the drug can kill all the cancer cells spread throughout the body, even away from cancer tumor. Chemo is generally used to control the cancer, though cure is the goal. There are more than 100 different chemo drugs in the market and depending on the type of cancer (more than 100 cancer types are identified) the drug is used either alone or in combination with other drugs. The mechanism of their action may involve the direct damage to DNA or interfere with its synthesis or block enzymes required for transcription or even interfere in the process of separation of double strands of DNA.[2] One of the most widely used drugs against a range of tumour types is Doxorubicin (Dox). Dox is a member of anthracycline antibiotics, which consist of an amino sugar linked through a glycosidic

bond to the C_7 of a tetracyclic ketone namely, doxorubicinone. The chemical structure of Dox is shown in Figure 2.1. In a widely accepted mechanism, Dox undergoes intercalation in between DNA base pairs which inhibits nucleic acid synthesis creating a marked cytotoxicity.[3]

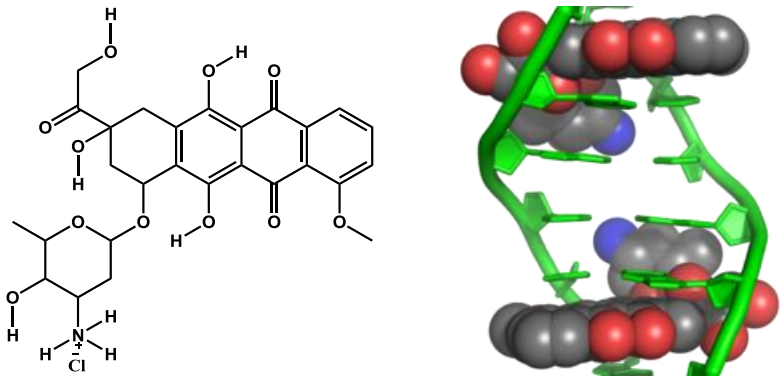

Figure 2.1. The chemical structure of doxorubicin and its intercalation with DNA causing its damage.

One of the common problems encountered in the chemo is the spread across the body of the administered drug causing toxicity to healthy tissues resulting in severe side effects. Additionally, many anticancer drugs have bulky polycyclic structures and are hydrophobic in nature. This results in poor bioavailability of these drugs and limited selectivity for cancer cells. In a bid to improve administration and reduce the side effects of chemo drugs, numerous attempts were made to deliver them in a controlled and localized manner at clinically relevant concentrations. One of the promising approaches is to encapsulate the drug in nano-sized drug delivery vehicles which prevents the metabolism, renal excretion and uptake of drug by immune systems.[4] Several of the drugs which were found less effective or toxic were found to be useful after encapsulation in drug carriers. Further, in a much-advanced drug delivery system, namely targeted drug delivery,[5] the drug encapsulated in a carrier is directly targeted to the affected area making the concentration of the drug higher near the tumor than other parts of body. In

order to improve the efficiency of chemotherapy, the delivery vehicle should be bio-compatible, targeting only to cancer cells, should have high drug loading efficiency and controlled release property. Nano-materials commonly used for delivering drugs include vesicles or liposomes,[6,7] micelles,[8] dendrimers,[7] hydrogels,[9] synthetic nano-particles[10] and several other supramolecular systems constructed in the aqueous medium. For example, Dox encapsulated in bilayer vesicles prepared by methoxy- polyethylene glycol is commercially available and sold as Doxil, which can protect patients from several side effects of doxorubicin. Drug administration by encapsulating it in nano-carriers is considered to be superior when compared to direct dosage and this technique is not only limited to cancer treatment but for almost all diseases where chemotherapy is involved. Many of the nano-carriers in the above category are dropped from further development to reach the clinical stage because of several reasons. Also, it has been observed that several of the self-assembled nano-materials are leaky and can release a lot of their loaded materials immediately on administration. Hence there is always a huge demand for novel drug carriers with advanced properties.

As discussed in Chapter 1, hydrogels, which are three dimensional networks of fibrils either connected by covalent or supramolecular interactions with trapped water, are increasingly used in bio-medical field. Particularly, they are widely used for controlled release of drugs because of their similarity with microenvironment of tissues of human body. Biodegradable natural polymeric hydrogels (chitosan, hyaluronic acid, dextran etc.) and synthetic polymeric hydrogels (polypeptides, polyesters etc.) are widely used for this purpose. Even though these hydrogels are generally used in medication, they have limitations because of their bulky irregular structure, incomplete release of drug, immunogenic behaviour etc. To overcome these difficulties small molecule based supramolecular hydrogels whose water content is more than 95% are increasingly used in

recent days. Zbigniew et al. for instance have recently reported that azobenzene connected L-lysine derivative forms a supramolecular hydrogel which could be effectively used for the controlled release of DNA and Dox.[11] The structure of the molecule and the mechanism of drug release are shown in Figure 2.2.

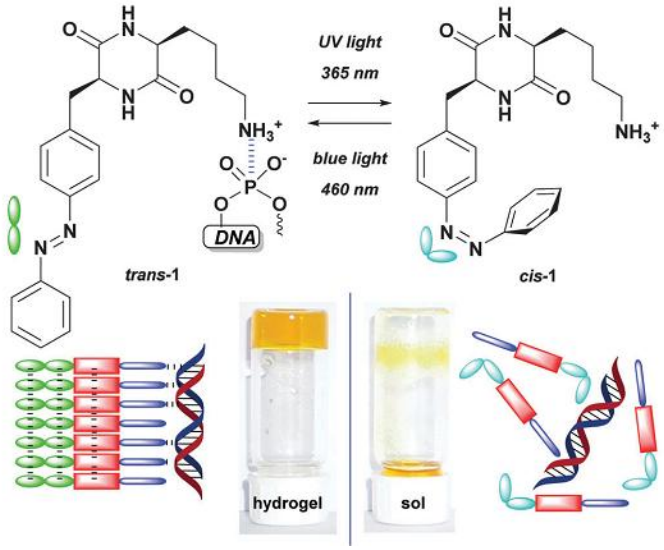

Figure 2.2. The supramolecular hydrogel formation by lysine derivative and its light triggered release of cargo. "Reprinted with permission from (Zbigniew. L. P. et al. *Chem. Commun.*, **2016,** *52,* 3143). Copyright 2016, The Royal Society of Chemistry 2016."

The drug release could be controlled by light, temperature, ionic strength and pH of the medium. The light active azobenzene unit in the *trans* form allows a long range order in the system to form the hydrogel. But the *cis* configuration of -azo group formed upon light irradiation destroys the hydrogel releasing the loaded cargo.

There is a large literature on different kinds of synthetic nano-carriers for the loading and unloading of active molecules in the biological system. In spite of the advances made in this area nano-carriers in practical use are generally limited to vesicles. As discussed in Chapter 1, the vesicles are formed by bilayers of amphiphiles and have an empty cavity at the center. It is for this cavity the researchers are always targeting for the encapsulation of active molecules. Although polymeric vesicles have high drug loading

capacity, those constructed by self-assembly approach have their own advantages because of their reversible nature. The host-guest assembly is a commonly used method for vesicle preparation by using secondary interactions. Liu and co-workers have recently reported two component vesicles based on p-sulfonatocalix[4]arene and asymmetric viologen by non-covalent approach which could uptake Dox (Figure 2.3).[12] The vesicles were multi stimuli-responsive and hence the loaded drug could be released by temperature, voltage as well as by competitive hosts such as CDs. All the components used for the vesicle construction are found to be nontoxic and safe to use in living cells. Hence authors carried out cell experiment with Dox-loaded vesicles and found that the therapeutic effect of Dox is not reduced but the damage for normal cells has reduced significantly.

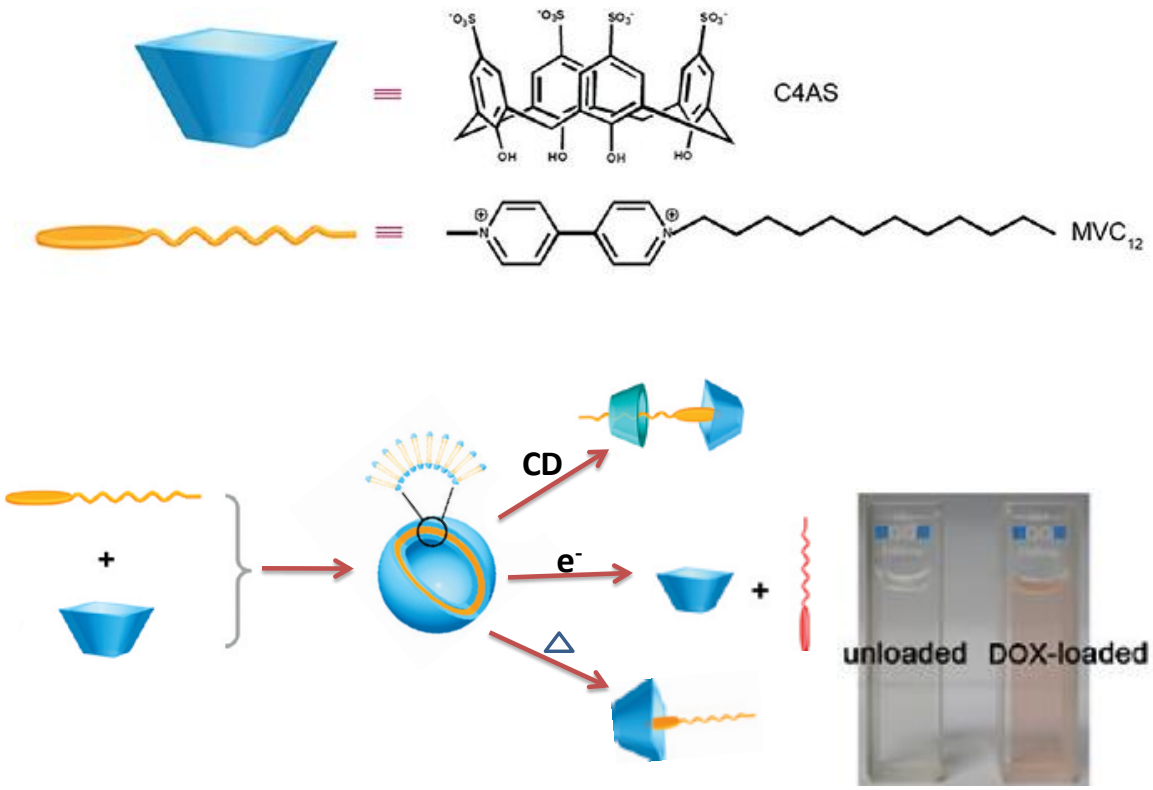

Figure 2.3. The molecular structures of chemicals used for the construction of vesicles, their multi-stimuli responsiveness and capacity to uptake Dox.

The vast literature of supramolecular vesicles prepared by using CDs as hosts is surveyed in Chapter 1. After reviewing the literature one can understand that the vesicles

are prepared by the careful construction of supramolecular amphiphiles wherein the CDs function as hydrophilic part and the guest acting as the hydrophobic part.

When an amphiphile is dissolved in the aqueous medium there will be polar non-polar interaction between water and hydrophobic part of the amphiphile. This high energy interaction makes the system less stable. In order to achieve stability, the amphiphile undergoes aggregation in such a way that the hydrophobic part is not exposed to water. To the best of our knowledge, almost all the amphiphiles possesses clearly distinguishable hydrophobic and hydrophilic parts and their aggregation follow the above rules. As a contradiction to this generalization, we have observed that purely hydrophilic amphiphile based on β-CD inclusion complex also can undergo spontaneous self-assembly in the aqueous medium to form vesicles. The present chapter deals with this unprecedented self-assembly process and its application in stimuli-responsive delivery of the anti-cancer drug Dox.

The adamantane group exhibits a very high tendency to form an inclusion complex with β-CD with the association constant in the range of 10^4 M^{-1}.[13] Based on this knowledge we have synthesized a ditopic 1,4-bis(4-pyridyl)ethane derivative bearing two adamantane moieties on either side of it (AD-AD). Facile aqueous solubility of this molecule is achieved by quarternizing the pyridine nitrogens. In the presence of two equivalents of β-CD, the bis-adamantane derivative AD-AD is expected to form host-guest inclusion complex to give the bis-inclusion complex β-CD⊂AD-AD⊃β-CD as shown in Scheme 2.1. Interestingly, we observed that the formed bis-inclusion complex undergoes spontaneous stacking which ultimately resulted in the formation of supramolecular vesicles. This unusual process was probed by isothermal titration calorimetry (ITC) and NMR titration experiments which supported the self-assembly

processes shown in Scheme 2.1. The vesicles were characterized by atomic force microscopy (AFM), transmission electron microscopy (TEM), scanning electron microscopy (SEM) and dynamic light scattering (DLS) experiments. Further, we also showed that, these vesicles can be loaded with the anti-cancer drug Dox and the loaded drug can be released upon addition of a competitive binding agent such as adamantane carboxylate (ADC).

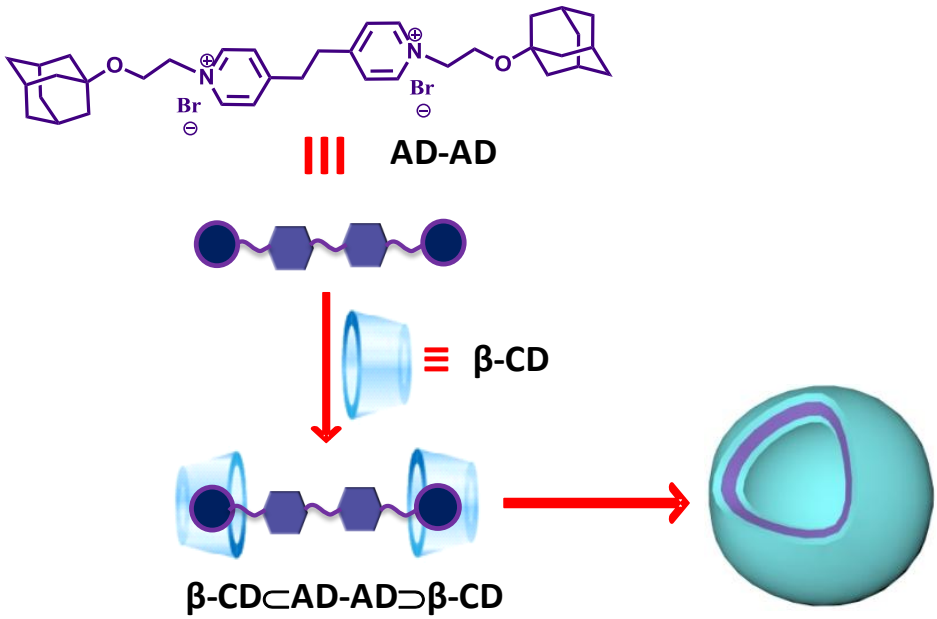

Scheme 2.1. Graphical illustration of chemical structure of AD-AD and its host-guest complexation induced self-assembly into vesicles.

2.3. Results and discussions

2.3.1. Synthesis and characterization of molecules

The chemical modification of adamantane is well documented in the literature.[14] We followed one of the procedures from literature with necessary modifications for the synthesis of AD-AD. The procedure adopted is shown in Scheme 2.2. 1-bromo adamantane (**1**) was used as the starting material which was refluxed with ethylene glycol as a reagent as well as solvent for 12 h in the presence of triethylamine as an acid

scavenger. The compound **2** was obtained as brown liquid in nearly 100% yield which was brominated by using Appel's reaction. The bromo derivative (**3**) was refluxed with 0.5 equivalent of commercially available compound 1,4-bis(4-pyridyl)ethane (**4**) in dry acetonitrile to get the final compound AD-AD (**5**) in 43% yield. The hydrophilicity of the final compound was effectively used for its purification by washing with organic solvent (Acetonitrile). All the intermediates and final molecule were extensively characterized by ^{1}H NMR, ^{13}C NMR, HRMS and FTIR techniques for their purity. The chemical structures of intermediates, final molecule and the equations of chemical reactions are given in Scheme 2.2.

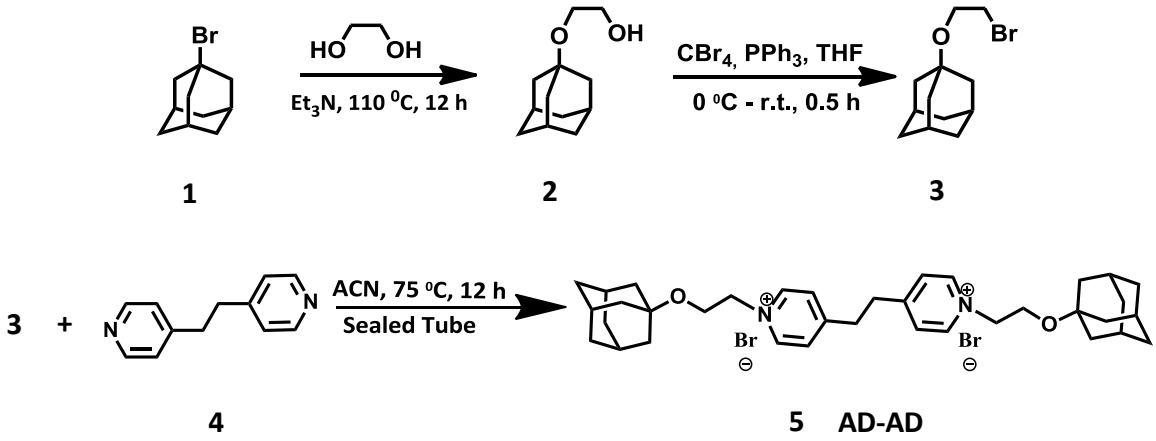

Scheme 2.2. Scheme for the synthesis of AD-AD.

2.3.2. Host-guest complexation studies

The ditopic molecule AD-AD was found to be highly soluble in the aqueous medium and solutions up to 20 × 10^{-2} M could be easily prepared without any precipitation. We have observed that when two equivalents of β-CD were reacted with AD-AD, it formed a stable host-guest complex in the aqueous medium in which both the adamantanes of AD-AD were capped by β-CD as shown in Scheme 2.1. This process was studied by ITC titration, NMR titration and 2D-rotating-frame overhauser effect spectroscopy (ROESY) NMR techniques. The details are given in the following sections.

2.3.2.1. Isothermal titration calorimetry studies

ITC is the modern technique for the direct measurement of binding stoichiometry *n*, the binding constant K_a, and the thermodynamic parameters ΔH, ΔS and ΔG for the host-guest interactions.[15] Basically the instrument has two cells namely sample and reference cells and the instrument measures the amount of power (μcal/s) required to maintain a constant temperature difference between the two cells. Instrument is provided with a syringe by which the titrant is added in a stepwise manner to the aliquot taken in the sample cell with stirring. Each addition will change the sample temperature depending on whether the reaction between the two is endothermic or exothermic. Accordingly the feedback system either raises or lowers the thermal power applied to compensate the same temperature between sample and reference cell which will be measured and converted to thermodynamic parameters.

Figure 2.4 shows the ITC titration curve for the β-CD/AD-AD interaction. The experiment was carried out by taking β-CD (2 mM, 200 μL) in the cell and AD-AD (10 mM, 40 μL) in the syringe. AD-AD was added from the syringe (2 μL at a time, 20 additions) to the solution taken in the cell. We presume that each addition of AD-AD to cell containing β-CD will result in the formation of host-guest complex in the cell. The host-guest complexation will generally be an exothermic process and the heat released during the reaction is monitored carefully. We observed that the titration curve became saturated and no further heat was released after 11 additions of AD-AD which suggested that no free β-CD is available in the cell. Nevertheless the addition of AD-AD was continued further to ensure the utilization of all the β-CD molecules for complexation. The experiment resulted in a sigmoidal curve which was fitted and analyzed using origin 7.0 software provided along with the instrument. The fitting gave values of $K_a = 6.4 \times 10^4$

M^{-1}, ΔH = -8.19 × 10^4 J mol^{-1} and ΔS = -178 J mol^{-1} deg^{-1} and n = 0.45. Interestingly, when the titration was carried out with AD-AD in the cell and β-CD in the syringe, value of n obtained was close to 2. These two trials suggested that AD-AD interacts with two β-CD molecules.

In an earlier study we reported K_a = 6.09 × 10^4 M^{-1}, ΔH = -3.47 × 10^4 J mol^{-1} and ΔS = -22.9 J mol^{-1} deg^{-1} and n = 1.0 for a similar system with only one adamantane unit.[14] Comparing the two, we see that when the number of adamantane moieties increased to two, -ΔH is more than doubled as expected which suggested that both adamantane units in AD-AD are included in the β -CD cavity as shown in β-CD⊂AD-AD⊃β-CD (Scheme 2.1). But there is a several fold increase in the –ΔS value (large decrease in the entropy of the system), which suggested that there is an additional ordering of the host-guest complex β-CD⊂AD-AD⊃β-CD formed. A minor contribution for the decrease in the entropy comes from the release of high energy water molecules from the cavity of CD upon guest complexation. Once the water molecules come out from the cavity, they can form regular hydrogen bonded structure with bulk water which is not possible for those water molecules inside the cavity.

It is known that dilution of solution can be either exothermic or endothermic process.[15] As the concentrations of the two components used in the ITC experiment above are not the same, control experiments were carried out to identify the effect of dilution on ITC data obtained. In a typical experiment, water in the cell was titrated against either β-CD or AD-AD taken in the syringe. It was found that the heat released during dilution is negligible when compared to heat released during host-guest complexation process.

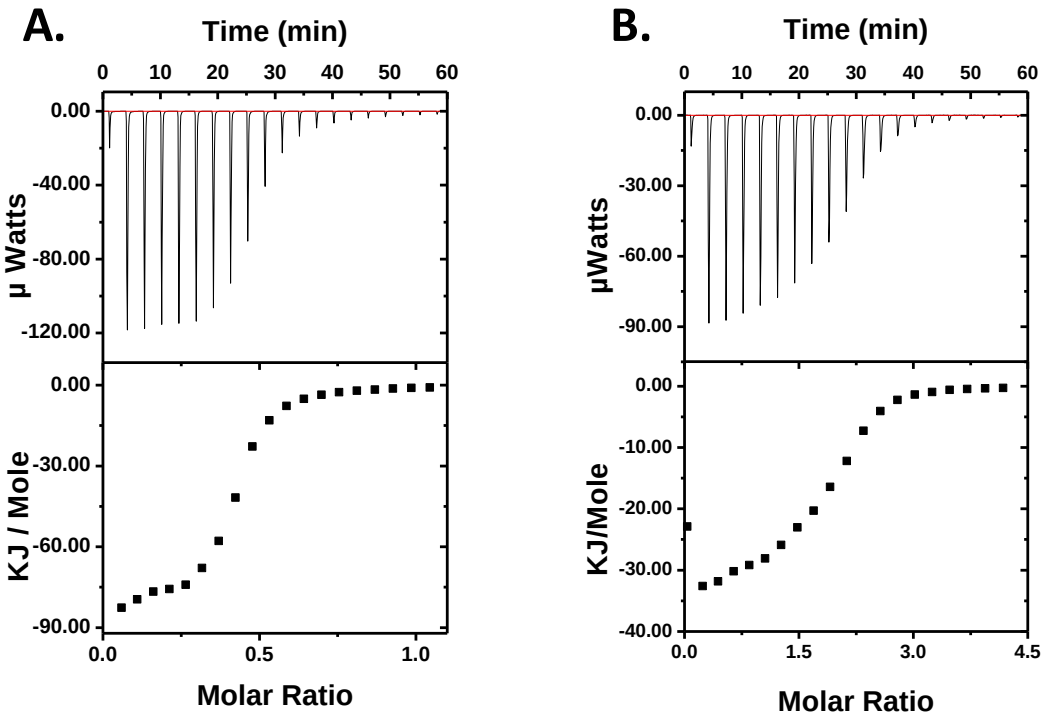

Figure 2.4. The ITC curve for titration of (A) AD-AD (10 mM) in syringe with β-CD (2 mM) in the cell. (B) AD-AD (1mM) in the cell with β-CD (10 mM) in the syringe.

2.3.2.2. 2D-ROESY NMR studies

In order to gain a deeper understanding of the structure of the bis-inclusion complex β-CD⊂AD-AD⊃β-CD complex and to confirm that the complex formation involves the inclusion of adamantane moiety into the β-CD cavity, 2D-NMR experiments were carried out. Nuclear overhauser effect (NOE) is the conventional method to confirm that the two sets of protons under study are very close to each other and to estimate the distance between them. In this method nuclear spin polarization is transferred from one set of protons to the other set of nearby protons via cross-relaxation. This transfer process occurs through space and not through bonds, hence the three dimensional arrangement of molecule could be derived from this technique. But for those molecules with higher molecular mass (above 1k Dalton), this technique generally fails.[16] In these cases advanced 2D experiments such as ROESY is found to be very useful. The spin transfer

process takes place only if the distance between the protons falls within ~4 Å units. As a result of this, ROESY can be used to locate the guest inside the host cavity and there are several such reports available in the literature. Hence we found this method could confirm the presence of adamantane moiety inside the cavity of β-CD.

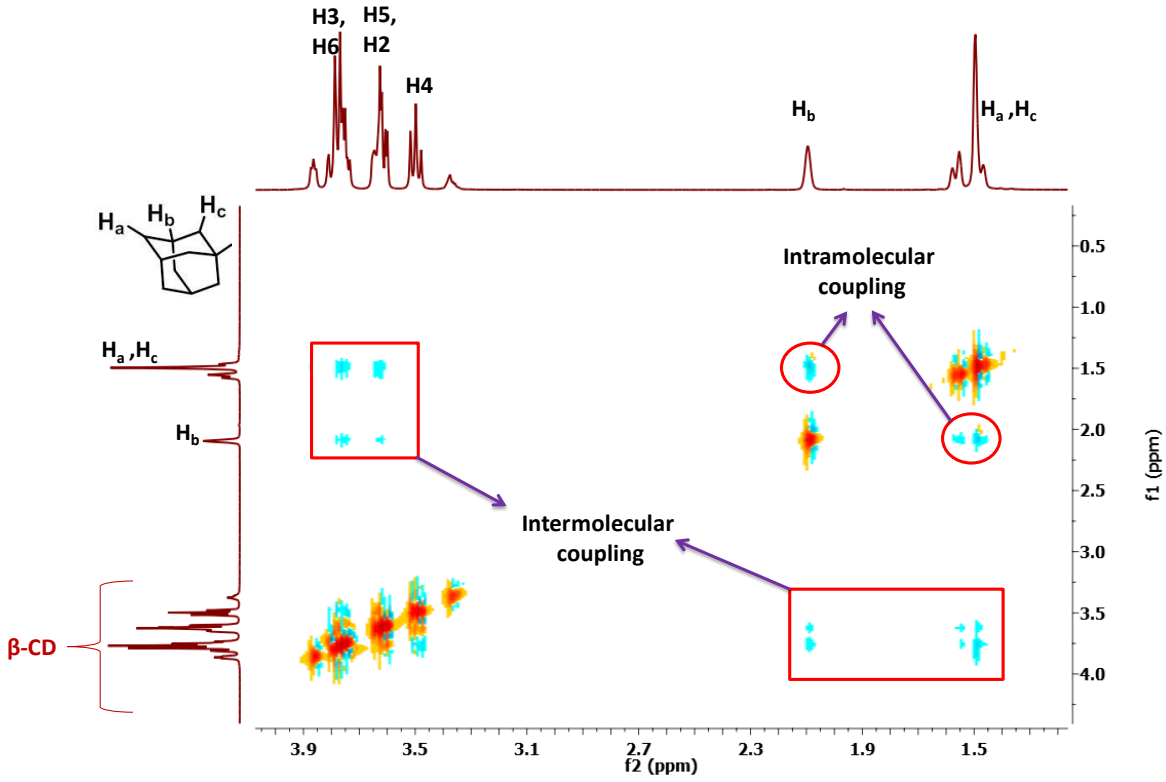

Figure 2.5. The selected area ROESY spectrum of AD-AD/β-CD supramolecular complex showing host-guest interaction.

Figure 2.5 shows the selected region 2D-ROESY spectrum of AD-AD/β-CD (1:2) system. In this figure the cross peaks are marked with box and circle highlighted in red. Also the protons of β-CD are indicated by numerical and protons of adamantane are identified by alphabets as suffixes with H. In the uncomplexed state adamantane exhibits three clear ^{1}H NMR signals for H_a, H_b and H_c protons. But upon inclusion into β-CD cavity, the signals due to H_a and H_c protons will merge to give a multiplet with downfield shift (vide infra). We observed clear cross peaks between adamantane H_a, H_b and H_c protons with H-3 and H-5 protons of β-CD (marked in rectangles). As explained in

Chapter 1, the H-3 and H-5 protons of β-CD are projecting towards the interior of the cavity and the cross peaks arise because of spatial interaction between these CD protons with adamantane protons. Hence we conclude that the adamantane moiety is inside the β-CD and the adamantane protons are close to (<4 Å units) H-3 and H-5 protons of β-CD.

The Figure 2.5 also shows two other cross peaks (marked in circles) which corresponds to the spatial interaction between H_a and H_b protons of adamantane group. Similar intramolecular cross peaks were also observed for aromatic protons. This intramolecular coupling arises because these two protons lie within a distance of 4 Å units in space.

2.3.2.3. ^{1}H NMR titration experiments

For the study of dynamic molecular process such as host-guest complexation, NMR titration is one of the most useful techniques available to chemists. In this technique, the chemical shift changes are measured as the concentration of one of the components changed. To use this technique, the guest (or host) should have at least one proton whose chemical shift value is different in the complexed state when compared to uncomplexed state. This difference in the magnitude of chemical shift value is useful for studying the structure of complexes and physical parameters such as association constant. In the present case ^{1}H NMR titration studies were carried out to confirm the formation of β-CD⊂AD-AD⊃β-CD where the adamantane group is expected to be inside the β-CD cavity.

Figure 2.6 shows the ^{1}H NMR spectra of AD-AD (10 mM) in the presence of varying amounts of β-CD, where the β-CD concentration changed from 0 – 2 equivalents with the lower panel showing the proton assignments of AD-AD. In Figure 2.6 the dotted vertical lines indicate the original peak positions and the change in peak positions is

indicated by arrow in the top panel. The 15 protons of mono-substituted adamantane derivatives gave three clear signals (H_a, H_b and H_c) in the ^{1}H NMR and they appeared in the δ1.4 – 2.0 ppm range. All these proton peaks shifted downfield in the presence of β-CD indicating encapsulation of the adamantyl moieties into the CD cavity. The change in the peak position upon complexation arises because of the change in the local environment of the adamantyl protons from hydrophilic medium to lipophilic medium within the CD cavity.

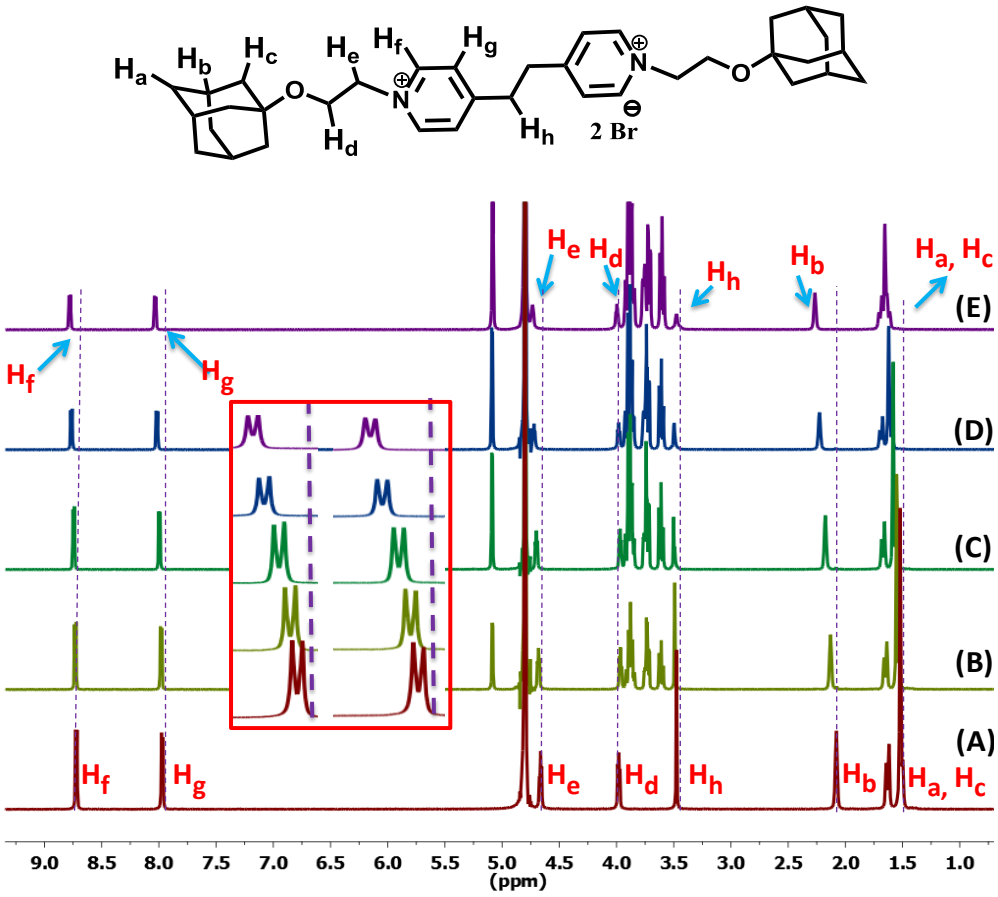

Figure 2.6. ^{1}H NMR titration spectra of AD-AD (10 mM) in the absence (A) and presence (B-E) of β-CD (0.5 – 2 eq.) in D_2O. The inset shows the shifts of H_f and H_g protons of AD-AD.

A careful observation of the titration spectrum revealed further details about additional interactions taking place in the medium along with host-guest complexation.

There was a constant downfield shift of almost all the protons of AD-AD upon increasing the β-CD concentration. The H_e protons of AD-AD shifted from δ4.66 ppm to δ4.74 ppm (Δδ=0.08 ppm) upon addition of two equivalents of β-CD. The H_d and H_h protons also showed similar shift to the downfield region with Δδ = 0.04 ppm. The inset in Figure 2.6 shows the gradual shift of aromatic protons (H_f and H_g) of 1, 2-bis(4-pyridy)ethane moiety in AD-AD upon increasing β-CD concentration. The H_f protons actually shifted from 8.72 ppm to 8.78 ppm (Δδ=0.06 ppm) and H_g protons showed a shift from 7.97 ppm to 8.04 ppm (Δδ=0.07 ppm) upon the addition of two equivalents of β-CD.

We calculated the molecular length of AD-AD by using its energy minimized structure and it is found to be around 5 nm while the cavity length of β-CD is reported to be 0.78 nm.[17] Hence the molecular dimensions of β-CD will not allow the inclusion of any other part of the AD-AD molecule other than adamantane group. Moreover, several β-CD molecules threading on AD-AD is not possible because the size of adamantane group is bigger compared to the diameter of narrow rim of β-CD. This stops the penetration of adamantane moiety near the narrow rim of β-CD. Also ITC experiment showed that AD-AD has only two binding sites with β-CD. Hence it could be easily proposed that 1,2-bis(4-pyridyl)ethane moiety of AD-AD cannot act as guest to complex with β-CD. In the absence of any of these interactions, by reviewing the literature we attribute the chemical shift changes observed for H_e, H_f, H_g and H_h protons in the β-CD/AD-AD system to the secondary interactions taking place in β-CD⊂AD-AD⊃β-CD along with host-guest complexation. In order to probe such secondary interactions we have subjected the β-CD complex of AD-AD to transmission electron microscope (TEM), atomic force microscope (AFM), scanning electron microscopy (SEM) and dynamic light scattering (DLS) studies.

2.3.3. Formation of supramolecular vesicles

^{1}H NMR studies confirmed the formation of β-CD⊂AD-AD⊃β-CD bis-inclusion complex by the host-guest recognition of β-CD and adamantane units. We observed that the bis-inclusion complex spontaneously self-assembled into supramolecular vesicles even in very dilute solution (10^{-5} M AD-AD). The vesicles, particularly those formed by secondary interactions find several applications in bio-medical field (Chapter 1). In the present case the formation of nano-structures were studied by different microscopic techniques and light scattering methods. The details of these experiments are given in the following sections.

2.3.3.1 High resolution transmission electron microscopy studies

Transmission electron microscopy (TEM) is a microscopy technique in which a beam of high energy electrons are transmitted through the specimen, similar to light used in an optical microscope. For taking the image of an object, there should be a correlation between wavelength of light used and dimensions of the object. When the size of the specimen is in the nano range, the normal light cannot be used because of this relationship. For small objects, the resolution of images taken in TEMs is significantly higher than optical microscopes because of the small wavelength of electrons. The interaction of matter in the specimen with electron beams generates an image of the object which can be viewed by a fluorescent screen or CCD camera.

Figure 2.7 shows the TEM images of the particles obtained upon drop casting an aqueous solution containing AD-AD (5×10^{-5} M) and β-CD (1×10^{-4} M). Spherical structures with diameters in the 70 – 500 nm range could be seen in the TEM. A distinguishable feature of each of these particles is a narrow dark particle skin and a central light region, which is typical for vesicle type structures.[6,18,19] The clear images of

vesicles could be obtained without using any staining agents, which are generally used for enhancing the contrast difference between vesicle skin and central space. The dark particle skin, which most probably corresponds to the vesicle membrane, had a thickness of 10 nm for a 250 nm sized particle. By using the energy minimized structure, we have estimated the approximate length of β-CD⊂AD-AD⊃β-CD complex and found to be about 5 nm. Hence the TEM studies suggest that the vesicle membrane is formed by bilayer assemblies of β-CD⊂AD-AD⊃β-CD complex. The TEM images also showed that the interiors of some of these particles contain dark objects which most probably are small aggregates of the inclusion complex which are captured inside the vesicles during their formation.

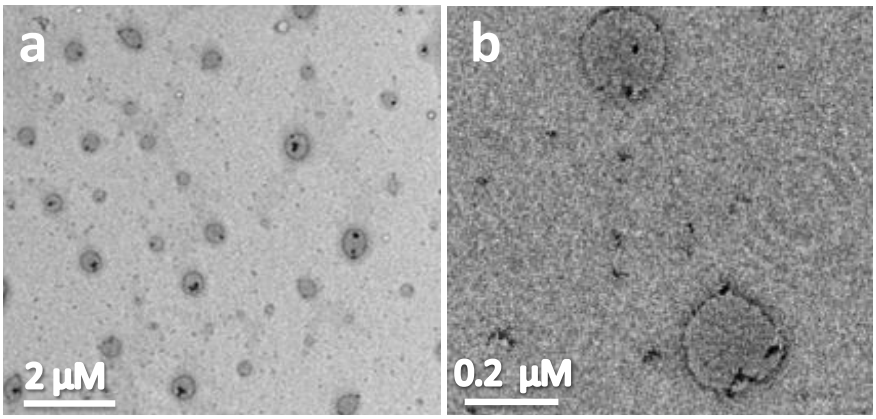

Figure 2.7. TEM images of supramolecular vesicles of β-CD (1×10^{-4} M) and AD-AD (5×10^{-5} M) in water.

2.3.3.2. Atomic force microscopy studies

AFM is a high resolution microscope discovered by Binnig, Quate, and Gerber in 1986 which is used regularly in determining the surface morphology of nanomaterials.[20,21] By using this technique the sample dimensions can be measured in all three axes resulting in the generation of a 3D image of the sample. The microscope contains a sharp piezoelectric tip (it is proposed that the end of tip contains only one atom) mounted on

low spring constant cantilever. The repulsive force (~10^{-9} N) between the atoms of tip and atoms of sample during scanning of the surface, deflects the cantilever (Hook's law) in the Z direction. This deflection in the cantilever is monitored by a sharp beam of laser which gives the height of the sample. The tip-sample interactions are finally processed to generate a 3D image of the surface. Important advantages of using this nanoscope are: (i) it does not require any vacuum environment for the operation (ii) non-conducting samples can be used and (iii) no special sample preparation skills are required. The quality of the image obtained is so high that the resolution of the images can go up to 0.1 nm in X-Y plane and 0.01 nm in Z direction which is atomic resolution. Recent advancements in AFM include measurement of the conductivity of nano-structures, surface roughness, phase images etc.[20]

We have used AFM for obtaining the three dimensional morphology of the vesicles along with their height. Figure 2.8a shows the AFM height image obtained by drop casting the AD-AD (1×10^{-4} M)/β-CD (2×10^{-4} M) solution on freshly cleaved mica surface. For better visualization of vesicles, AFM magnitude images were also taken in the same region (Figure 2.8b). Both the experiments revealed that the majority of vesicles are mono-disperse in nature with a narrow size distribution of 80 - 400 nm, which was in agreement to the data obtained by TEM. The height (Figure 2.8c) of the so formed vesicles also could be recorded which showed particle height ranging between 8 nm to 12 nm suggesting that these vesicles are sufficiently flattened on the mica surface.

It should be noted that the height of the vesicles obtained by AFM measurement is almost similar to the dimensions of the vesicle skin obtained by TEM experiment. While the width of vesicles obtained in the AFM experiment is comparable to that of vesicles measured in solutions, the experiment will not provide the actual height of the vesicles.[6] This is understandable because during drying of vesicles on mica surface, the thin

membrane of vesicle cannot support the spherical shape of vesicle. As a result of this the supramolecular framework will collapse onto the matrix. Hence it is proposed that the height measured for an ideal polymeric dried vesicle on uniform surface using AFM actually corresponds to thickness of the two collapsed walls.

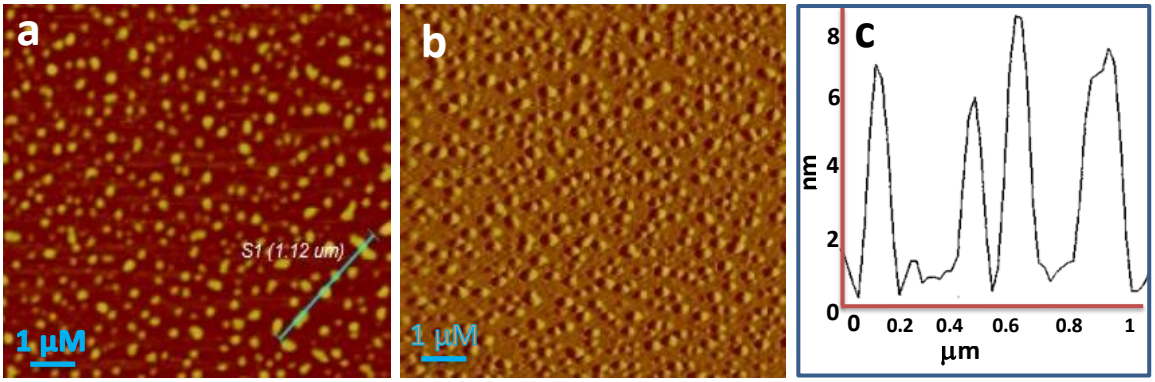

Figure 2.8. (a) AFM height and (b) magnitude images of AD-AD/β-CD vesicles. (c) The height profile of vesicles.

2.3.3.3. Scanning electron microscopy studies

SEM is a high resolution microscope used regularly for viewing the morphology of objects of dimensions in nano meter to micrometer range. Similar to TEM, this instrument also uses a high energy beam of electrons instead of normal light as used in the optical microscopes for imaging the objects. In TEM the electron beam is transmitted through the sample, but in SEM the electron beam is reflected from the surface of sample or secondary electrons are produced by the sample which is detected by a detector placed at 90° from source. Hence this technique gives clear morphology for conducting materials, electron rich samples such as ceramics etc. The sample is prepared on aluminium studs and on the sample thin layer of gold or silver is deposited for smooth conduction of electrons and to avoid the sample disturbance in high vacuum during imaging.

The vesicles formed by the self-assembly of β-CD⊂AD-AD⊃β-CD bis-inclusion complex were also characterized by SEM method. Figure 2.9 shows the SEM image obtained by casting an aqueous solution of β-CD (1×10^{-4} M)/AD-AD (5×10^{-5} M) system on aluminium stud. In the image, the spherical particles of mono-dispersive nature could be seen which were similar in dimensions to those obtained by TEM and AFM.

However it is reported that the SEM cannot be used to visualize the vesicle cavity,[6] hence it is difficult to differentiate between a particle and a vesicle. For viewing the cavity by SEM, ultrasonication or high vacuum has to be applied during sample preparation and this process induces holes by rupturing the vesicle walls.[22] We have applied high vacuum for the supramolecular vesicles during drying and the dried samples were examined under SEM. We were successful in obtaining SEM images of destroyed or opened particles (Figure 2.9b, c) which confirmed that the particles are vesicles possessing hollow interior cavities. Thus, SEM experiments confirmed formation of vesicles from the bis-inclusion complex.

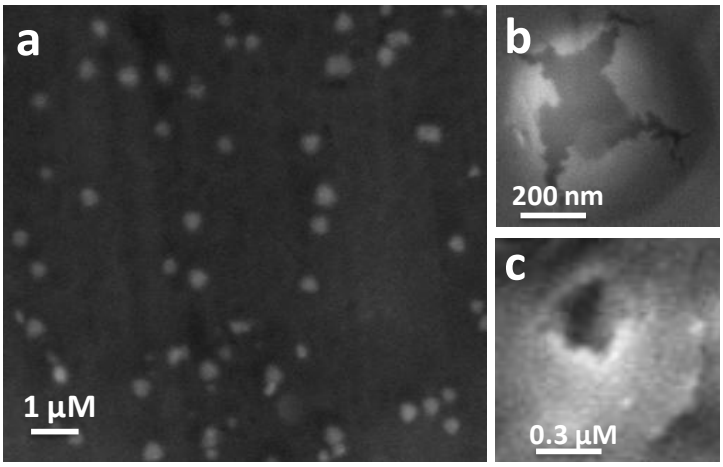

Figure 2.9. (a) The SEM image of β-CD⊂AD-AD⊃β-CD vesicles, (b, c) SEM images of opened up vesicles.

2.3.3.4. Light scattering experiments

The particles in solution will be under constant Brownian motion in random directions. According to Stokes-Einstein equation the diffusion coefficient of particles (measure of Brownian motion) in solution (D) is inversely related to the hydrodynamic radius (d) of particles [D α 1/d]. If the dimensions of particles are in micrometer or nanometers domain, the movements cannot be observed by naked eyes but could be detected by light scattering experiments, particularly by using Laser. Dynamic Light Scattering (DLS) is one such technique where in the light from a laser is passed through the sample cell containing sub-micron particles and the intensity of the light scattered by particles is measured by a detector, which is set at an angle of 90° from the laser.[23] This technique is widely used in the literature for obtaining the actual radius of particles in solution because the radius obtained by microscopic methods is that of dried particles which will be always less than wet particles. Mathematically radius is defined for spherical objects and hence DLS method could only be used for determining the radius of spherical particles. The microscopic experiments (TEM, SEM and AFM) revealed that the β-CD⊂AD-AD⊃β-CD vesicles are spherical in nature and thus we employed DLS technique for determining the hydrodynamic radius of vesicles.

The DLS profile of freshly prepared supramolecular vesicles of β-CD⊂AD-AD⊃β-CD is shown in Figure 2.10a. The study showed a narrow size distribution of 150 - 400 nm for the particles with an average hydrodynamic diameter corresponding to 256.7 nm. The data obtained was in close agreement with microscopic data obtained for vesicles prepared under similar conditions.

One of the oldest methods to confirm the presence of nano-aggregates in solution is by using Tyndall scattering. We have employed this technique for confirming the presence of nano particles in the solution. A narrow beam of laser was passed through

freshly prepared vesicle solution of β-CD/AD-AD which showed a clear path of light as it passed through the solution Figure (2.10b). The path of light could not be identified in pure β-CD or AD-AD solution (2.10c) which clearly confirmed the absence of such nano-aggregates in these solutions.

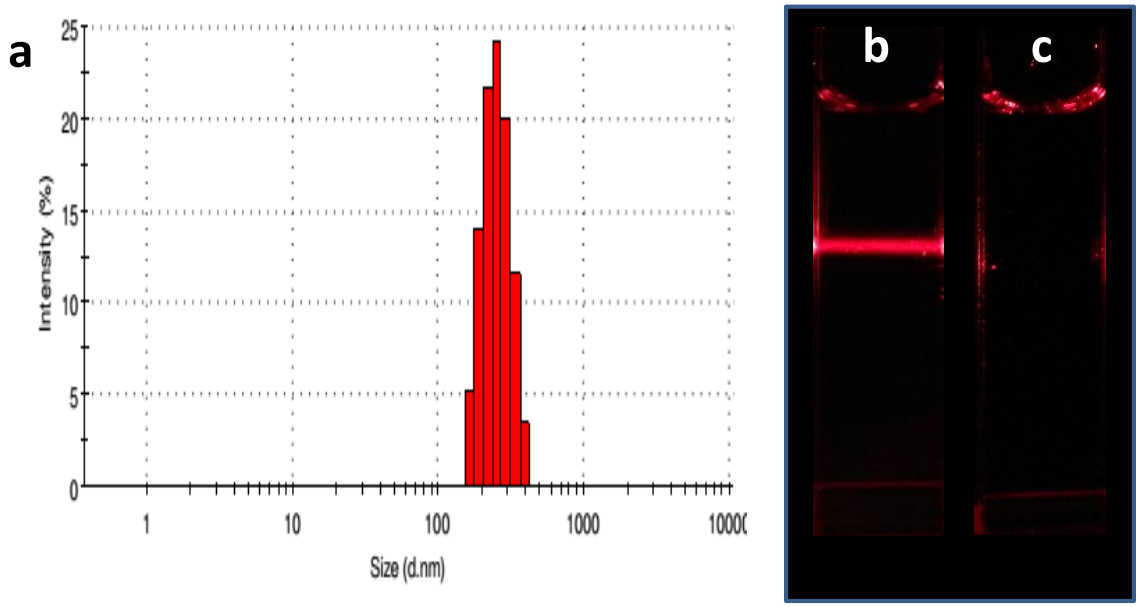

Figure 2.10. (a) DLS size distribution and (b) Tyndall effect in aqueous AD-AD (5×10^{-5} M)/β-CD (1×10^{-4} M) solution showing nano-aggregates and (c) absence of nano-particles in true solution of AD-AD.

2.3.4. Mechanism of vesicle formation

The TEM, SEM and AFM images obtained clearly showed that the β-CD/AD-AD bis-inclusion complex β-CD⊂AD-AD⊃β-CD self-assembled to form vesicles which was further supported by light scattering experiments. These vesicles are in fact stable for more than three weeks. Vesicle formation can occur only if the inclusion complex undergoes stacking as shown in Scheme 2.3. By using energy minimized structure, we have calculated the length of the bis-inclusion complex β-CD⊂AD-AD⊃β-CD and it was found to be ~5 nm. We propose that the bis-inclusion complex undergoes stacking one above the other which forms layered arrangement of β-CD⊂AD-AD⊃β-CD with width of

layer being ~5 nm. The diameter of wider rim of β-CD is reported to be 1.5 nm which is discussed in Chapter 1 of this thesis. Hence the minimum distance between two adjacent bis-inclusion complex units in the layered arrangement should be 1.5 nm as shown in Scheme 2.3. We have found from TEM studies that the vesicles have average membrane thickness of 10 nm which suggested that the vesicles are formed by bilayer assemblies of the inclusion complex as shown in Scheme 2.3. The two layers may be held together by hydrogen bonding interactions involving the hydroxyl groups at the narrow rims of the β-CD.[24] The seven hydroxyl groups in the primary rim of β-CD are not involved in any intramolecular hydrogen bonding as observed in the case of hydroxyl groups of secondary rim. Hence these hydroxyl groups can be engaged in interlayer hydrogen bonding and stabilize the bilayer structure. In order to achieve further stability in the system, the bilayer structure can fold to form vesicles with empty interior cavity.

Formation of vesicles from native or functionalized CD inclusion complexes have been reported by several groups and some of them are described in Chapter 1. For example, Tao *et al.* have reported inclusion complex formation between adamantane functionalized long chain alkane and polyglycerol-grafted β-CD and self-assembly of the inclusion complex into vesicles.[25] Zhang *et al*. reported bis-inclusion complex formation between *N,N'*-bis(ferrocenylmethylene)diaminohexane and native β-CD to give a supramolecular bola-amphiphile, which underwent self-assembly into vesicles.[26] In all these cases one can identify the inclusion complex as a 'supramolecular amphiphile' or 'supramolecular bola-amphiphile', with the CD acting as the hydrophilic head group and the alkyl or aryl residue acting as the hydrophobic tail or hydrophobic core.

In the present case under investigation, the AD-AD molecule is water soluble even though adamantyl group is hydrophobic and its hydrophilicity can be attributed to

the presence of two positive charges in the central 1, 2-bis(4-pyridinium)ethane core. In the presence of β-CD, the supramolecular complex β-CD⊂AD-AD⊃β-CD is formed in which the adamantane moieties are deeply inserted into the β-CD cavity and together they constitute the head group. Thus β-CD masks the hydrophobicity of adamantane group and the head group is hydrophilic in β-CD⊂AD-AD⊃β-CD. Upon reaction with β-CD the hydrophilicity of AD-AD should remain same if not increased and hence β-CD⊂AD-AD⊃β-CD is not a bola-amphiphile in the conventional sense. The core unit is water soluble and in fact the whole supramolecular complex is hydrophilic. In the complex, the +ve charges on the pyridinium nitrogens of adjacent layers are expected to repel each other and the inclusion complex β-CD⊂AD-AD⊃β-CD was not expected to stack one over the other as shown in Scheme 2.3.

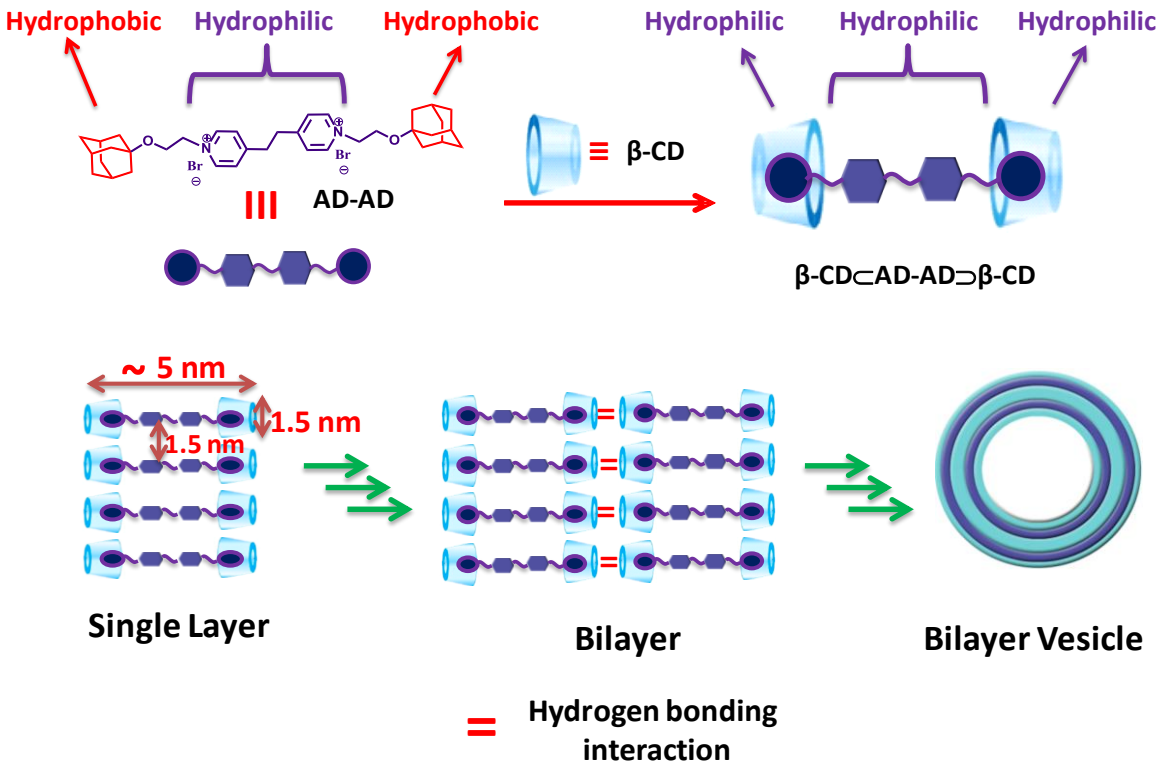

Scheme 2.3. Schematic representation of hydrophilicity of β-CD⊂AD-AD⊃β-CD bis-inclusion complex and its stacking to get bilayer vesicles.

The fact that stacking occurs and vesicles are formed suggests that the repulsive forces do not play a dominant role here and that the core unit is sufficiently hydrophobic to drive the self-assembly process. The outer diameter of β-CD is 1.53 nm and geometrical requirements suggest that the core units in successive layers (Scheme 2.3) are also separated at least by the same distance. Thus the distance between adjacent pyridinium moieties is sufficiently large and hence the repulsive forces could be very weak.[27,28] A few water molecules can also be present near the charged sites leading to screening of the repulsive interactions. Alternatively, the positive pyridinium ions and counter bromide ions may form tight ion pairs, which also can eliminate repulsion between successive layers.

2.3.5. Disassembly of the vesicular structures

Most of the applications of vesicles reported in the literature are focused on mimicking cells, encapsulation and drug delivery. For use in these applications, the study of responsiveness of vesicles to chemical, temperature, pH, ionic strength etc. is an important research area because it can change morphology, size and shape and also can release the active materials loaded into the cavity of vesicles. The different external stimuli applied for this purpose are pH, temperature, light, chemicals etc. For all types of stimuli except chemical responsiveness, the stimuli-responsive group must be the part of the vesicle structure (for example azobenzene unit for light responsive vesicles). But for chemical responsive vesicles, an extra component is added externally to the vesicle solution which brings about the disassembly.

In the present case, the formation of vesicles from AD-AD/β-CD mixture has its origin in the inclusion binding of adamantane moiety of AD-AD in β-CD cavities. A widely used competitive guest in the literature to displace adamantane moiety from the

cavity of β-CD is adamantane carboxylate (ADC). This is because ADC has very high β-CD binding constant of 2.9×10^5 / M[29, 30] , while we observed K_a for the binding of adamantane moiety of AD-AD as 6.4×10^4 M^{-1} by ITC experiment. The high association constant of ADC with β-CD is due to the better penetration ability of ADC into the β-CD cavity with the carboxylate group entering through wider rim and protruding out from the smaller rim. Thus in the case ADC⊃β-CD complex, the cavity of β-CD is completely occupied while the adamantane inclusion leaves considerable space in the CD cavity.We used this difference in the mode of inclusion and higher value of K_a (for ADC) for the disassembly of β-CD⊂AD-AD⊃β-CD vesicles. We have followed the disassembly process of vesicles by the TEM and AFM. The images did not show the presence of vesicles but showed irregular structures formed by the disassembly of vesicles. The disassembly process was also followed by ^{1}H NMR titration method and the spectrum of this experiment is shown in Figure 2.11. In this figure, the lower panel (a) shows the assignment of ADC protons (H_1, H_2 and H_3) upon reaction with one equivalent of β-CD. The three signals for these protons appeared at δ 1.7, δ 1.87 and δ 2.04 ppm and were broadened indicating that ADC is inside the β-CD cavity. In Figure 2.11, the spectra (b) and (c) respectively show the assignment of AD-AD protons before and after complexation with β-CD. The change in peak position is indicated by arrow which shows that almost all the protons of AD-AD has shifted downfield region after reaction with β-CD. In section 2.3.2.3 we have explained this shift of H_a - H_c protons of AD-AD for the inclusion of adamantyl moiety of AD-AD into β-CD cavity to get β-CD⊂AD-AD⊃β-CD complex and shift in H_d - H_h protons of AD-AD for the stacking of β-CD⊂AD-AD⊃β-CD to get vesicles.

When we added ADC to vesicle solution, there was upfield shift of all the protons of AD-AD (panel d) to their original position as observed for uncomplexed AD-AD

(panel b). The upfield shift of adamantyl protons of AD-AD to their original chemical shift values as observed for AD-AD indicates that adamantyl moiety is no longer in the β-CD cavity. The pushing out of adamantyl group from cavity of β-CD will break the bis-inclusion complex which brings about disassembly of vesicles. The cavity of β-CD is now occupied by ADC which is proved by comparing the similar positions of ADC protons (H_1 - H_3) as shown in panel (a) and panel (d) in Figure 2.11. Thus the experiment confirmed that the competitive binder ADC pushes out the adamantane group of AD-AD from AD from β-CD cavity before forming inclusion complex with it which is the key process in the vesicle disassembly.

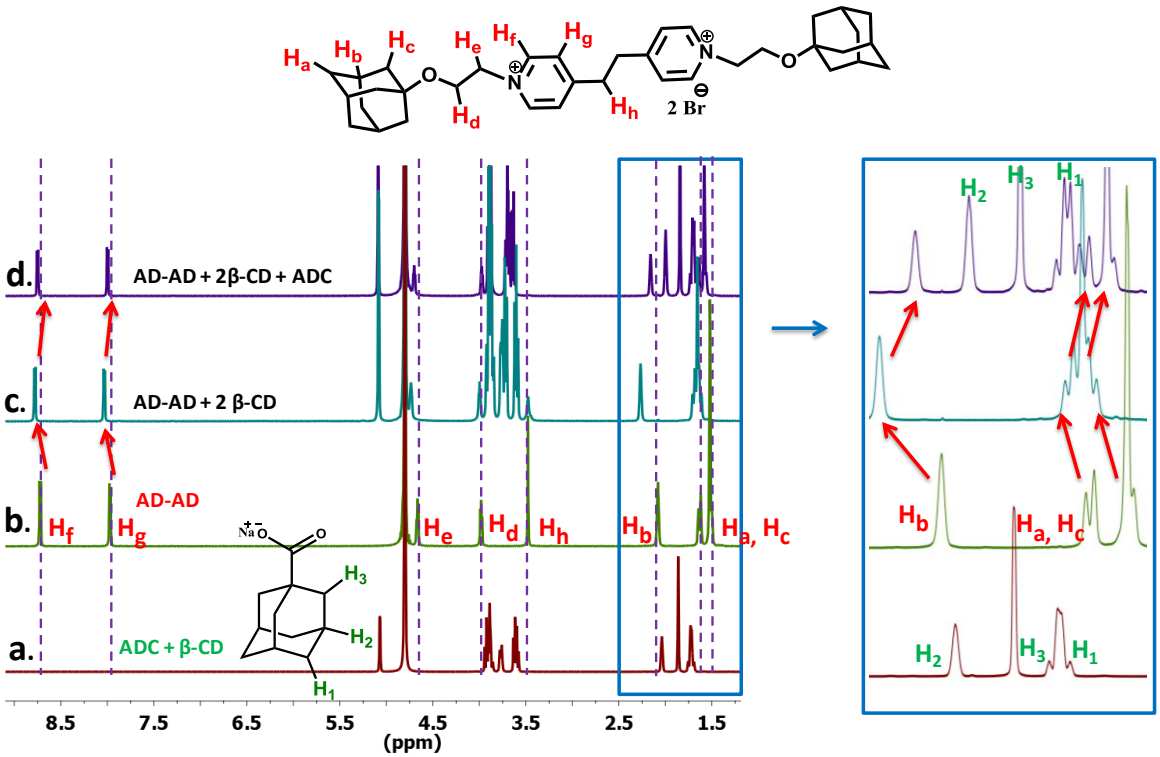

Figure 2.11. ^{1}H spectra of (a) ADC + β-CD, (b) AD-AD, (c) AD-AD/β-CD (2:1) vesicle and (d) spectrum after addition of ADC (2.25 eq.) to (c).

2.3.6. β-CD/AD-AD vesicles as drug carriers

Stimuli-responsive vesicles prepared from bio-compatible molecules such as CDs are promising anti-cancer drug delivery agents. The last few decades have witnessed

significant amount of work reported in this area. Stimuli-responsive slow disruption for the controlled release of drug is an essential requirement for a good drug delivery vehicle. For those delivery systems which are responsive only to externally added agents, the slow release can be controlled easily by varying the doses of external agents. Further, as they are not responsive to temperature, light, pH etc. the drug will not be released by these stimuli's and can remain in the body with loaded drug. Once the active material is transported to the desired location in the body, the doses of releasing agents can be administered into the body. This is the intelligent way of drug delivery because other stimuli such as temperature, pH, enzyme concentration etc. can vary irregularly for a patient. Finally, once the drug is completely released from the carrier, the remaining of the disassembled vesicles could be easily excreted out from the body. Hence the use of CDs for the vesicle preparation is a great choice because of their nontoxic nature and biodegradability.[31]

The fact that β-CD/AD-AD vesicles can be disrupted by ADC suggested that these vesicles may have potential applications as drug carriers. In order to see if the β-CD/AD-AD vesicles can actually carry drug molecules, we have attempted to load the anti-cancer drug Dox into these vesicles. In a typical experiment, Dox hydrochloride solution (1×10^{-3} M) was mixed with the vesicle solution (1×10^{-3} M of β-CD and 5×10^{-4} M of AD-AD) and kept aside overnight followed by dialysis to remove the uncomplexed Dox. The Dox has bright luminescence in the 500 nm to 700 nm region and hence we choose Confocal Laser Scanning Microscope (CLSM) to confirm the drug loading. The CLSM is an optical imaging technique useful for viewing objects in the micrometer range by utilizing the light emitted by the fluorescent objects. This microscope is routinely used in Biology for localizing the drug or imaging agents inside living cells. The CLSM images of the Dox-loaded vesicles are shown in Figure 2.12. The

bright red luminescence due to Dox inside the vesicles can be clearly seen in Figure 2.12c, which confirms that these vesicles are loaded with Dox.

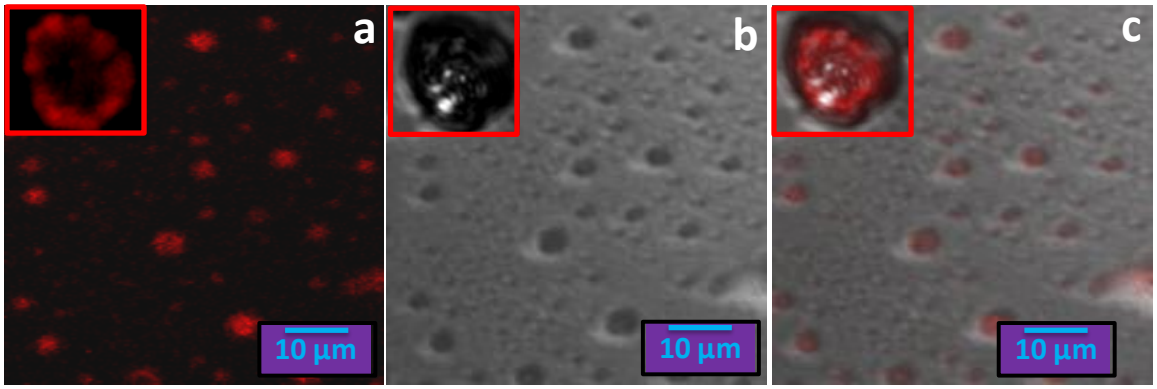

Figure 2.12. (a) Confocal laser scanning microscope, (b) transmission, and (c) merged images of Dox-loaded β-CD/AD-AD vesicles. Insets show enlarged image of a Dox-loaded vesicle.

Figure 2.13 shows the absorption spectra of free Dox and Dox inside the vesicles. We observed negligible change in the spectroscopic characteristics of Dox after its loading into vesicles which indicates no strong binding of Dox with vesicles. Instead the drug is trapped in the cavity of vesicles.

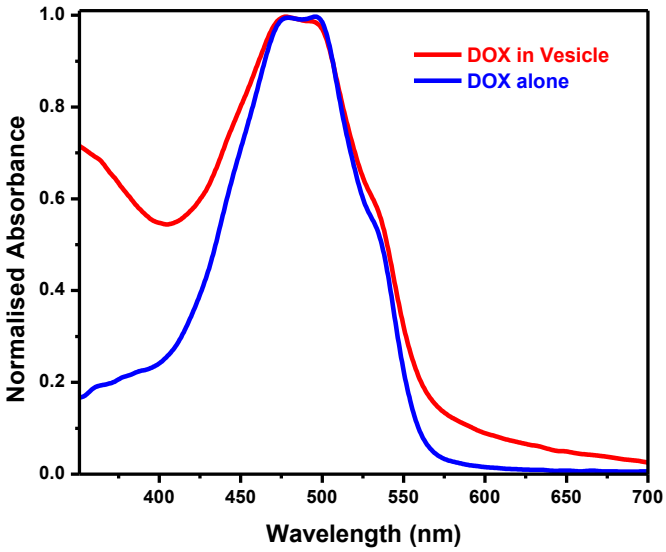

Figure 2.13. The absorption spectra of free Dox and Dox inside vesicles.

The concentration of encapsulated Dox was determined using molar extinction coefficient (**ε**) of Dox at 480 nm (11,500 cm^{-1} M^{-1}).[4,32] From this data, we found the Dox loading efficiency of the vesicles to be 7.06%. This value compares very well with the reported 5.02% loading efficiency of pillar[6]arene based supramolecular vesicles.[32] Both the empty and Dox-loaded vesicles were found to be stable for at least 3 weeks which was confirmed by SEM and DLS studies.

We have shown that the vesicles can be disassembled by the addition of ADC. The same strategy was used for disassembling the Dox-loaded vesicles. We found that addition of ADC brings about the disruption of vesicles thereby releasing the loaded drug. For the release study, a solution of ADC (2.25 eq. of AD-AD) was added to the Dox-loaded vesicle and the solution was kept aside for 2 h.

The CLSM images of the solution drop cast on glass slide after addition of ADC are shown in Figure 2.14. In Figure 2.14, we can see that majority of vesicles are disrupted into irregular structures. The fluorescence of the dye is seen in most of the viewing area indicating that the fluorescent drug is released from vesicles because of rupturing of the vesicles.

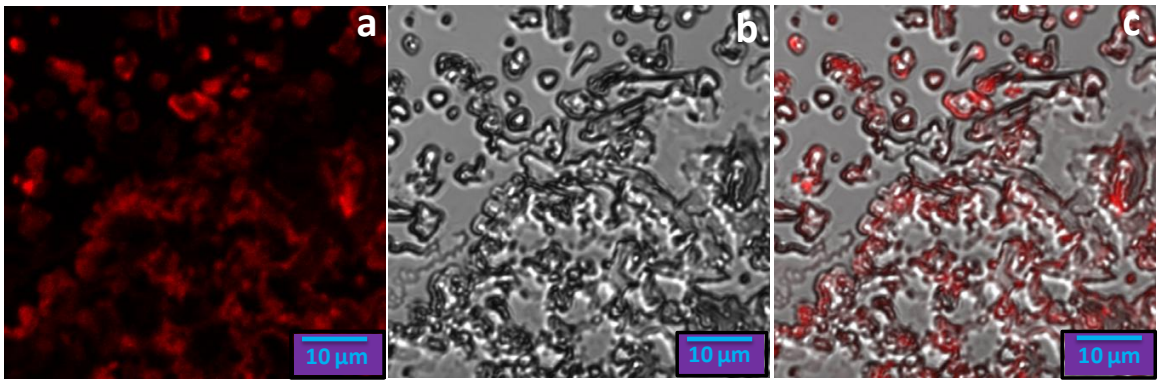

Figure 2.14. (a) Confocal laser scanning microscope, (b) transmission, and (c) merged images of β-CD/AD-AD vesicles upon addition ADC showing stimuli-responsive Dox release.

2.4. Conclusions

In this chapter we have studied the interactions of the novel molecule AD-AD with native β-CD in the aqueous solution which yielded a hydrophilic supramolecular complex. The supramolecular complex formed between β-CD and AD-AD is confirmed by ITC, ROESY and ^{1}H NMR titration studies. Further the β-CD/AD-AD bis-inclusion complex formed spontaneously self-assembled into vesicles which are stable for several weeks. Formation of the bis-inclusion complex and it's self-assembly into vesicular structures are proved by SEM, TEM, AFM and light scattering studies. It is important to note that in the present case the supramolecular complex is not expected to form vesicles as it is hydrophilic. Also we have shown that these vesicles can be loaded with the anti-cancer drug Dox. The loaded drug can also be released upon addition of the disassembling motif ADC showing that the vesicles have potential applications in bio-medical field as a drug carrier.

2.5. Experimental section

2.5.1. General methods

A. Instrumentation and sample preparation details: The electronic absorption spectra were recorded using Shimadzu 2401PC UV-VIS-NIR scanning spectrophotometer. ITC data were obtained using microcal iTC 200. The raw data obtained were fitted and analyzed using origin 7.0 software provided along with the instrument. All NMR data were recorded in D_2O purchased from Aldrich, using a 500 MHz Bruker Avance DPX spectrometer. High-resolution mass spectra were obtained by using a JOEL JMS600 mass spectrometer. AFM measurements were carried out using NTEGRA (NT-MDT) instrument using micro fabricated TiN cantilever tips (NSG-10) with a resonating

frequency of 299 kHz and a spring constant of 20-80 Nm^{-1} and multimode scanning probe microscope (Nanoscope IV controller, digital instruments), using tapping mode techniques. The samples for AFM were prepared by drop casting the solution on freshly cleaved mica surface and the excess solvent was evaporated. DLS analyses were carried out with a Zetasizer Nano S from Malvern Instruments and the measurements were performed after mixing and equilibrating the sample for 2 min. The average hydrodynamic radii were calculated from Stork-Einstein equation $Rh = kBT/6\pi\eta D$. TEM analyses were performed using a FEI-TECNAI T30 G^2S-TWIN, 300 kV HRTEM microscope with an accelerating voltage of 100 kV and the samples were prepared by drop casting the solution on a formvar coated copper grid (400 mesh) and evaporating excess solvent. The SEM images were recorded by using ZEISS EVO MA and LS series scanning electron microscope. The operating range was between 100 - 230 V at 50 - 60 Hz single phase with a consumption of 2.5 kVA. The sample solution in water was drop cast directly on to the top of the aluminium grid and the solvents were allowed to evaporate at ambient conditions. CLSM images were obtained on a Lecica-DMIR2 optical microscope by collecting the emission in the 550 - 610 nm regions at 20x magnification. Samples for CSLM were prepared by drop casting the vesicle solution on a glass slide followed by slow evaporation.

B. Procedure for preparation of vesicles: The compounds AD-AD and β- CD were taken in the 1:2 ratios in water. The solution was heated to ensure dissolution of both the compounds and allowed to cool to room temperature. The supramolecular complex formed spontaneously self-assembled into vesicles.

C. Procedure for loading and releasing of Dox into vesicles: Dox-loaded vesicles were prepared by mixing a solution of Dox hydrochloride (1 mM) with β-CD/AD-AD vesicle (5×10^{-4} M AD-AD and 1×10^{-3} β-CD). The solution was kept aside overnight and then

dialyzed in a dialysis membrane (MW cut off = 3500) to remove free Dox for 3 h using distilled water. For drug release study, ADC (2.25×10^{-3} M) was added to the above solution and kept aside for 2 h.

D. Calculation of Dox encapsulation efficiency of vesicles: The Dox encapsulation efficiency was calculated using following equation.

$$\text{Encapsulation efficiency (\%)} = \left(\frac{\text{Mass of Dox encapsulated in vesicles}}{\text{Mass of Dox added}} \right) \times 100 \qquad \textbf{(2.1)}$$

A known concentration (1 mM) of Dox solution was prepared and loaded into β-CD/AD-AD vesicles. After dialysis the absorption of Dox encapsulated vesicles was measured. By using this absorbance data and known **ε** of Dox, the mass of drug encapsulated into vesicles was calculated. By using these two mass values, the efficiency of Dox encapsulation was calculated using Equation 2.1.

2.5.2. Molecules and materials

β-CD and Doxorubicin were purchased from Aldrich and used as received. ADC was prepared by neutralizing 1-adamantane carboxylic acid with sodium carbonate taken in iso-propanol. The solvents and reagents were dried and purified by standard methods prior to use. The procedure for the synthesis of AD-AD is described below.

A) Synthesis of 2:

A solution of 1-bromoadamantane (**1**) (1.5 g, 6.972 mmol) and triethylamine (2.17 mL, (1.52g), 15.54 mmol) in ethylene glycol (30 mL) was heated at 110 °C for 12 h. The mixture was allowed to cool to room temperature, 50 mL of CH_2Cl_2 was added, and the solution was washed with 1 M HCl (3 × 20 mL) and water (2 × 20 mL). The organic layer was dried over Na_2SO_4, and the solvent was evaporated under reduced

pressure. **2** was obtained as a light yellow liquid. Yield 0.92 g (67%). ^{1}H NMR (500 MHz, $CDCl_3$) δ: 3.68 (t, 2 H), 3.52 (t, 2 H), 2.15 (br.s, 1 H), 1.96 (br.s, 3 H), 1.72 (br.s, 6 H), 1.57 (m, 6 H).^{13}C NMR (125 MHz, $CDCl_3$) δ: 74.59, 63.41, 61.95, 41.37, 36.23, 30.48.

B) Synthesis of 3:

Compound **2** (0.81 g, 4.15 mmol) and tetrabromomethane (1.72 g, 5.18 mmol) were dissolved in dry THF under inert atmosphere. Triphenylphosphine (1.35 g, 5.18 mmol) was added to this at 0 $^{\circ}$C and stirred at room temperature for 0.5 h. The reaction was quenched with a few drops of water, and was partitioned between CH_2Cl_2 (150 mL) and H_2O (100 mL). The organic layer was washed with water (3 × 50 mL) and brine (50 mL). The organic layer was dried over Na_2SO_4, and the solvent was evaporated under reduced pressure. The compound was purified by column chromatography over silica gel. Elution with chloroform gave compound **3** as a light brown liquid. Yield 0.77 g (72%). ^{1}H NMR (500 MHz, $CDCl_3$) δ: 3.71 (t, 2 H), 3.40 (t, 2 H), 1.94 (br.s, 3 H), 1.67 (br.s, 6 H), 1.57 (m, 6 H). ^{13}C NMR (125 MHz, $CDCl_3$) δ: 72.51, 60.14, 41.33, 36.27, 33.54, and 31.42.

C) Synthesis of AD-AD:

Compound **4** (0.050 g, 0.27 mmole) and compound **3** (0.140g, 0.54 mmole) were heated in dry acetonitrile (5ml) for 12 h in a sealed tube.The white precipitate formed was filtered and washed repeatedly with dry acetonitrile.Yield of the product: 0.063g (42.8 %). This reaction was repeated six times so as to get sufficient amount of AD-AD (~ 400 mg) which was used for all the studies. ^{1}H NMR (500 MHz, D_2O) δ: 8.60 (d, 4H), 7.8(d, 4H), 4.5(t, 4H), 3.8(t, 4H), 3.3(t, 4H) 1.95(s, 6H), 1.5(m, 6H) and 1.3(m,

18H). ^{13}C NMR (125 MHz, D_2O) δ:160.89, 144.29, 127.72, 74.89, 61.44, 58.80, 40.36, 35.36,34.06, 30.14.

ESI-HRMS: Mass calculated for $C_{36}H_{50}N_2O_{22}^+$ is 542.38 and mass obtained was 542.38.

2.6. References

(1) Siegel, R. L.; Miller, K. D.; Jemal, A.: Cancer statistics, 2016. *CA: A Cancer Journal for Clinicians* **2016**, *66*, 7.

(2) Tacar, O.; Sriamornsak, P.; Dass, C. R.: Doxorubicin: An update on anticancer molecular action, toxicity and novel drug delivery systems. *J. Pharm. Pharmacol.* **2013**, *65*, 157.

(3) Harrison, C.: Anticancer drugs: Double boost for doxorubicin therapy. *Nat. Rev. Drug Discov.* **2014**, *13*, 178.

(4) Sanson, C.; Schatz, C.; Le Meins, J. F.; Soum, A.; Thevenot, J.; Garanger, E.; Lecommandoux, S.: A simple method to achieve high doxorubicin loading in biodegradable polymersomes. *J. Control. Release* **2010**, *147*, 428.

(5) Ulbrich, K.; Holá, K.; Šubr, V.; Bakandritsos, A.; Tuček, J.; Zbořil, R.: Targeted drug delivery with polymers and magnetic nanoparticles: Covalent and noncovalent approaches, release control, and clinical studies. *Chem. Rev.* **2016**, *116*, 5338.

(6) Jiang, W.; Zhou, Y.; Yan, D.: Hyperbranched polymer vesicles: From self-assembly, characterization, mechanisms and properties to applications. *Chem. Soc. Rev.* **2015**, *44*, 3874.

(7) Tiwari, G.; Tiwari, R.; Sriwastawa, B.; Bhati, L.; Pandey, S.; Pandey, P.; Bannerjee, S. K.: Drug delivery systems: An updated review. *Int. Journal of Phar. Investigation* **2012**, *2*, 2.

(8) Zhang, Y.; Huang, Y.; Li, S.: Polymeric micelles: Nano-carriers for cancer-targeted drug delivery. *AAPS PharmSciTech* **2014**, *15*, 862.

(9) Li, J.; Mooney, D. J.: Designing hydrogels for controlled drug delivery. *Nature Rev. Materials* **2016**, *1*, 16071.

(10) Singh, R.; Lillard, J. W.: Nanoparticle-based targeted drug delivery. *Exp. Mol. Pathol.* **2009**, *86*, 215.

(11) Pianowski, Z. L.; Karcher, J.; Schneider, K.: Photoresponsive self-healing supramolecular hydrogels for light-induced release of DNA and doxorubicin. *Chem. Commun.* **2016**, *52*, 3143.

(12) Wang, K.; Guo, D. S.; Wang, X.; Liu, Y.: Multistimuli responsive supramolecular vesicles based on the recognition of p-sulfonatocalixarene and its controllable release of doxorubicin. *ACS Nano* **2011**, *5*, 2880.

(13) Carrazana, J.; Jover, A.; Meijide, F.; Soto, V. H.; Vazquez Tato, J.: Complexation of adamantyl compounds by β-cyclodextrin and monoaminoderivatives. *J. Phys. Chem. B* **2005**, *109*, 9719.

(14) Krishnan, R.; Gopidas, K. R.: β-cyclodextrin as an end-to-end connector. *J. Phys. Chem. Lett.* **2011**, *2*, 2094.

(15) Freyer, M. W.; Lewis, E. A.: Isothermal titration calorimetry: Experimental design, data analysis, and probing macromolecule/ligand binding and kinetic interactions. *Methods in cell biology*; Academic Press, **2008**; Vol. 84; pp 79.

(16) Krishnan, R.; Rakhi, A. M.; Gopidas, K. R.: Study of β-cyclodextrin–pyromellitic diimide complexation. Conformational analysis of binary and ternary complex structures by induced circular dichroism and 2D nmr spectroscopies. *J. Phys. Chem. C* **2012**, *116*, 25004.

(17) Szejtli, J.: Introduction and general overview of cyclodextrin chemistry. *Chem. Rev.* **1998**, *98*, 1743.

(18) Jürgen-Hinrich, F.; Tianyu, W.: Bolaamphiphiles. *Chem. Rev.* **2004**, *104*, 2901.

(19) Liu, Y.; Yu, C.; Jin, H.; Jiang, B.; Zhu, X.; Zhou, Y.; Lu, Z.; Yan, D.: A supramolecular janus hyperbranched polymer and its photoresponsive self-assembly of vesicles with narrow size distribution. *J. Am. Chem. Soc.* **2013**, *135*, 4765.

(20) Giessibl, F. J.: Advances in atomic force microscopy. *Reviews of Modern Physics* **2003**, *75*, 949.

(21) Jalili, N.; Laxminarayana, K.: A review of atomic force microscopy imaging systems: Application to molecular metrology and biological sciences. *Mechatronics* **2004**, *14*, 907.

(22) Xing, P.; Sun, T.; Hao, A.: Vesicles from supramolecular amphiphiles. *RSC Advances* **2013**, *3*, 24776.

(23) Ross Hallett, F.: Particle size analysis by dynamic light scattering. *Food Research Int.* **1994**, *27*, 195.

(24) Rekharsky, M. V.; Inoue, Y.: Complexation thermodynamics of cyclodextrins. *Chem. Rev.* **1998**, *98*, 1875.

(25) Tao, W.; Liu, Y.; Jiang, B.; Yu, S.; Huang, W.; Zhou, Y.; Yan, D.: A linear-hyperbranched supramolecular amphiphile and its self-assembly into vesicles with great ductility. *J. Am. Chem. Soc.* **2012**, *134*, 762.

(26) Zhang, H.; Shen, J.; Liu, Z.; Hao, A.; Bai, Y.; An, W.: Multi-responsive cyclodextrin vesicles assembled by 'supramolecular bola-amphiphiles'. *Supramol. Chem.* **2010**, *22*, 297.

(27) Ma, X.; Tian, H.: Stimuli-responsive supramolecular polymers in aqueous solution. *Acc. Chem. Res.* **2014**, *47*, 1971.

(28) Yang, H.; Ma, Z.; Wang, Z.; Zhang, X.: Fabricating covalently attached hyperbranched polymers by combining photochemistry with supramolecular polymerization. *Polymer Chemistry* **2014**, *5*, 1471.

(29) William C. Cromwell, K. B., and Maurice R. Eftink: Cyclodextrin-adamantanecarboxyiate inclusion complexes: Studies of the variation in cavity size. *J. Phys. Chem.* **1985**, *89*, 326.

(30) Falvey, P.; Lim, C. W.; Darcy, R.; Revermann, T.; Karst, U.; Giesbers, M.; Marcelis, A. T.; Lazar, A.; Coleman, A. W.; Reinhoudt, D. N.; Ravoo, B. J.: Bilayer vesicles of amphiphilic cyclodextrins: Host membranes that recognize guest molecules. *Chem. Eur. J.* **2005**, *11*, 1171.

(31) Crini, G.: Review: A history of cyclodextrins. *Chem. Rev.* **2014**, *114*, 10940.

(32) Cao, Y.; Hu, X. Y.; Li, Y.; Zou, X.; Xiong, S.; Lin, C.; Shen, Y. Z.; Wang, L.: Multistimuli-responsive supramolecular vesicles based on water-soluble pillar[6]arene and saint complexation for controllable drug release. *J. Am. Chem. Soc.* **2014**, *136*, 10762.

Chapter 3

Integrative Self-sorting in a Three Component System Leading to Formation of Long Fibrous Structures

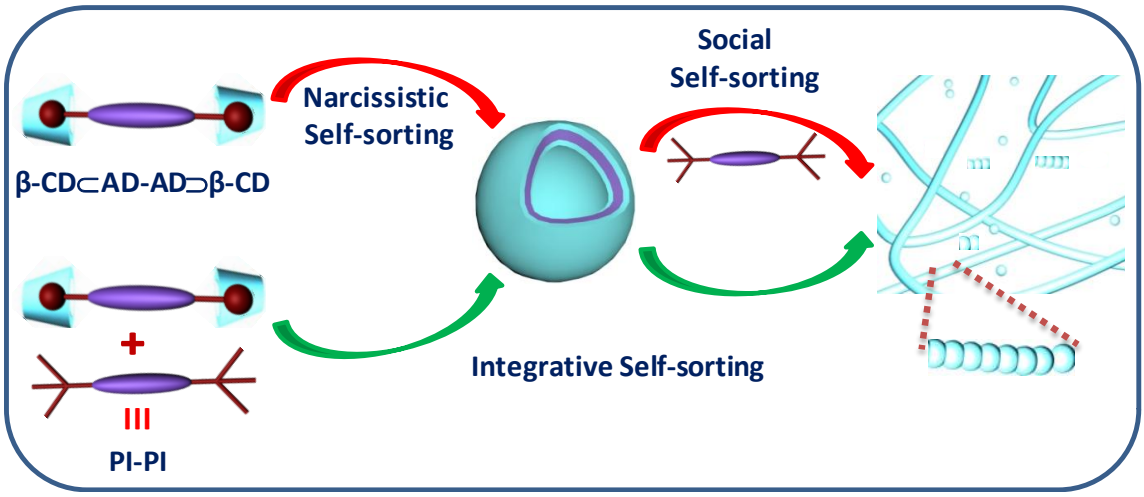

3.1. Abstract

In the present chapter, we report the integrative self-sorting processes in a three-component system consisting of β-CD, a bis-adamantane derivative of 1,4-bis(4-pyridyl)ethane (AD-AD) and a bis-pyromellitic diimide derivative of 1,4-bis(4-pyridyl)ethane (PI-PI) in a 2:1:1 ratio in an aqueous medium. The process actually led to the slow evolution of ultra-long supramolecular fibers wherein the intermediate stages during fiber formation could be observed. Using TEM, AFM and time-dependent ICD measurements of the three-component system and the constituent two-component systems (β-CD/AD-AD/PI-PI and β-CD/AD-AD), the involvement of two social self-sorting and two narcissistic self-sorting processes were identified. In a mixture consisting of three components, initially a bis-inclusion complex of β-CD and AD-AD is formed through a social self-sorting process. The bis-inclusion complex undergoes a narcissistic self-

assembly to give vesicles which were same to those described in Chapter 2. Vesicle formation is followed by rim-binding interaction which led to joining of the vesicles to give long fibrous structures. The rim-binding motif is effectively exploited herein to perform the functions of vesicle recognition and vesicle joining.

3.2. Introduction

Because of the hydrophobic cavity, almost all applications of CDs deal with the formation of host-guest complexes.[1] In almost all of such complexes, the guest will enter into the CD cavity through the wider rim even if the narrow rim is not substituted. In Chapter 1 of this, thesis we have discussed an anomalous behavior of certain *N*-alkyl pyromellitic diimides (PMDI) towards the β-CD cavity for complex formation which we named as 'rim-binding' association.[2,3] In this mode of binding, the PMDI core remains just outside of the smaller rim while the N-alkyl group enters the cavity through the smaller rim. After the detailed investigation, we concluded that the rim-binding is independent of the alkyl substituents with the *tert*-butyl derivative exhibiting the highest association constant. We have also established that the cavity of β-CD can simultaneously hold adamantane (AD) and *tert*-butyl PMDI moieties by inclusion and rim-binding modes of association, respectively, to give ternary complexes. Using these modes of interactions, we could assemble a donor-acceptor system for PET reaction, where a β-CD assembled the donor by inclusion binding and acceptor by rim-binding. We also designed a ditopic molecule with PMDI at one end and AD moiety at the other which in the presence of β-CD formed long fibers through iterative inclusion and rim-binding interactions.[4]

In Chapter 2 of this thesis we reported the preparation and characterization of the supramolecular bis-inclusion complex β-CD⊂AD-AD⊃β-CD. The β-CD⊂AD-AD⊃β-CD bis-inclusion complex underwent spontaneous self-assembly to give stable bilayer

vesicles having diameters in the range 70-500 nm.[5] The outer surface of these vesicles is made up of the narrow rim of β-CD containing the seven primary hydroxyl groups. Previous studies from our laboratory had established that the narrow rims could bind to PMDI derivatives in the rim-binding mode. Since the outside of the β-CD⊂AD-AD⊃β-CD vesicles are loaded with the primary faces of β-CD, the vesicle surface can, in principle, provide large numbers of rim-binding sites for PMDI derivatives. In other words, the outer surface of the vesicles can recognize PMDI moieties and undergo rim-binding with them as shown in Scheme 3.1. Using the same reasoning one can argue that ditopic molecule containing PMDI moieties at both ends can undergo rim-binding interactions with two β-CD⊂AD-AD⊃β-CD supramolecular vesicles simultaneously as shown in Scheme 3.1. If a ditopic molecule can interact with two vesicles as shown in Scheme 3.1, these interactions will bring the two vesicles closer and ultimately lead to fusion of the vesicles. Thus, the rim-binding interactions illustrated in Scheme 3.1, in principle, can be exploited to perform the functions of vesicle recognition, adhesion and fusion leading to formation of larger structures. In this chapter we report our studies in this direction.

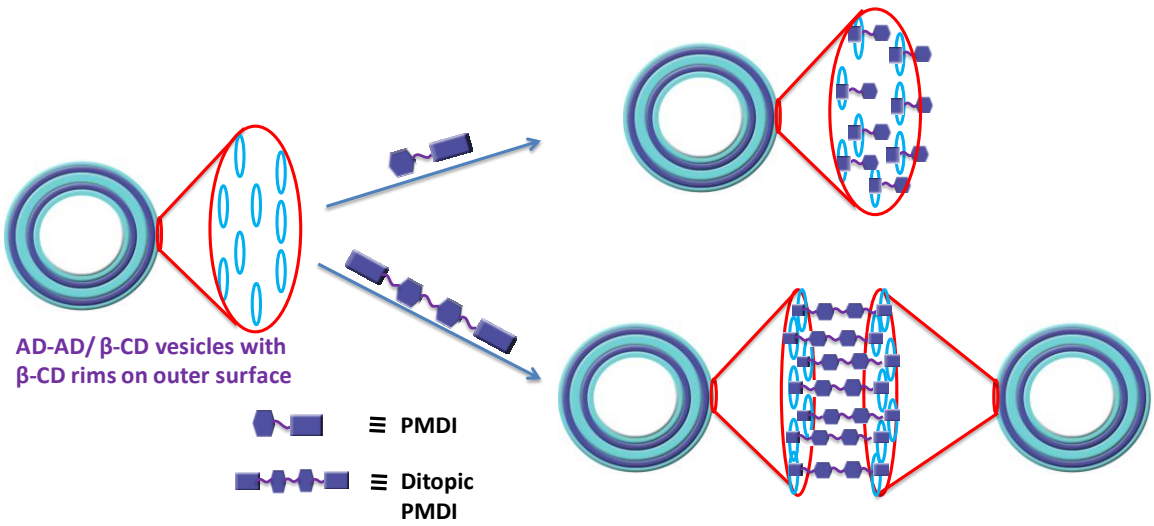

Scheme 3.1. Schematic of vesicle surface recognition by mono- and ditopic PMDI.

In order to see if Scheme 3.1 is a practical proposition we used PMDI derivatives PI and PI-PI and the AD derivative AD-AD and interactions of these molecules with β-CD were investigated. Synthesis and characterization of AD-AD and its interaction with β-CD leading to the formation of β-CD⊂AD-AD⊃β-CD vesicles are discussed in Chapter 2 of the thesis. These processes are schematically shown in Scheme 3.2(1). In earlier papers from our laboratory, we have reported the synthesis and characterization of PI.[3] We have shown that PI can undergo rim-binding interaction with β-CD to give β-CD≻PI as shown in Scheme 3.2 (2). PI can also undergo rim-binding with AD/β-CD inclusion complexes to form ternary complexes.[3] Synthesis and characterization of the ditopic molecule PI-PI is described in this chapter. Based on previous studies we expect PI-PI to interact with two β-CD molecules in the rim-binding mode to give the bis-rim-binding complex β-CD≻PI-PI≺β-CD shown in Scheme 3.2(3). We have studied the PI-PI/β-CD interaction using different techniques and the results are reported herein. In a solution containing β-CD, AD-AD and PI-PI, ternary complex AD-AD⊃β-CD≻PI-PI shown in Scheme 3.2(4) can also form through co-operative inclusion and rim-binding interactions. If these interactions occur in an iterative manner long fibers would result.

Thus, in an aqueous solution containing AD-AD, PI-PI and β-CD in a 1:1:2 ratio, one cannot apriori predict the structure of the final product, as the product formation would be governed by the strengths of the various interactions described in Scheme 3.2 and the preference for any sorting processes that may occur in the system. Upon mixing AD-AD, PI-PI and β-CD (1:1:2) in an aqueous medium, we actually observed slow evolution of long fibers in the system during a three-day period. Mechanistic investigations of the evolution of the fibrous structures are presented herein. We also report that these fiber-like structures can be disassembled readily into smaller fragments

upon addition of the competitive β-CD binder such as adamantane carboxylate (ADC), which confirms the non-covalent nature of the assembly.

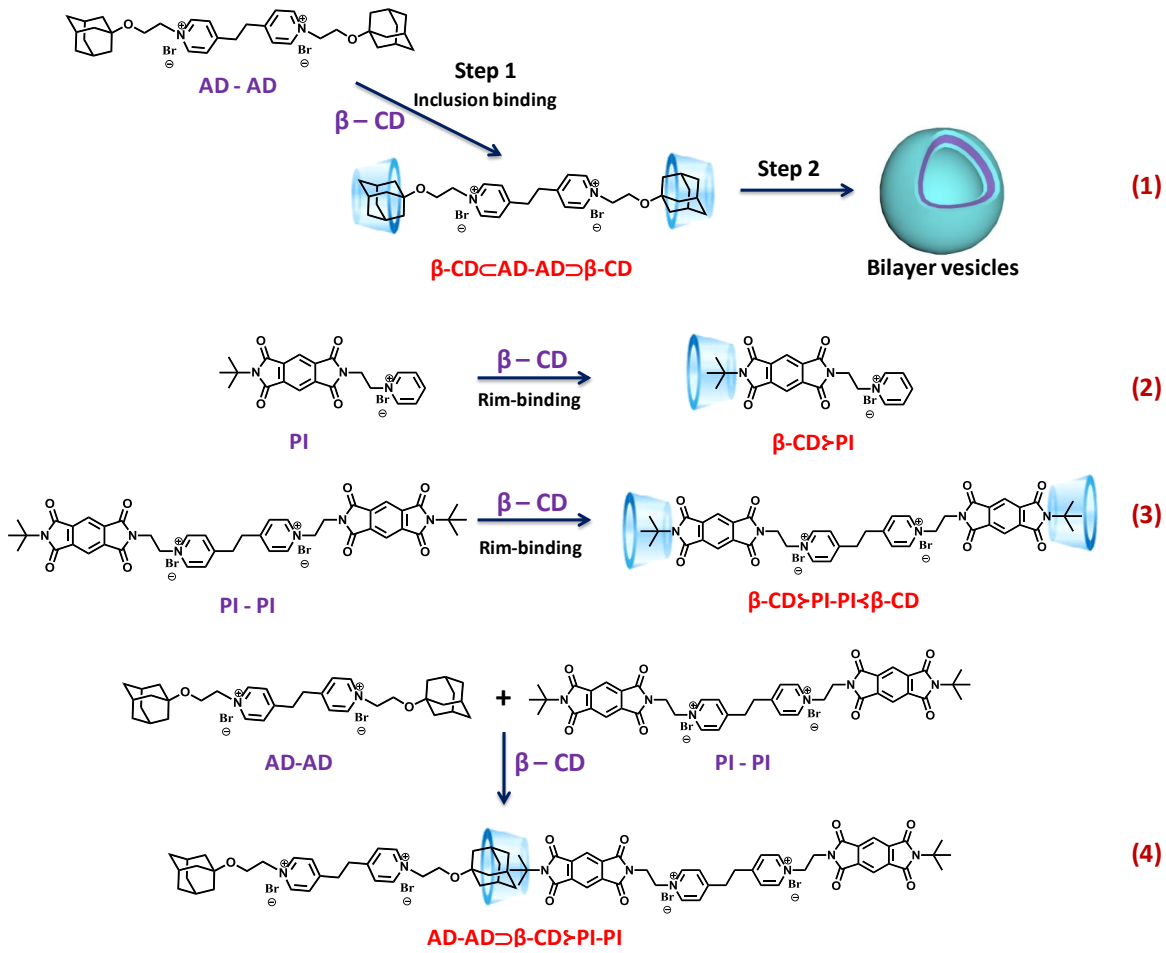

Scheme 3. 2. Structures of PI, PI-PI, AD-AD and their β-CD complexes used in this study.

3.3. Results and discussions

3.3.1. Synthesis and characterization of molecules

The asymmetric functionalization of pyromellitic dianhydride is well studied by our group and several reports are also available in the literature.[3] We used one such procedure with necessary modifications for the synthesis of PI-PI which is shown in Scheme 3.3. Commercially available pyromellitic dianhydride (**1**) was initially stirred with *tert*-butyl amine and ethanolamine at RT in anhydrous DMF. The mixture was then

refluxed at an elevated temperature of 130 °C for 12 h and the residue was column purified to get **2** in 12-14 % yield as a white solid. **2** was brominated by Appel's procedure using CBr_4 and PPh_3 in dry THF to get the bromo derivative **3** as pale brown solid in nearly 100% yield. **3** was heated in a sealed tube in the presence of 0.5 eq. of 1,4-bis(4-pyridyl)ethane (**4**) in dry acetonitrile. The product precipitated as brown solid which was repeatedly washed with chloroform to get pure PI-PI (**5**) in 40% yield. All the intermediates and final product were thoroughly characterized by ^{1}H and ^{13}C NMR, HRMS and FTIR techniques.

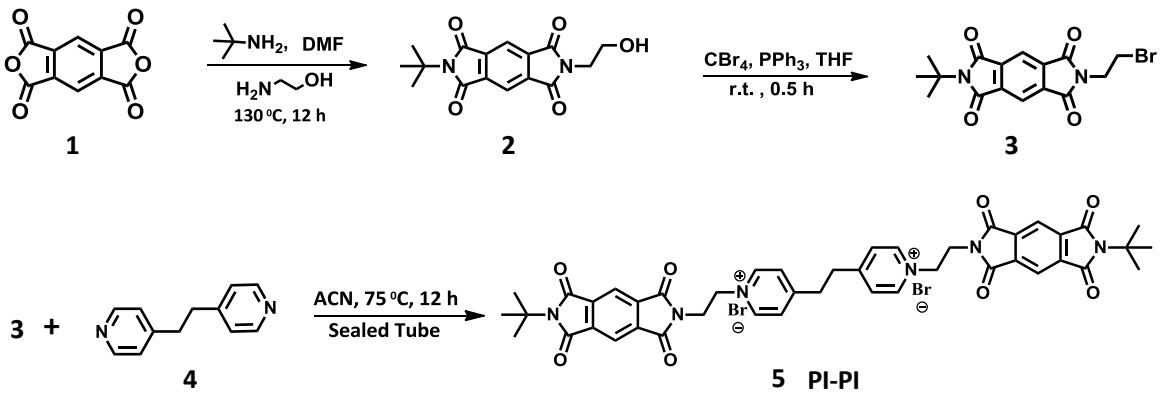

Scheme 3.3. Scheme for the synthesis of PI-PI.

Synthesis and characterization of AD-AD used for the preparation of vesicles is described in Chapter 2 (scheme 2.2).

3.3.2. Host-guest complexation studies between PI-PI and β-CD

Because of the presence of charged sites, PI-PI is found to be highly soluble in water. In Chapter 1, we have explained that certain N-alkyl PMDI derivatives rim-bind to β-CD and hence the ditopic molecule PI-PI is expected to rim-bind with β-CD at both ends to give the bis rim-binding complex β-CD⊱PI-PI⊰β-CD as shown in Scheme 3.2(3). Formation of this complex was studied by MALDI-TOF, ICD, ITC and ^{1}H NMR titrations as described below.

3.3.2.1. MALDI-TOF analysis

Previous studies from our group have confirmed the formation of a stable rim-binding complex between β-CD and PI to give β-CD⊱PI as shown in Scheme 3.2(2).[3] We have characterized this interaction using MALDI-TOF wherein we observed a peak at 1514.12, which was assigned to β-CD⊱PI. Figure 3.1 shows the MALDI-TOF data of a 1:2 mixture of PI-PI (10^{-2} M) and β-CD (2×10^{-2} M) in the presence of 2-(4'-Hydroxybenzeneazo) benzoic acid as the matrix in aqueous solution. The observed peak at m/z of 3053.37 was corresponding to the molecular mass of two β-CD and one PI-PI units without counter ion. The experiment provided clear evidence for the formation of a 1:2 host-guest complex between PI-PI and β-CD in aqueous medium which was sufficiently stable for MALDI-TOF analysis. The experiment, however, did not reveal the mode of binding between β-CD and PI-PI in the supramolecular complex.

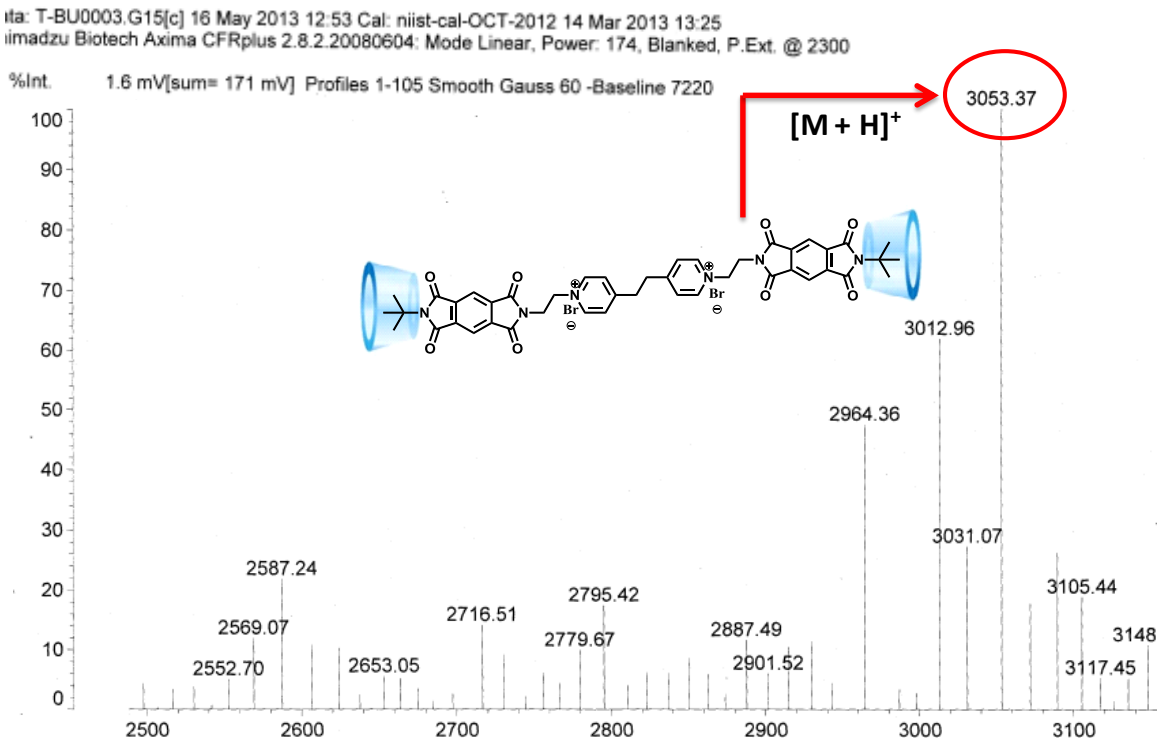

Figure 3.1. MALDI-TOF spectra of PI-PI (10^{-2} M)/β-CD (2×10^{-2} M) adduct.

3.3.2.2. ^{1}H NMR titration studies

The β-CD⊱PI supramolecular complex was characterized by ^{1}H NMR titration method in our previous study.[3] In that study, the *tert*-butyl protons observed at δ 1.67 ppm showed a downfield shift upon addition of β-CD and this shift was attributed to the entry of the *tert*-butyl group into the β-CD cavity. The aromatic protons of PMDI which appeared at δ 7.9 ppm showed a small upfield shift at higher concentrations of β-CD possibly due to the stacking of PMDI core. In order to gather information about the mode of PI-PI/β-CD interaction we have carried out ^{1}H NMR titration studies.

Figure 3.2 shows the ^{1}H NMR spectra of PI-PI in the presence of varying amounts of β-CD, where the β-CD concentration changed from 0 to 2 equivalents. The lower panel shows the assignments of the various protons in PI-PI with the dotted vertical lines indicate the original peak positions and the changed peak positions are indicated by arrow in the top panel. Figure 3.2 shows that the signal due to the *tert*-butyl protons (H_a protons) at **δ** 1.67 ppm undergoes 0.11 ppm down-field shift which is attributed to inclusion of the *tert*-butyl group into the β-CD cavity through the narrow rim in the rim-binding mode based on the observation made for the β-CD⊱PI system. This chemical shift changes actually occurs because of the change in the local environment of complexing moiety (-*tert* butyl group) from bulk of water to hydrophobic environment of β-CD.

We can also notice that the H_b protons of PI-PI, which appear as singlet at δ 7.95 did not undergo any change till one equivalent of β-CD was added, but exhibited slight down field shift upon further addition of β-CD. In an earlier study we showed that when the narrow rim of β-CD is functionalized with an anthracene derivative, rim-binding association is prevented and the PMDI molecules undergo inclusion binding in the β-CD cavity and this is characterized by an upfield shift of the PMDI aromatic proton by ~0.4

ppm with considerable peak broadening.[2] Hence the down field shift we see at higher β-CD concentration is not due to inclusion binding. Most probably some kind of stacking of the hydrophobic PMDI chromophore may be taking place in aqueous medium.[6] It should be noticed that the H_c, H_d, H_e, H_f and H_g protons of PI-PI did not exhibit any change in the presence of β-CD. The NMR results thus suggest that PI-PI binds to β-CD in the rim-binding mode to give the bis-complex β-CD⊱PI-PI⊰β-CD as shown in Scheme 3.2(3).

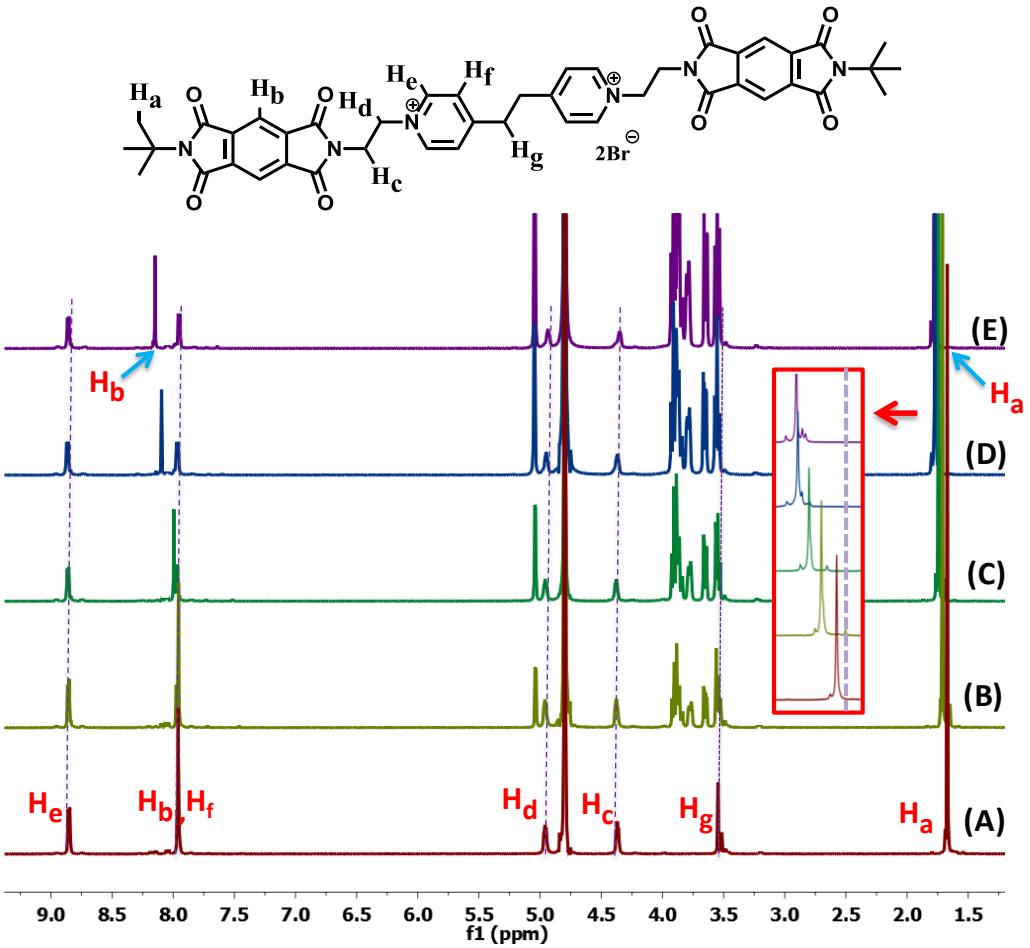

Figure 3.2. ^{1}H NMR titration spectra of PI-PI (10 mM) in the absence (A) and presence (B-E) of β-CD (0.5 – 2.0 eq.) in D_2O. The inset shows shifts of H_a protons.

3.3.2.3. Induced circular dichroism studies

To get further insights into the interactions between β-CD and PI-PI we have carried out ICD studies. The sign and intensity of ICD signals are extensively used in the

literature to identify the orientation of guest inside the host for the complexes of chiral macrocycles, using a set of rules derived by Harata and Kodaka.[7,8] The rules predict that (1) The sign of ICD is positive for a transition polarized parallel to the axis of the macrocyclic host and negative for that polarized perpendicular to the axis. (2) The sign of ICD is reversed when a chromophore moves from the inside of the host cavity to the outside, while keeping the direction of the transition moment unchanged. (3) The absolute value of ICD is greater when a chromophore exists on the outside of the narrower rim than when it is on the outside of the wider rim. (4) The ICD value of a transition polarized perpendicular to the axis of a macrocycle is −1/2 of that of a parallel-polarized one and the sign of ICD changes at 54.7°.

The rim-binding complex between β-CD and PI was previously confirmed by negative ICD signal at 320 nm (inset in Figure 3.3). Figure 3.3 shows the ICD spectra of PI-PI in the presence of increasing amounts of β-CD. As seen from the spectra, PI-PI did not exhibit any ICD signal in the absence of β-CD. Upon addition of β-CD the ICD signal was observed and its intensity steadily increased with increase in the concentration of β-CD and reached a value of -9 in the presence of two equivalents of β-CD. It is reported in the literature that, the PMDI chromophore in PI-PI has electronic absorption maxima at 321 nm and is polarized along the axis connecting the two imide nitrogen atoms.[9] In Figure 3.3 we observed negative ICD signal for PI-PI molecule in the presence of β-CD. Hence, based on above rules we confirm that PMDI chromophore is outside the β-CD cavity with only *tert*-butyl group is entering into the CD cavity. The ^{1}H NMR titration (Figure 3.2) experiment also indicated similar interaction of PI-PI with β-CD thus confirming the structure of β-CD⊱PI-PI⊰β-CD host-guest complex as shown in Scheme 3.2(3).

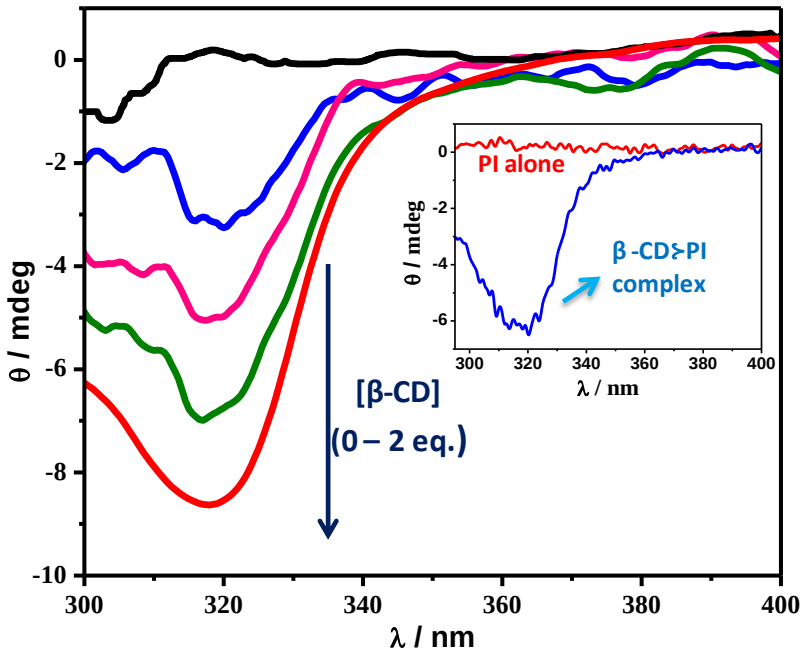

Figure 3.3. ICD spectra of PI-PI (4×10^{-4} M) in the presence of β-CD (0.0, 0.5, 1.0, 1.5 and 2.0 eq.). The inset shows the ICD curves for PI in the absence (red) and presence (blue) of one equivalent of β-CD.

3.3.2.4. Isothermal titration calorimetry studies

ITC experiments were carried out by taking β-CD (2.5 mM, 200 µL) in the cell and PI-PI (25 mM, 40 µL) in the syringe. Figure 3.4 shows the ITC titration curve for the PI-PI/ β-CD system. Heat changes observed for PI-PI/β-CD complexation was moderately high and fit of the data yielded values of K_a = 3.1 × 10^3 M^{-1}, ΔH = -5.53 × 10^4 J mol^{-1} and ΔS = -116 J mol^{-1} deg^{-1} and n = 0.5. The dilution experiment of PI-PI yielded very small heat changes. The number of binding sites n = 0.5 suggested that PI-PI has two binding sites for β-CD which further supports the structure of β-CD≻PI-PI≺β-CD complex as shown in Scheme 3.2(3). In the earlier study we obtained values of K_a = 3.36 × 10^3 M^{-1}, ΔH = -3.64 × 10^4 J mol^{-1} and ΔS = -52 J mol^{-1} deg^{-1} for β-CD and PI interaction.[4] The large negative value of entropy change for the β-CD/PI-PI system compared to the β-CD/PI system suggested the binding of β-CD to both ends of PI-PI resulting in a high degree of ordering in the β-CD≻PI-PI≺β-CD complex.

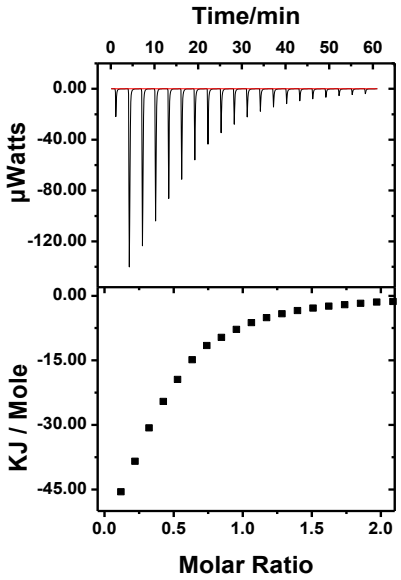

In cell (β-CD)		2.5 mM, 200 µL
In syringe (PI-PI)	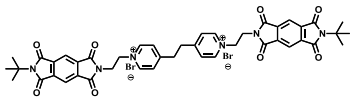	25 mM, 40 µL

Number of binding sites	0.5
Binding constant M^{-1}	3.1 E3
ΔH k joules/mol	-55.3
ΔS joules/mol/deg	-116

Figure 3.4. ITC data for the titration between β–CD (2.5 mM) and PI-PI (25 mM).

3.3.3. Self-assembly studies

As discussed in Chapter 2, the β-CD⊂AD-AD⊃β-CD supramolecular complex can spontaneously self-assemble into vesicles of dimensions ranging between 70-500 nm. The outer surface of these vesicles are loaded with the primary faces of β-CD and hence each vesicle can provide large numbers of rim-binding sites (or ternary complexation sites) for PMDI derivatives. In order to see if rim-binding interaction actually occurs we have added PI to the β-CD⊂AD-AD⊃β-CD vesicle solution and monitored the interaction using CD spectroscopy. Since the β-CD⊂AD-AD⊃β-CD vesicles are CD silent and rim-binding interaction proceeds with observation of negative ICD signals, CD spectroscopy was identified as the most convenient tool for studying the above interaction. Figure 3.5 shows the formation of the CD spectrum due to the rim-binding interaction of PI to β-CD⊂AD-AD⊃β-CD vesicles. The maximum CD intensity obtained was -3 mdeg at 320 nm upon addition of one equivalent of PI (w.r.t AD-AD). Thus Figure 3.5 supports out the proposal that PI can recognize the vesicle surface and interact with it in the rim-binding mode.

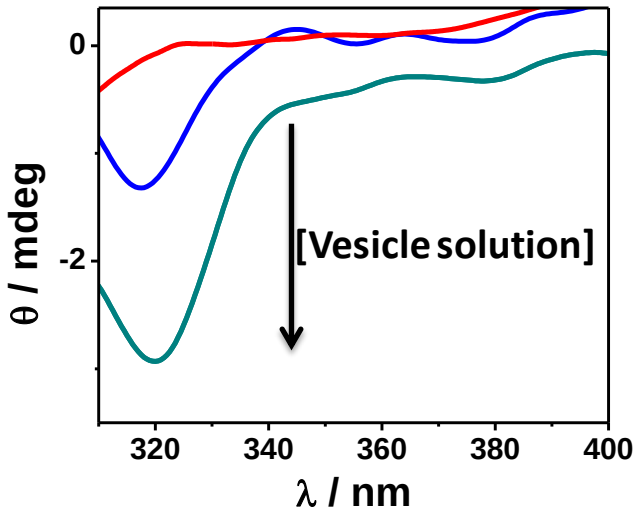

Figure 3.5. Evolution of ICD signals upon addition of PI to β-CD⊂AD-AD⊃β-CD vesicles.

TEM and AFM images of β-CD⊂AD-AD⊃β-CD vesicles in the presence of one equivalent of PI were also recorded. Only vesicles could be identified in these solutions. The wall thickness of vesicles before and after addition of PI remained similar. This can be attributed to the low association constant of rim-binding interaction over inclusion binding because of which only few PI molecules may be complexed on to the outer surface of the vesicles. We also examined the time dependence of the ICD signal intensity, but no such dependence was observed.

We observed that the β-CD⊂AD-AD⊃β-CD vesicle solution exhibited ICD signals in the presence of PI-PI also. In this case the ICD intensity, however, varied with time. Hence we performed a time dependence study of the evolution of the ICD signal. Figure 3.6 shows the variation of ICD signal intensity monitored for three days after addition of one equivalent of PI-PI to the pre-formed β-CD⊂AD-AD⊃β-CD vesicles. In this figure, the negative ICD signal intensity starts increasing almost immediately upon adding PI-PI to the vesicles. As seen from Figure 3.6, the negative signal intensity increased continuously for 70 h and reached the maximum limit of -4.5 mdeg after nearly 90 h.

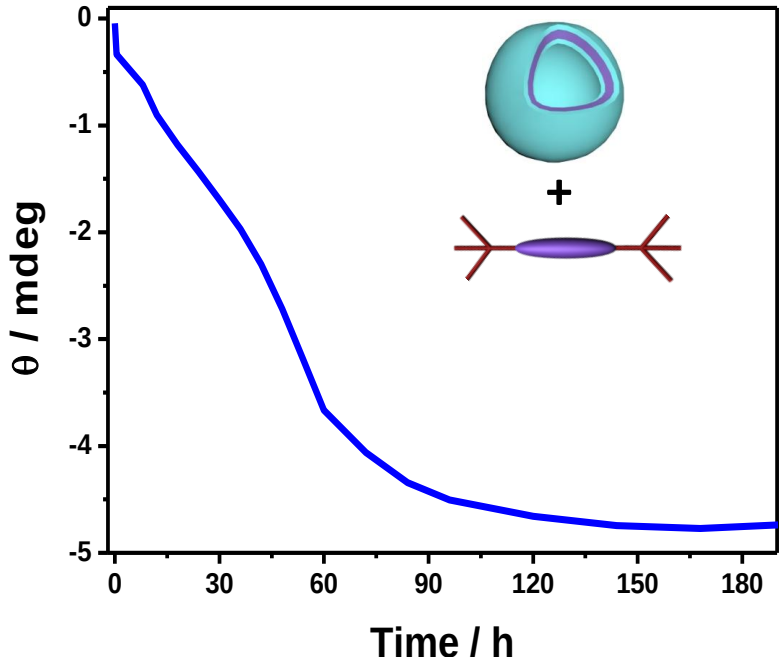

Figure 3.6. Time-dependent ICD changes (at 320 nm) observed upon addition of PI-PI (4 × 10^{-4} M) to β-CD⊂AD-AD⊃β-CD supramolecular vesicles. [AD-AD] = 4×10^{-4} M and [β-CD] = 8×10^{-4} M.

We proposed that the ditopic linker PI-PI can interact with two vesicles and link them together and most probably the observed time-dependent changes in the ICD signal can be attributed to such a process. In order to check whether this linking process is leading to any changes in the vesicle morphology and to study the mechanistic details of the self-assembly process we obtained AFM and TEM images of the sample at different time intervals. Initially, we have recorded the TEM and AFM images by drop casting this aqueous solution after 5 h of adding PI-PI which showed large numbers of spherical nano-structures (Figure 3.7 a, b). From TEM image we concluded that the nano-structures are actually vesicles because of clear contrast difference between interior and periphery of each nano-structure. Also these vesicles were similar in dimensions and properties to the β-CD⊂AD-AD⊃β-CD vesicles reported in Chapter 2. This suggested that in the first 5 h of addition of PI-PI, even though vesicle linking process has started (as indicated by ICD), the majority of the vesicles are still maintaining their spherical structure.

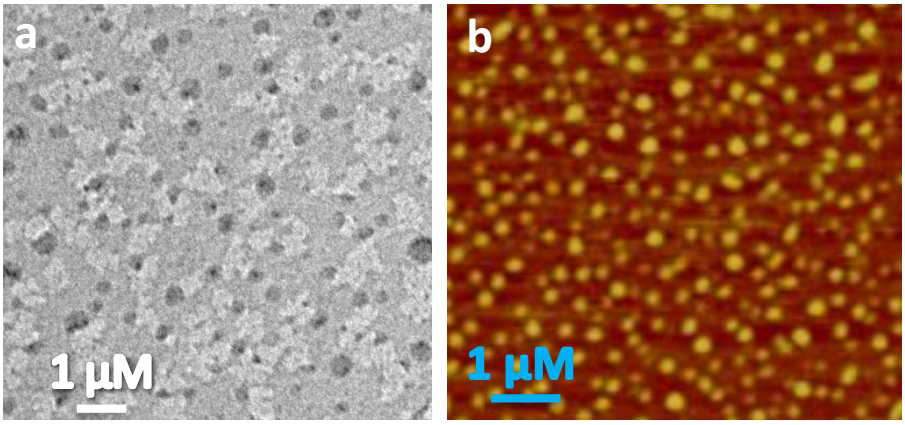

Figure 3.7. TEM (a) and AFM (b) images of vesicles formed in the β-CD/AD-AD/PI-PI (2:1:1) system at 5 h after mixing. [β -CD] = (1×10^{-4} M), [AD-AD] = [PI-PI] = 5×10^{-5} M.

We have preserved the three component solution without disturbing and after 24 h the same solution was again cast on freshly cleaved mica and carbon coated copper grid and analysed respectively by AFM and TEM. The AFM and TEM images (Figure 3.8) showed that the vesicles are joining together to give fibrous structures. In most of the images obtained the vesicles are seen co-existing with fibers and joining of two or more vesicles can be seen very clearly (Insets in Figure 3.8b). This fact is further confirmed by capturing the AFM magnitude image of the vesicle joining process (Figure 3.8c). The inset in the Figure 3.8d shows that the height of vesicles and height of fiber formed by joining of vesicles are same which further supports our argument.

TEM and AFM images were again obtained from three day-old solutions and the images obtained are shown in Figure 3.9. Examination of the images shows that most of the vesicles have disappeared and long fibers are seen over most of the viewing area. The AFM height analysis (Inset in Figure 3.9b) shows that fibers have an average height of 8-10 nm which was similar to that of vesicles. The AFM 3D image (Figure 3.9c) showed continuous crests and troughs along the backbone of nano-fibers. We believe that these supramolecular fibers are formed by joining of the vesicles as proposed by us earlier.

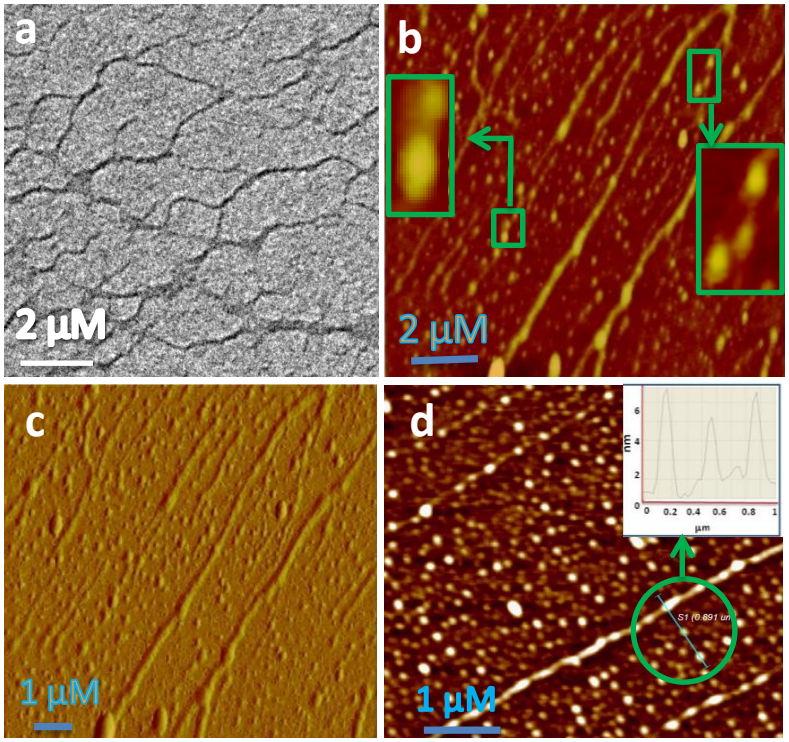

Figure 3.8. TEM (a), AFM height (b, d), and AFM magnitude (c) images of vesicles and fibers formed in the β-CD/AD-AD/PI- PI (2:1:1) system after 24 h.

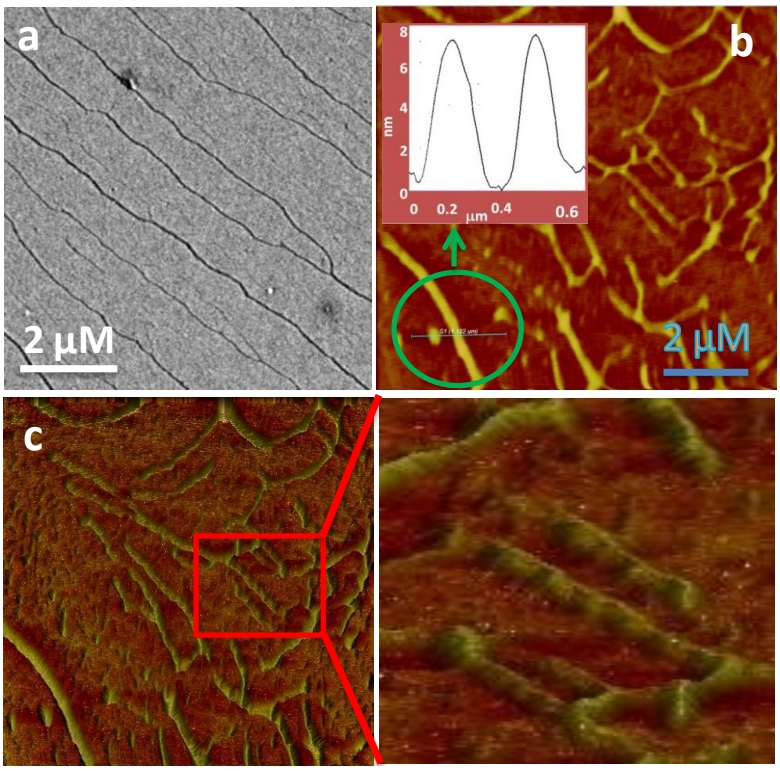

Figure 3.9. TEM (a) and AFM images (b, c) of vesicles and fibers formed in the β-CD/AD-AD/PI- PI (2:1:1) system taken after 72 h.

In Scheme 3.1 we proposed joining of β-CD⊂AD-AD⊃β-CD vesicles by PI-PI and Figure 3.9 shows that vesicles are joined upon addition of PI-PI to give long fibrous structures. To obtain these images we have added one equivalent of PI-PI (w.r.t. to AD-AD). Scheme 3.1, however, does not demand the presence of one equivalent of PI-PI for vesicle joining to happen. Even small amounts of PI-PI could initiate fiber formation. In order to check this we obtained TEM images of β-CD⊂AD-AD⊃β-CD vesicle solutions containing 0.25, 0.5 and 0.75 equivalents of PI-PI (w.r.t. to AD-AD) and these are shown in Figure 3.10.

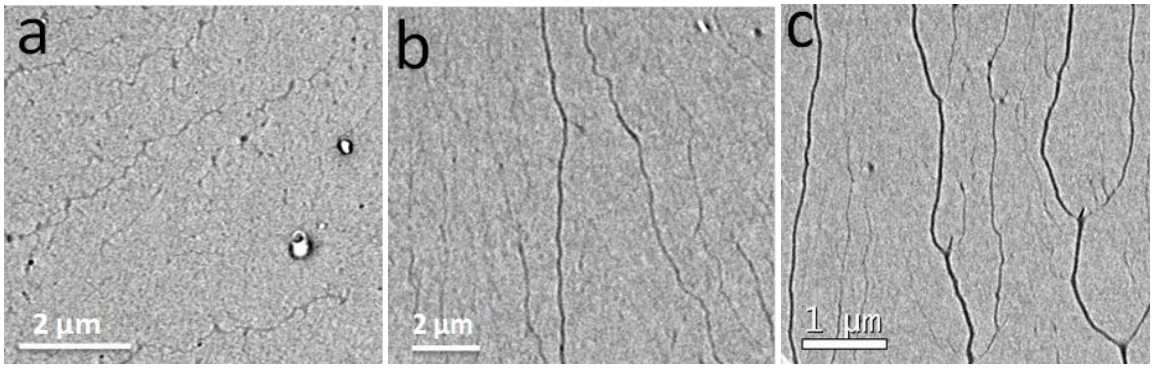

Figure 3.10. TEM images of fibers obtained by addition of varying equivalents of PI-PI to β-CD/AD-AD vesicles AD-AD (5×10^{-5} M) and β-CD (1×10^{-4} M). [PI-PI] were: (a) 0.25 eq., (b) 0.5eq. and (c) 0.75 eq. w.r.t AD-AD.

In a 1:1:2 aqueous solution of AD-AD, PI-PI and β-CD, ternary complexes AD-AD⊃β-CD⊱PI-PI (Scheme 3.2(4)) can also be formed through co-operative inclusion and rim-binding interactions. Iterative interactions of this type can lead to the formation of long fibers. Such fibers are expected to be very thin with diameters equal to the outer diameter of β-CD (< 2.0 nm). One can argue that the fibers seen in Figure 3.9 are formed through bundling of such narrow fibers. Our observations in Figure 3.10 rules out the above possibility also. Iterative interactions leading to long –(AD-AD⊃β-CD⊱PI-PI⊰β-CD)$_n$- fibers can occur only if AD-AD, PI-PI and β-CD are present in 1:1:2 ratio. The

formation of fibers even in the presence of 0.25 eq. of PI-PI clearly confirms our proposal that fibers are formed by vesicles joining and not by the bundling of small fibers.

In principle, long fibers can form if one equivalent of AD-AD is added to the pre-formed bis-rim-binding complex β-CD≻PI-PI≺β-CD. The mechanism would involve iterative addition of AD-AD to β-CD≻PI-PI≺β-CD. Since β-CD≻PI-PI≺β-CD exhibited reasonably good ICD signal the formation of long fibers, if any, can be followed by time-dependent ICD measurements. With this aim in mind, we have added one equivalent (w.r.t. PI-PI) of AD-AD to a solution containing PI-PI (4×10^{-4} M) and β-CD (8×10^{-4} M) and monitored the changes in the ICD signal intensity as a function of time. This PI-PI/β-CD (1:2) solution exhibited negative ICD signal due to formation of the bis-rim-binding complex. Before the addition of AD-AD the ICD signal exhibited an intensity of ~ -8.5 mdeg at 320 nm. Time dependence of the ICD intensity for 180 h following the addition of AD-AD is shown in Figure 3.11.

Figure 3.11 shows that addition of AD-AD led to an immediate disassembly of the bis-rim-binding complex as suggested from the sudden decrease of the ICD intensity to a near zero value. For the next several hours the ICD signal intensity remained close to zero and then started increasing (in the negative direction) till about 70 h. The final intensity attained is nearly the same as that in Figure 3.6. Time dependence of the ICD signal shown in Figure 3.11 shows that the expected long –(AD-AD⊃β-CD≻PI-PI≺β-CD)$_n$-fibers are not formed. Formation of such fibers would involve insertion of AD into the cavities in β-CD≻PI-PI≺β-CD such that all β-CD molecules would hold one AD moiety in the inclusion mode and one PI moiety in the rim-binding mode. Such an interaction is expected to reduce the ICD signal intensity due to β-CD≻PI-PI≺β-CD initially but thereafter the signal intensity should remain constant. Based on Figure 3.11 we suggest that β-CD≻PI-PI≺β-CD disassembles upon addition of AD-AD to its constituents. At that

time the solution would contain AD-AD, PI-PI and β-CD in 1:1:2 ratio, and the system then undergo self-assembly to give a super structure which contains PI-PI in the rim-binding mode.

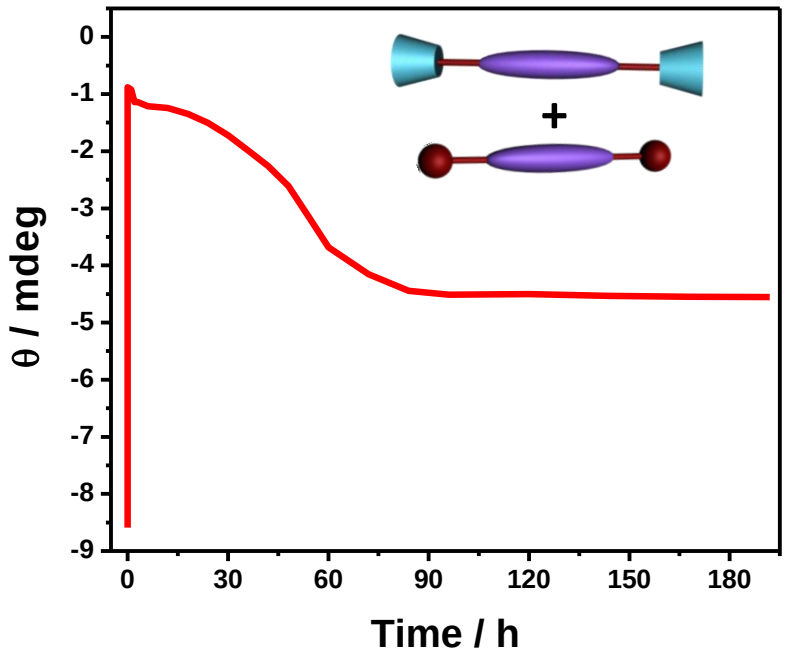

Figure 3.11. Time-dependent ICD changes observed upon addition of AD-AD (4×10^{-4} M) to β-CD⊱PI-PI⊰β-CD (8×10^{-4} M β-CD and 4×10^{-4} M PI-PI) supramolecular complex.

In order to obtain further clarification, we performed time-dependent ICD measurements on the three-component system. A mixture of AD-AD, PI-PI and β-CD (1:1:2) was dissolved in water and the ICD intensity was monitored at 320 nm. Immediately after mixing the observed ICD intensity was ~ -1.0 and then the signal intensity remained nearly the same for the next several hours. At ~ 15 h the signal intensity starts increasing (in the negative direction) and reached maximum around 90 h. No changes were observed thereafter.

In order to investigate the self-assembly processes in the three component system, we have carried out AFM and TEM experiments. The TEM and AFM images taken immediately after mixing the three components did not show the presence of any nano-

structures but showed only irregular aggregates. The AFM and TEM after 5 h showed the presence of vesicles which were having the same dimensions as in Figure 3.7. It should be noted that the supramolecular rim-bound complex β-CD≻PI-PI≺β-CD did not self-assemble to form any nano-structures. Thus we propose that the vesicles seen after mixing all the three components are the β-CD⊂AD-AD⊃β-CD vesicles. Morphological features of the 3-component system at 45 and 90 h are also shown as inserts in Figure 3.12. Interestingly the changes in morphology of this three component system with time were similar to that observed in Figure 3.8 and 3.9. Based on this observation, we propose that, in the three component system, initially β-CD⊂AD-AD⊃β-CD vesicles are formed which were later joined by PI-PI.

Figures 3.6, 3.11 and 3.12 deal with time-dependent ICD changes of a three component system consisting of AD-AD, PI-PI and β-CD (1:1:2) system. The only difference in the experiments was the mode of mixing. For the Figure 6 experiment PI-PI was added to the pre-mixed AD-AD/β-CD system. For the Figure 3.11 experiment AD-AD was added to pre-mixed PI-PI/β-CD system and for Figure 3.12 all components were mixed at the same time. In all three figures the final ICD intensity observed were same. We also noted that the self-assembled structure exhibited AFM and TEM images as shown in Figure 3.9. Comparing Figures 3.11 and 3.12 we observe that time-dependent changes observed in the ICD signals after ~10 h are nearly identical. The differences in these cases are only in the first 30 min after mixing. In the case of Figure 3.11 the initial intensity was ~ -8.5 mdeg, which decreased to ~ 0 immediately after adding AD-AD. As mentioned previously this is attributed to disruption of the β-CD≻PI-PI≺β-CD complexes. In the case of Figure 3.12, the ICD signal intensity was ~ -1.0 mdeg immediately after mixing, which suggest that nearly 10% PI-PI are engaged in rim-binding initially. When the components are mixed we expect binary complexes to form in a ratio dectated by the

ratio of their formation constants. For β-CD/AD-AD interaction K_{AD} obtained by ITC was 6.4×10^4 M^{-1}. For β-CD/PI-PI rim-binding we obtained $K_{PI} = 3.1 \times 10^3$ M^{-1} from ITC studies (Figure 3.4). The observed initial ICD intensity is slightly more than expected based on the ratio of the strengths of β-CD/AD-AD and β-CD/PI-PI interactions (as dictated by the magnitude of K_{AD}/K_{PI}). Most probably some amount of ICD active ternary complex AD-AD⊃β-CD⊱PI-PI (Scheme 3.2) may also be present at zero time.

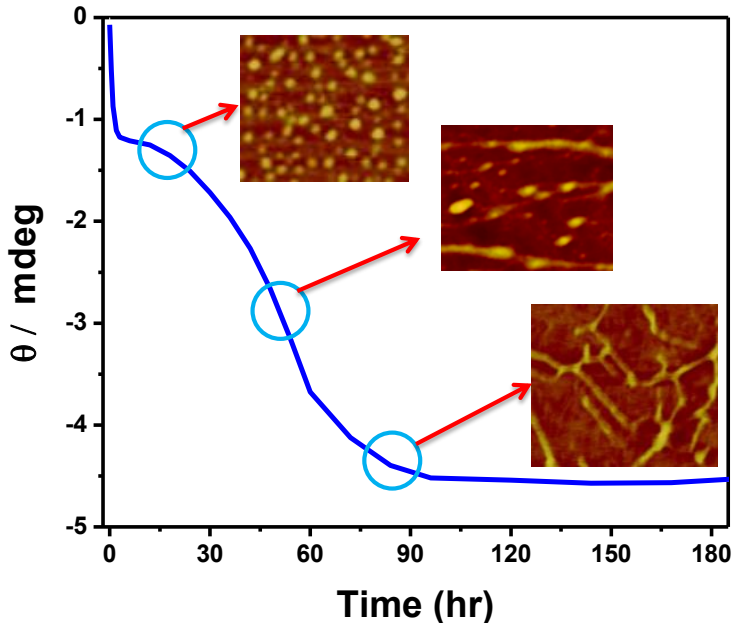

Figure 3.12. Evolution of ICD signal with time for the β-CD/AD-AD/PI-PI (2:1:1) system. The AFM images correspond to the times indicated. [PI-PI] = [AD-AD] = 4×10^{-4} M and [β-CD] = 8×10^{-4} M.

In experiments leading to Figures 3.11 and 3.12 we noticed that AFM and TEM images taken before 15 h of mixing did not indicate presence of nano-structures other than vesicles. The vesicles are not CD active and development of the negative ICD signal and formation of fibrous structures is initiated only around 15 h after mixing in these cases. This lag phase, however, is not observed in Figure 3.6 where PI-PI was added to preformed vesicles. The difference between these experiments is the pre-formed vesicles in the case of Figure 3.6. Thus we attribute the lag phase observed in Figures 3.11 and 3.12 to the time taken for vesicle formation.

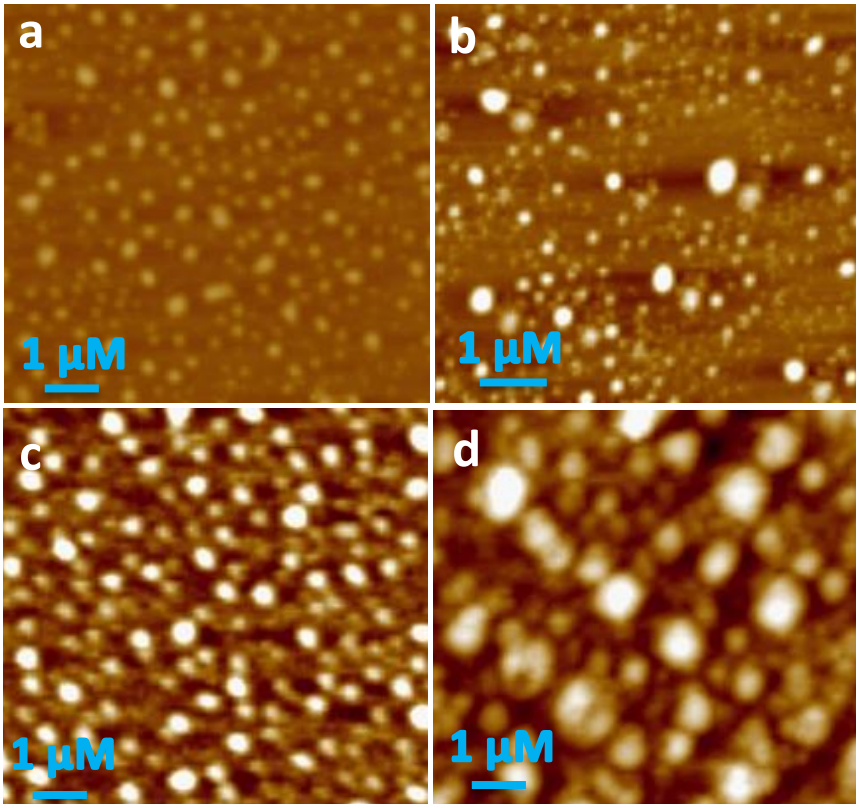

Figure 3.13. Time dependent AFM images of AD-AD/ β-CD/PI-PI (1:2:1) system at (a) 5 h, (b) 8 h, (c) 11 h and (d) 14 h after mixing. The average width of vesicles is found to be 165 nm, 220 nm, 285 nm and 368 nm, respectively, for a-d. [β -CD] = (1×10^{-4} M), [AD-AD] = [PI-PI] = 5×10^{-5} M

In order to confirm this proposal control experiments were carried out with β-CD/AD-AD/PI-PI (2:1:1) system. AFM images were obtained in this case every three hours after mixing. Vesicles could be seen only after 5-6 h of mixing and these gradually grow in size till 24 h (Figure 3.13). The lag phase observed in Figures 3.11 and 3.12 suggested that joining of vesicles can take place only after the vesicles have grown to certain sizes. This is understandable because vesicle joining can occur only if large numbers of PI-PI molecules undergo rim-binding interactions at a given area on the vesicle surface.

The above experiments clearly established that in the three-component system AD-AD/PI-PI/β-CD (1:1:2) long-fibrous structures slowly evolved over a period of 3-5

days, regardless of the mode of mixing the components. The fibrous structures incorporated all the 3 components within it in a particular sequence. This type of self-assembly is known as "integrated self-sorting". In order to understand the mechanistic details of the self-assembly process a discussion about self-sorting is essential. This is presented in the following section.

3.3.4. The concept of self-sorting in supramolecular chemistry

Because of the advancement in the synthetic methodologies, chemists can design and synthesize almost any complex molecule using 'covalent bonds' between atoms and molecules. Although the making and breaking of covalent bonds is a tedious and time consuming process, several thousands of useful molecules are prepared every year. In recent decades supramolecular chemistry is increasingly used for the arrangement of molecules to yield complex molecular structures.[10] In this case small molecules which are connected by primary interactions such as covalent bonds are linked further by secondary interactions such as hydrogen bonding, π-π interactions, hydrophobic interactions etc. for generating supramolecular structures. The dynamic nature of secondary interactions is effectively used for the addition or deletion of components from the macromolecules during synthesis which is otherwise done by tedious covalent modifications. In this way a chemist saves a lot of time, energy and reduces the cost of materials.

The supramolecular synthesis is taken into next level by the introduction and effective usage of the novel concept known as self-sorting.[11,12] The supramolecular systems constructed by the traditional bottom-up approach are generally symmetrical in nature because of similar repeating units, limiting their multiple applications. It is argued that the idea of self-sorting in supramolecular synthesis can integrate different subunits with precise positional control into the macromolecular architecture. In 2003, Isaacs and co-workers defined self-sorting in artificial self-assembling systems as the spontaneous,

high fidelity recognition of self from non-self within a mixture of similar components.[12] Because of this phenomenon, specific pairs are formed in the mixture of compounds rather than a library of all possible non-covalent complexes. Inorder to achieve this, the molecular instructions i.e suitable recognition elements on the components should be incorporated during chemical synthesis. Although the concept of self-sorting is relatively new in artificial systems, in the biological system this is ubiquitous in nature. Self-sorting manifests itself from the very simple processes such as the separation of oil/water mixture into immiscible layers to the organization of large numbers of constituents into functional assemblies such as organelle and cells. One of the primitive example is DNA whose function is to store genetic instructions. DNA is made up of four base pairs namely adenine (**A**), thymine (**T**), guanine (**G**) and cytosine (**C**). In the mixture of four components each of the component identifies its complementary nitrogenous base and self-sort to form two base pairs (**AT** and **GC**).[13] Both these base pairs are formed by the help of H-bonding interactions and it is important to note that other combination of base pairs such as **AG** or **GT** will never form even though H-bonding is possible in these pairs.

Self-sorting is basically classified into two types viz. social self-sorting[14,15] and narcissistic self-sorting[16] (Figure 3.14). Social self-sorting refers to the self-assembly of different species whereas narcissistic self-assembly refers to assembly of the same species. Recently Schally and co-workers further classified the self-sorting processes into integrative, wherein all the components get integrated into a single assembly and non-integrative where the self-assembly process yield more than one final product.[17,18]

Isaacs and co-workers from the University of Maryland are the pioneers in developing integrative and non-integrative self-sorting systems. In a recent report, they have used two crown-ethers, namely dibenzo-24-crown-8 (**A**) and benzo-21-crown-7 (**B**) along with two secondary ammonium derivatives **6** and **7** to form pseudorotaxanes

(Figure 3.15a).[19] In an aqueous equimolar mixture of these four components, **A** combined with **6** and **B** combined with **7** to form **A6** and **B7** pseudorotaxanes by non-integrative self-sorting method. It is important to note that despite similar binding sites on **6** and **7** for crown-ethers, **A** never formed complex with **7** and **B** with **6**. The phenyl group of **6** is too bulky to enter through the cavity of **B** and slim alkyl chain of **7** will easily slide out from wide cavity of **A**. This difference in the bulkiness on **6** and **7** is the reason for the high fidelity of the self-sorting process observed.

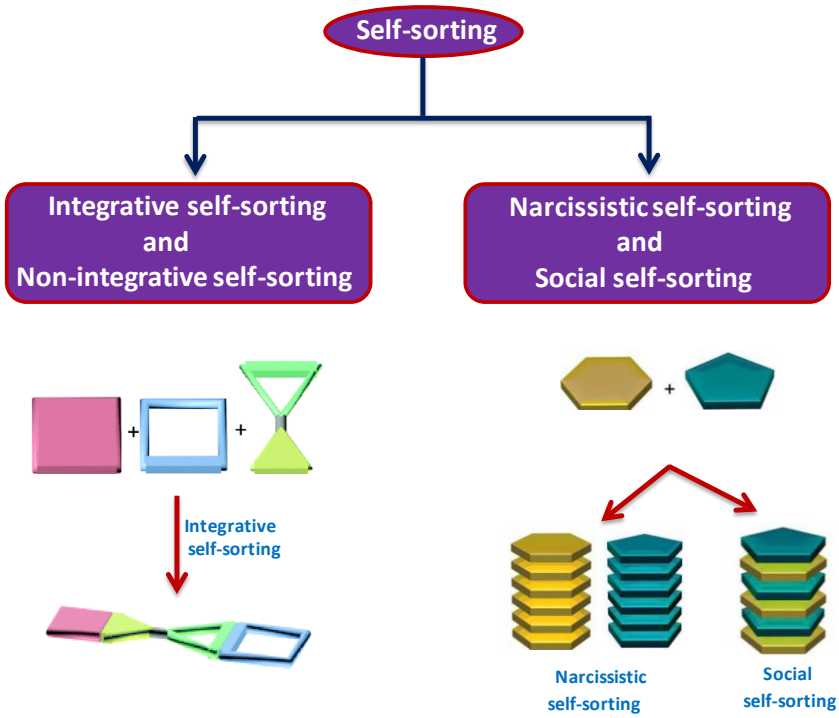

Figure 3.14. Schematic representation of the different types of self-sorting.

In further continuation of this work, the authors synthesized a molecule by combining the two binding sites present on **6** and **7** to get a heteroditopic secondary amine (**8**) as shown in Figure 3.15b.[19] This molecule upon reaction with **A** and **B** formed a hetero[3]rotaxane by a straight forward self-assembly process. Authors have successfully applied the concept of integrative self-sorting for the construction of this molecular machine wherein all the three components integrate into a single assembly.

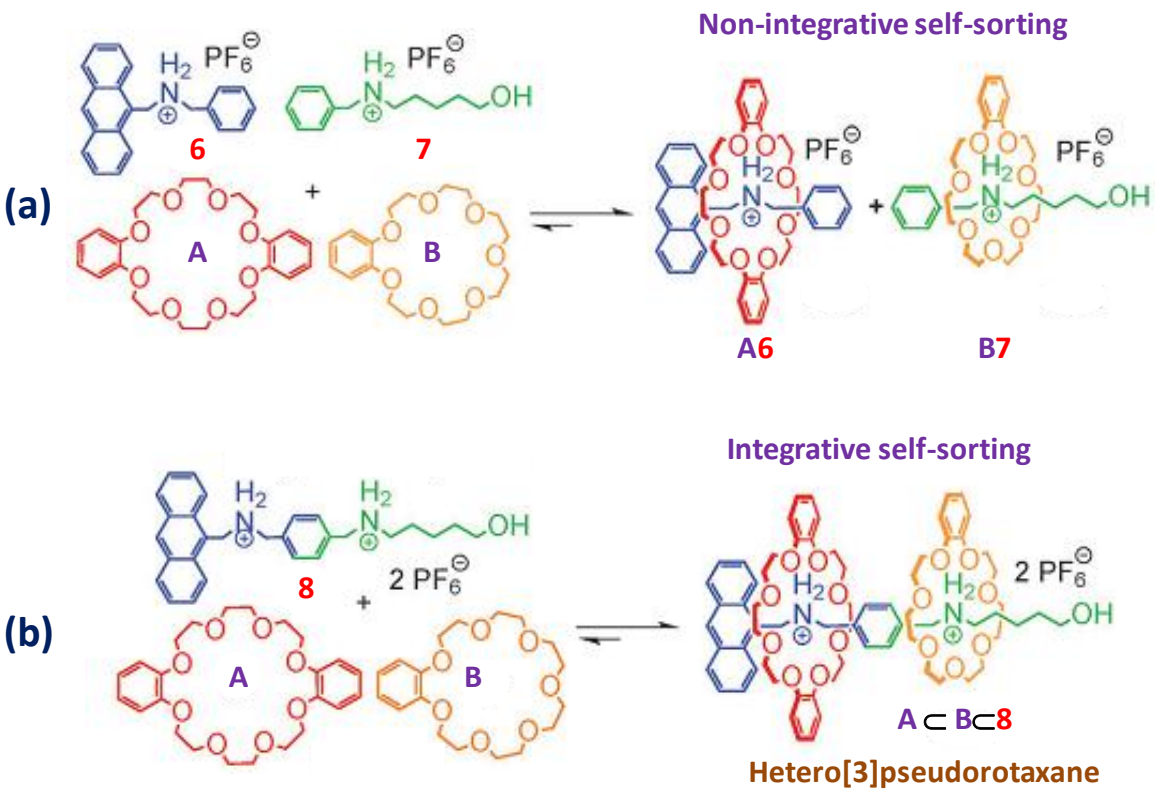

Figure 3.15. (a) Four component non-integrative self-sorting system constructed from an equimolar mixture of **6, 7, A** and **B**. (b) Formation of hetero[3]pseudorotaxanes by using equimolar mixture of **A, B** and **8**.

The concept of integrative self-sorting is taken to next level by the same group for the construction of even more complex assemblies by combining the strategies discussed above. The crown ethers **A** and **B** used in the previous work (Figure 3.15) were linked by using anthracene to get the homo-ditopic crown ethers **C** and **D** as shown in Figure 3.16. The secondary amine derivative (**8**) used previously (Figure 3.15) was used here also. When two equivalents of **8** were mixed with one equivalent each of **C** and **D**, the complex molecular architecture shown in Figure 3.3 was formed.[20,21] The structure of the complex was unambiguously confirmed by ^{1}H NMR (by monitoring the shift in the a-h protons of molecule **8**) and ESI mass techniques. The small cavity size of C will not allow phenyl group to penetrate through it. As a result of this **C** cannot occupy the position of **D** in the supramolecular structure and prefers to form a stable complex with slim alkyl chain. Thus

self-sorting allowed the construction of structurally diverse and complex supramolecular systems with controlled positions of each component whose synthesize by covalent method will be very challenging.

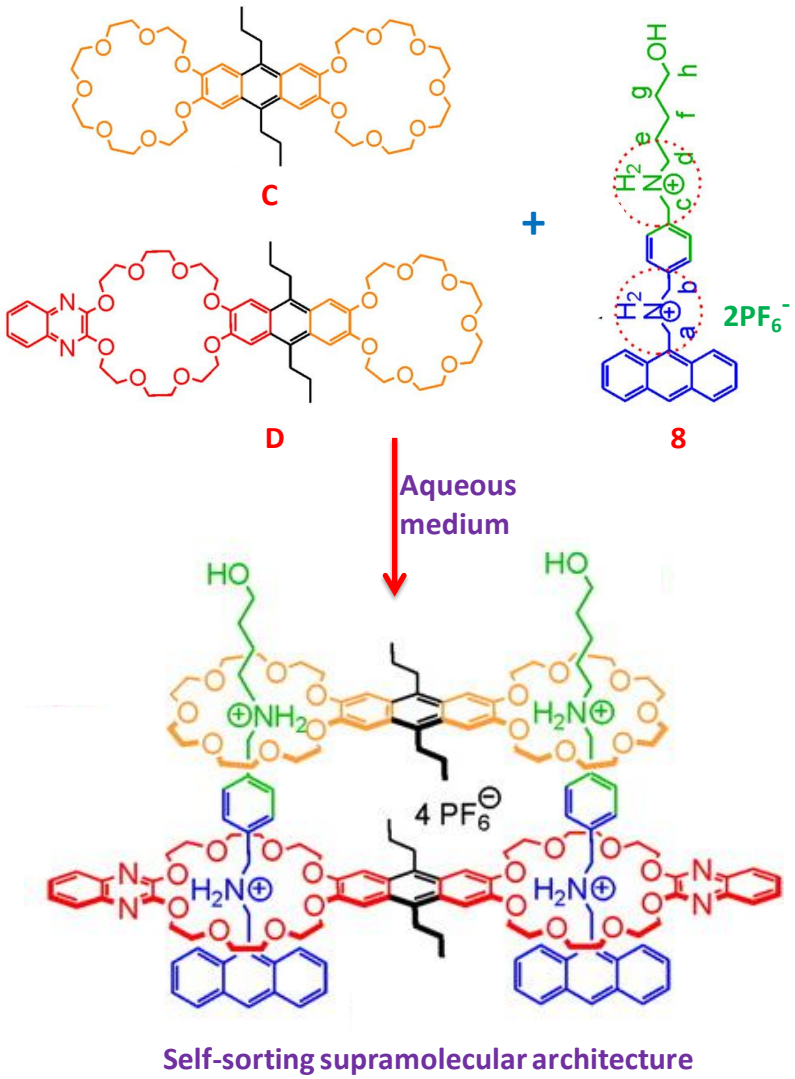

Figure 3.16. Schematic illustration of integrative self-sorting complex formation.

It is very clear from the above examples that integrative self-sorting is a powerful strategy to combine highly unsymmetrical molecular structures. For the characterization one has to relay on ^{1}H NMR and ESI mass spectroscopy. As the complexity in the molecular structure increases, ^{1}H NMR generally fails and tandem mass spectrometric experiment is the only available characterization method.

The self-sorting concept has been further extended for the fabrication of functional assemblies with higher order. For instance, Zhang and co-workers have prepared supramolecular polymers in which the polymerisation is controlled by utilizing the concept of self-sorting which is schematically shown in Figure 3.17.[22] They have synthesised a ditopic naphthalene derivative linked to both sides of p-phenylene moiety (Naph-Phen-Naph). It is well known in the literature that the phenyl group forms a stable host-guest complex with cucurbit[7]uril (CB[7]) while two naphthalene moieties can simultaneously enter into cucurbit[8]uril (CB[8]) cavity. Hence in an equimolar solution of Naph-Phen-Naph, CB[7] and CB[8] a linear supramolecular polymer was formed with high molecular weight. In the mixture, the CB[7] forms a complex with phenyl group of Naph-Phen-Naph thus making a rigid supramolecular complex. The naphthalene moieties at the ends of this complex can enter into CB[8] and this process can be repetitive in both directions which leads to linear polymerization. In the absence of CB[7], the two naphthalene moieties of single Naph-Phen-Naph may enter into the same CB[8] unit which prevents polymerization. Hence the authors could easily control the molecular weight of supramolecular polymer by varying the equivalents of CB[7]. In the mixture of all the three components, the CB[7] selectively complexes with phenyl group and CB[8] selectively complexes with naphthalene group because of self-sorting.

Most of the artificial systems studied based on social self-sorting are in organic solvents and the mechanism is very rarely observed in aqueous medium. This is in contrast to biological systems where social self-sorting in aqueous medium is routine. Harada and co-workers have recently reported an alternating supramolecular copolymer based on structurally similar isomers of α-CD in aqueous medium that can be considered as an example of social self-sorting (Figure 3.18).[15]

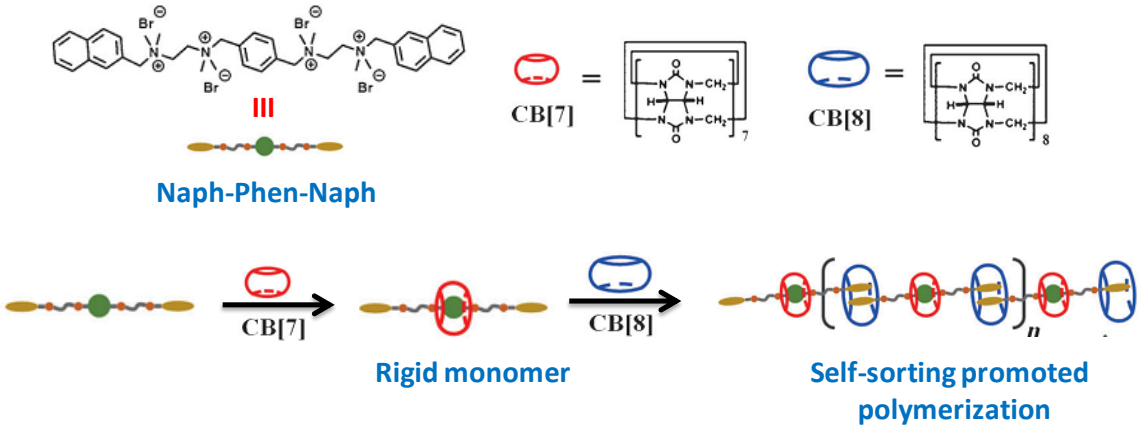

Figure 3.17. Scheme showing CB-based supramolecular polymerization promoted by self-sorting.

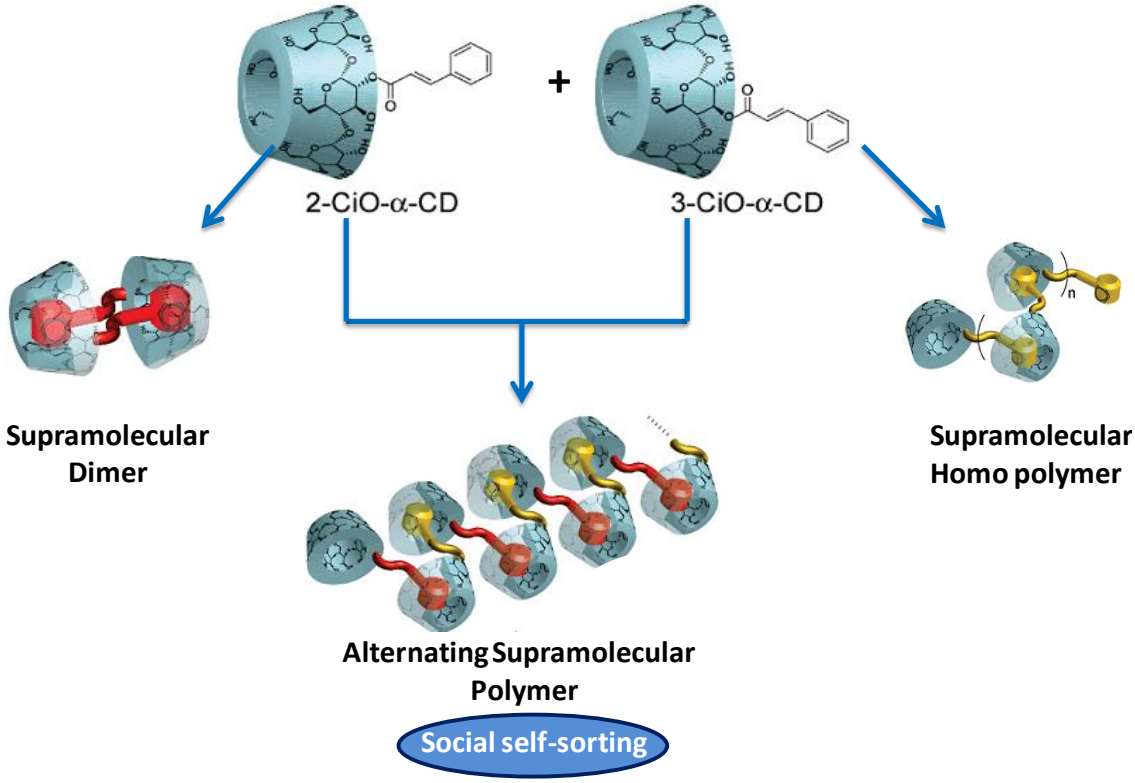

Figure 3.18. Schematic illustration of two isomers of α-CD with their isolated self-assembly and self-sorting assisted co-polymer formation in the mixture.

The two isomers of cinammoyl appended cyclodextrins 2-Cio-α-CD and 3-Cio-α-CD formed dimers and homopolymers in aqueous medium which were well characterized. When these two isomers are mixed in 1:1 ratio, the otherwise sparingly

soluble 2-Cio-α-CD became highly soluble in water. The ROESY spectrum of their equimolar mixture showed correlation peaks between CD inner protons of 2-Cio-α-CD with cinammoyl protons of 3-Cio-α-CD and vice-versa. However, the olefinic protons of 2-Cio-α-CD and 3-Cio-α-CD, respectively, did not correlate with their own inner CD protons in the mixture which suggested the formation of an alternating supramolecular polymer as shown in Figure 3.18. A social self-sorting could be identified in this case because one isomer prefers the other component rather than itself for the higher order assembly.

Since the fibrous structures obtained in the self-assembly of AD-AD/PI-PI/β-CD (1:1:2) system after 3 days integrates all the three components, its formation is an example of integrative self-sorting in a three component system. Various stages involved in the integrative self-sorting process can be summarized as in Scheme 3.4. The first step (marked as step **a** in Scheme 3.4, is a social self-sorting process which involves 2:1 inclusion complexation to form β-CD⊂AD-AD⊃β-CD and 2:1 rim-binding complexation to form β-CD≻PI-PI≺β-CD. A small fraction of the components may also be involved in ternary complex (PI-PI≺β-CD⊂AD-AD) formation. Both β-CD≻PI-PI≺β-CD and PI-PI≺β-CD⊂AD-AD are ICD active and together constitute ~10% of the social self-sorting process. β-CD⊂AD-AD⊃β-CD formed then undergo narcissistic self-assembly to give layered arrangement of the complex (step **b**). Once a bilayer arrangement is formed, it folds to give supramolecular vesicles and the process again can be identified as narcissistic self-sorting (step **c**). It should be noted that, during processes **b** and **c,** PI-PI is present in the medium and can always complex with β-CD along with AD-AD. But this did not happen, rather β-CD showed high preference towards AD-AD over PI-PI. Once the AD-AD is completely used for vesicles formation and vesicles are sufficiently large,

the PI-PI starts linking of these vesicles through another social self-sorting process (step **d**) to give the fibrous structures.

The outer surface of the β-CD⊂AD-AD⊃β-CD vesicles are made up of the small rim of β-CD as mentioned earlier. The outer surface of the vesicles can recognize PMDI moieties and undergo rim-binding with them. Hene the ditopic molecule PI-PI can also undergo rim-binding with vesicles with its both ends. When several PI-PI molecules get involved in bis rim-binding interaction with two vesicles, a mechanism for joining of vesicles as shown in Scheme 3.1 will be established.

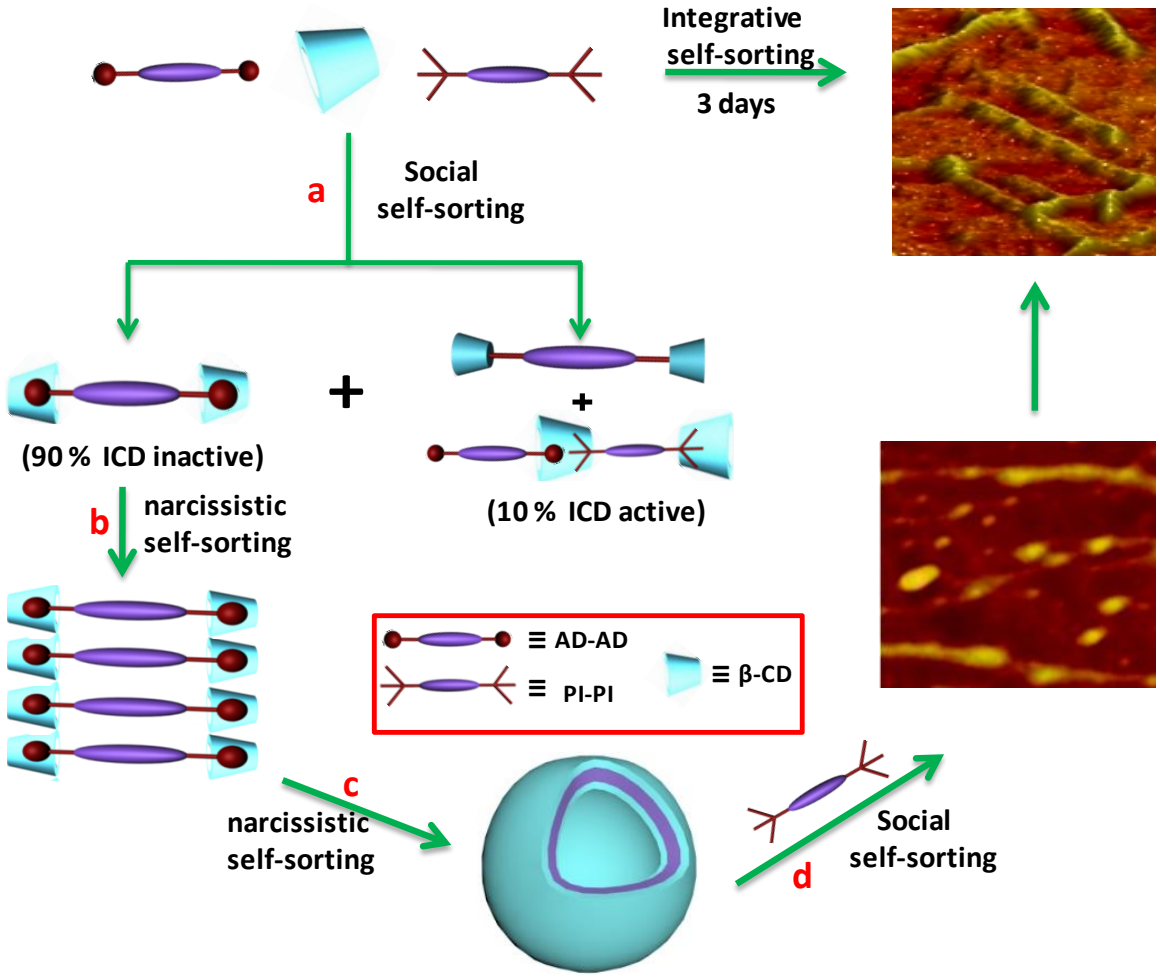

Scheme 3.4. Various self-sorting processes in β-CD/AD-AD/PI-PI (2:1:1) system.

3.3.5. Disassembly of nano-fibers

As discussed in Chapter 2, the guest included in β-CD cavity can be displaced out by using another guest with higher association constant.[23] When adamantane and tertiary butyl groups are complexed with β-CD, respectively, by inclusion binding and rim-binding interactions, adamantane carboxylate alone can push these two guests from β-CD cavity and form ADC⊃β-CD complex. Hence we used ADC for disassembling the nano-structures obtained by integrated self-assembly in the AD-AD/PI-PI/β-CD system. For the disassembly we used 2.25 equivalent of ADC w.r.t to the β-CD. We observed that addition ADC to β-CD⊂AD-AD⊃β-CD/PI-PI fiber solutions led to disappearance of the fiber structures in few hours as evidenced by the absence of these structures in TEM and AFM images (Figure 3.19a,b). Previous experiments showed that the long fibers obtained exhibited negative ICD signal, suggesting that PI-PI is incorporated in it in the rim-binding mode. Addition of ADC to these supramolecular fibers led to disappearance of ICD signal, which further confirmed the disassembly process (Figure 3.19c). The disassembly study also confirmed that the fibrous and vesicle structures are formed through non-covalent interactions.

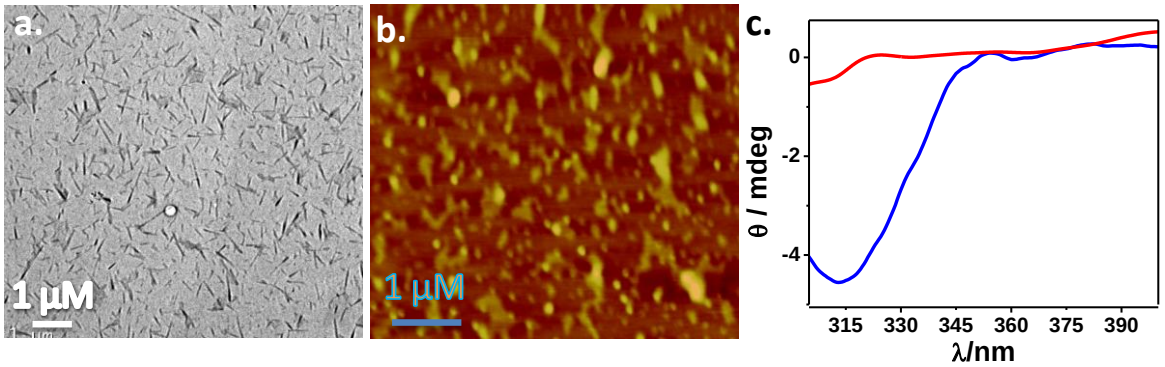

Figure 3.19. a) TEM and b) AFM images of nanofibers obtained 3 h after addition of 2.25 eq. ADC to 4-day old AD-AD/PI-PI/β-CD solution. c) ICD spectrum of nano-fibers before (blue trace) and after addition of ADC. [β -CD] = (1×10^{-4} M), [AD-AD] = [PI-PI] = 5×10^{-5} M for a and b. [β-CD] = (8×10^{-4} M), [AD-AD] = [PI-PI] = 4×10^{-4} M for experiment c.

3.4. Conclusions

We observed integrative self-sorting in an aqueous solution containing β -CD, AD-AD and PI-PI in 2:1:1 ratio. Long fibrous structures slowly evolved from the aqueous β-CD /AD-AD/PI-PI solution over a period of three days. The fibers can also form by the addition of PI-PI to pre-formed β-CD⊂AD-AD⊃β-CD vesicles. Alternately, addition of AD-AD to preformed bis rim-binding complex β-CD≻PI-PI≺β-CD also resulted in the formation of fibers. In this case, β-CD≻PI-PI≺β-CD will disassemble (as evidenced by the immediate disappearance of ICD) and the fibers have to evolve through all the stages shown in Scheme 3.4. All the evidences suggested that the fibers are formed through the joining of vesicles induced by the ditopic rim-binding interaction of PI-PI. In this study we have shown that the rim-binding motif can be effectively exploited to perform the functions of vesicle recognition and joining leading to formation of larger structures. In principle, the rim-binding motif invoked here for vesicle recognition and joining is applicable to all native β-CD based vesicles because the outer surfaces of these vesicles are comprised of the narrow rim of β-CD.

3.5. Experimental section

3.5.1. General methods

All NMR data were recorded in D_2O purchased from Aldrich, using a 500 MHz Bruker Avance DPX spectrometer. High-resolution mass spectra were obtained by using a JOEL JMS600 mass spectrometer. ITC data were obtained using microcal iTC 200. The raw data obtained were fitted and analyzed using origin 7.0 software provided along with the instrument. AFM measurements were carried out using NTEGRA (NT- MDT) instrument using micro fabricated TiN cantilever tips (NSG-10) with a resonating frequency of 299 kHz and a spring constant of 20-80 Nm^{-1} and multimode scanning

probe microscope (Nanoscope IV controller, digital instruments), using tapping mode techniques. The samples for AFM were prepared by drop casting the solution on freshly cleaved mica surface and evaporating the excess solvent. TEM analyses were performed using a FEI-TECNAI T30 G^2S-TWIN, 300 kV HRTEM microscope with an accelerating voltage of 100 kV and the samples were prepared by drop casting the solution on a formvar-coated copper grid (400 mesh) and evaporating excess solvent. ICD spectra were obtained on a JASCO-J-810 Circular Dichroism Spectropolarimeter. MALDI-TOF mass spectrometry was conducted on an AXIMA-CFR-plus instrument with 2-(4'-Hydroxybenzeneazo) benzoic acid as the matrix. Unless stated otherwise, all experiments were performed at 22 ^{0}C.

3.5.2. Molecules and materials

β-CD and 1,2-bis(4-pyridyl)ethane were purchased from Aldrich and used as received. ADC was prepared by neutralizing 1-adamantane carboxylic acid with sodium carbonate taken in 2-proponol. The solvents and reagents were dried and purified by standard methods prior to use. The procedure for the synthesis of AD-AD is described in chapter 2. The procedure for synthesis of PI-PI is described below.

A) Synthesis of 2:

Compound **2** was prepared by modifying a reported procedure.[3] Pyromellitic dianhydride (**1**) (3.0 g, 13.7 mmol) was dissolved in dry DMF (30 mL) and *tert*-butyl amine (1.0 g, 13.7 mmol) was added. After 12 h, 2-amino-1-ethanol (0.84 g, 13.7 mmol) was added and refluxed for 12 h at 130 ^{0}C. The reaction mixture after cooling was added to ice-cold water and the resulting precipitate was filtered and dried. This was purified by column chromatography over silica gel. Elution with methanol/chloroform (5:95) gave compound **2**. Yield: 0.55 g (12%), m.p. 184-185 ^{0}C. ^{1}H NMR (500 MHz DMSO-d_6,) δ:

8.10 (s, 2 H), 4.88 (br.s, 1 H), 3.69 (t, 2 H), 3.60 (t, 2 H), 1.64 (s, 9 H). ^{13}C NMR (125 MHz DMSO-d_6,) δ: 167.27, 166.32, 137.08, 136.60, 116.79, 60.28, 57.77, 40.79, 28.40.

B) Synthesis of 3:

Compound **2** (0.2 g, 0.64 mmol) and tetrabromomethane (0.27 g, 0.80 mmol) were dissolved in dry THF under inert atmosphere. Triphenylphosphine (0.21 g, 0.80 mmol) was added to this at 0 ^{0}C and stirred at room temperature for 0.5 h. The reaction was quenched with a few drops of water, and was partitioned between CH_2Cl_2 (100 mL) and H_2O (80 mL). The organic layer was washed with water (3 × 50 mL) and brine (50 mL) and dried over Na_2SO_4, and the solvent was evaporated under reduced pressure. This was purified by column chromatography over silica gel. Elution with chloroform gave Compound **3** as a pale brown solid. Yield: 0.21g (100%), m.p. 182 ^{0}C. ^{1}H NMR (500 MHz, $CDCl_3$) δ: 8.2 (s, 2 H), 4.18 (t, 2 H), 3.66 (t, 2 H), 1.72 (s, 9 H). ^{13}C NMR (125 MHz, $CDCl_3$) δ: 167.31, 165.91, 137.45, 136.67, 118.07, 59.08, 39.83, 28.96.

C) Synthesis of PI-PI:

1,2-Bis(4-pyridyl)ethane (**4**) (0.07 g, 0.38 mmol) and compound **3** (0.3 g, 0.79 m mol) were dissolved in dry acetonitrile (2 mL) was taken in a sealed tube and heated for 12 h. The solid obtained was filtered and washed with minimum amount of dry acetonitrile and repeatedly washed by chloroform to give **PI-PI** (**5**). Yield 0.25 g (40 %).

^{1}H NMR (500 MHz, CD_3CN) δ: 8.8 (d, 4H), 8.1 (s, 4H), 7.8 (d, 4H), 4.8 (t, 4H), 4.2 (t, 4H) 3.3 (t, 4H) and 1.67 (s, 18H); ^{13}C NMR (125 MHz D_2O,) δ: 190.74, 168.60, 167.04, 144.17, 137.11, 135.99, 128.48, 117.46, 59.22, 39.40 and 27.88. ESI-HRMS calculated for $C_{44}H_{42}N_6O_8^{2+}$ is 782.30 and found is 781.30.

3.6. References

(1) Hedges, A. R.: Industrial applications of cyclodextrins. *Chem. Rev.* **1998**, *98*, 2035.

(2) Balan, B.; Sivadas, D. L.; Gopidas, K. R.: Interaction of pyromellitic diimide derivatives with β-cyclodextrin and anthracene-appended β-cyclodextrin: Rim binding vs inclusion complexation. *Org. Lett.* **2007**, *9*, 2709.

(3) Krishnan, R.; Rakhi, A. M.; Gopidas, K. R.: Study of β-cyclodextrin–pyromellitic diimide complexation. Conformational analysis of binary and ternary complex structures by induced circular dichroism and 2D nmr spectroscopies. *J. Phys. Chem. C* **2012**, *116*, 25004.

(4) Krishnan, R.; Gopidas, K. R.: β-cyclodextrin as an end-to-end connector. *J. Phys. Chem. Lett.* **2011**, *2*, 2094.

(5) Nayak, N.; Gopidas, K. R.: Unusual self-assembly of a hydrophilic β-cyclodextrin inclusion complex into vesicles capable of drug encapsulation and release. *J. Mater. Chem. B* **2015**, *3*, 3425.

(6) Yu, Z.; Wang, H.; Bai, B.; Qu, S.; Li, F.; Ran, X.; Sun, J.; Jin, G.; Li, M.: A novel pyromellitic diimide derivative: Synthesis, gelation and spontaneous colorimetric sensing of dihydroxybenzene isomers. *Materials Science and Engineering: C* **2010**, *30*, 699.

(7) Kodaka, M.: A general rule for circular dichroism induced by a chiral macrocycle. *J. Am. Chem. Soc.* **1993**, *115*, 3702.

(8) Kodaka, M.: Sign of circular dichroism induced by β-cyclodextrin. *J. Phys. Chem* **1991**, *95*, 2110.

(9) Gawroński, J.; Brzostowska, M.; Kacprzak, K.; Kołbon, H.; Skowronek, P.: Chirality of aromatic bis-imides from their circular dichroism spectra. *Chirality* **2000**, *12*, 263.

(10) Lehn, J. M.: Supramolecular chemistry. *Science* **1993**, *260*, 1762.

(11) Safont-Sempere, M. M.; Fernandez, G.; Wurthner, F.: Self-sorting phenomena in complex supramolecular systems. *Chem. Rev.* **2011**, *111*, 5784.

(12) Wu, A.; Isaacs, L.: Self-sorting: The exception or the rule? *J. Am. Chem. Soc.* **2003**, *125*, 4831.

(13) Watson, J. D.; Crick, F. H. C.: Molecular structure of nucleic acids: A structure for deoxyribose nucleic acid. *Nature* **1953**, *171*, 737.

(14) Mukhopadhyay, P.; Wu, A.; Isaacs, L.: Social self-sorting in aqueous solution. *J. Org. Chem.* **2004**, *69*, 6157.

(15) Tomimasu, N.; Kanaya, A.; Takashima, Y.; Yamaguchi, H.; Harada, A.: Social self-sorting: Alternating supramolecular oligomer consisting of isomers. *J. Am. Chem. Soc.* **2009**, *131*, 12339.

(16) Johnson, A. M.; Wiley, C. A.; Young, M. C.; Zhang, X.; Lyon, Y.; Julian, R. R.; Hooley, R. J.: Narcissistic self-sorting in self-assembled cages of rare earth metals and rigid ligands. *Angew. Chem. Int. Ed.* **2015**, *54*, 5641.

(17) He, Z.; Jiang, W.; Schalley, C. A.: Integrative self-sorting: A versatile strategy for the construction of complex supramolecular architecture. *Chem. Soc. Rev.* **2015**, *44*, 779.

(18) Zhang, Q.; Tian, H.: Effective integrative supramolecular polymerization. *Angew. Chem. Int. Ed.* **2014**, *53*, 10582.

(19) Jiang, W.; Winkler, H. D. F.; Schalley, C. A.: Integrative self-sorting: Construction of a cascade-stoppered hetero[3]rotaxane. *J. Am. Chem. Soc.* **2008**, *130*, 13852.

(20) Jiang, W.; Schalley, C. A.: Integrative self-sorting is a programming language for high level self-assembly. *Proc. Natl. Acad. Sci. U. S. A.* **2009**, *106*, 10425.

(21) Jiang, W.; Sattler, D.; Rissanen, K.; Schalley, C. A.: [4]pseudorotaxanes with remarkable self-sorting selectivities. *Org. Lett.* **2011**, *13*, 4502.

(22) Huang, Z.; Yang, L.; Liu, Y.; Wang, Z.; Scherman, O. A.; Zhang, X.: Supramolecular polymerization promoted and controlled through self-sorting. *Angew. Chem. Int. Ed.* **2014**, *53*, 5351.

(23) William C. Cromwell, K. B., and Maurice R. Eftink: Cyclodextrin-adamantanecarboxylate inclusion complexes: Studies of the variation in cavity size. *J. Phys. Chem.* **1985**, *89*, 326.

Chapter 4

Study of Photoinduced Electron Transfer in Donor-β-Cyclodextrin-Acceptor Supramolecular Nano-fibers Under Aqueous Conditions

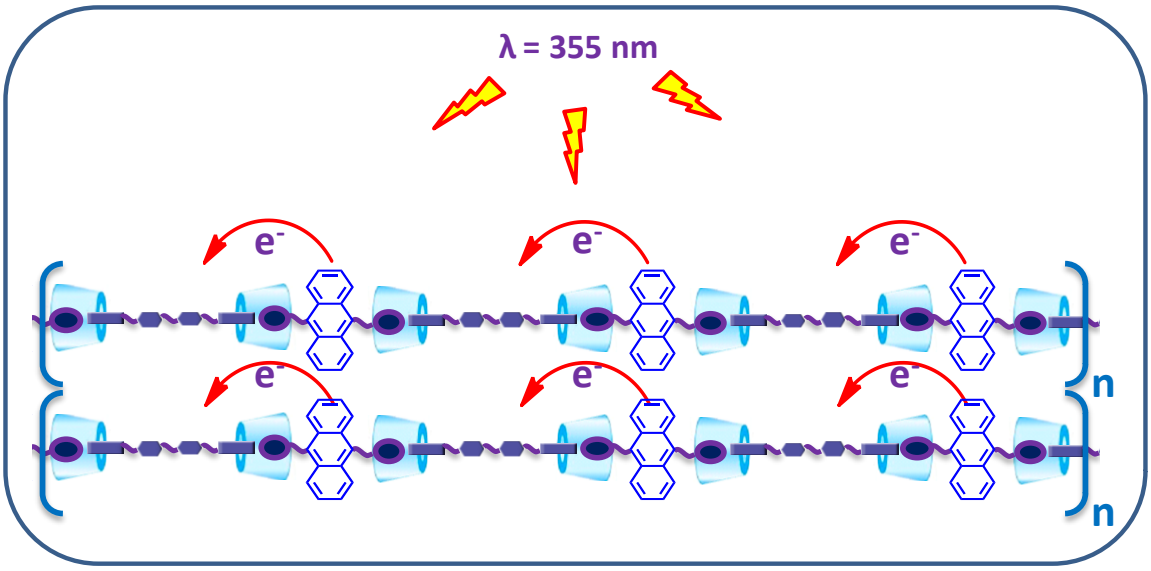

4.1. Abstract

This chapter deals with the study of photoinduced electron transfer (PET) process in a self-assembled donor-acceptor system in an aqueous medium which resulted in the formation of a long-lived charge separated state. We have selected anthracene as the donor and attached two adamantyl groups to its 9- and 10- positions to give the ditopic derivative AD-AN-AD, which now has two sites for the inclusion binding with β-CD cavity. AD-AN-AD in the presence of two equivalents of β-CD formed a stable host-guest complex β-CD⊂AD-AN-AD⊃β-CD in the aqueous medium which was characterized by ^{1}H NMR titration, ITC and UV-visible spectroscopic studies. Further, we observed that the β-CD⊂AD-AN-AD⊃β-CD bis-inclusion complex spontaneously self-assembled into a

rigid supramolecular polymer as confirmed by TEM, AFM and 2D-WAXS studies. The acceptor used in this study is a bis-pyromellitic diimide derivative of 1,4-bis(4-pyridyl)ethane (PI-PI) and as mentioned in the previous chapter this molecule can undergo rim-binding interactions with two β-CD residues. The addition of one equivalent of PI-PI to β-CD⊂AD-AN-AD⊃β-CD resulted in the formation of supramolecular nano-fibers which were different from the β-CD⊂AD-AN-AD⊃β-CD nano-structures. A possible structure for this three-component nano-structure is proposed. We observed efficient PET taking place in three component nano-structure upon excitation of the anthracene chromophore. The PET process was studied by steady state fluorescence quenching, nanosecond laser flash photolysis and EPR techniques. The PET in β-CD/AD-AN-AD/PI-PI system resulted in the formation of radical cation of AN and radical anion of PMDI which survived for nearly 59 μs in the aqueous medium. The lifetime of PMDI radical anion, which is normally unstable in water, could be attributed to wrapping of the anion radical in supramolecular polymeric environment.

4.2. Introduction

Conversion of solar energy into chemical energy in the form of chemical fuels such as hydrogen sometimes referred to as artificial photosynthesis, has been one of the top priority research areas in Chemistry and Physics for the last three decades. The artificial photosynthesis inspired by natural photosynthesis includes the design of artificial systems capable of harvesting sunlight and to store it in the form of chemical bonds. Natural photosynthesis generally stores energy in the form of glucose but a chemist can think of very simple molecule namely hydrogen to begin with, for storing solar energy. This can be achieved if water can be split into hydrogen and oxygen using sunlight (solar water splitting).[1,2] Hydrogen is considered as a clean fuel because burning of hydrogen will not produce hazardous emissions and also the energy stored per mole of

hydrogen is higher compared to fossil fuels.[3] It should be noted that 71% of earth's surface is covered with water and the sun is the primary energy source for the planet. Hence the photolysis of water using sunlight could solve earth's energy crisis to a large extent and artificial photosynthesis aims at achieving this goal. Despite large numbers of experimental and theoretical work carried out in this area for the last three decades, artificial photosynthetic methods are still confined to the laboratory when compared to the solar cell industry which is a mature technology today. This is mainly because water can only absorb sunlight in the far UV region, most of which is blocked by the ozone layer. Hence suitable organic/inorganic systems capable of absorbing visible light and reducing water into molecular hydrogen need to be developed. After absorbing the solar energy, these systems should efficiently transfer the absorbed energy to a reaction center where water splitting occurs and the mechanism may involve energy transfer/electron transfer or a combination of the two.[4,5]

Electron transfer (ET) involves the transfer of an electron from a donor moiety (D) to an acceptor moiety (A) and the process can take place with the help of light, heat, and sonication or even spontaneously. For example, during the formation of ionic bonds the valence electrons are lost from one atom (oxidation) which is gained by another (reduction). ET process which takes place with the aid of light and which does not involve making and breaking of chemical bonds is called photoinduced electron transfer (PET).[6,7] The products formed in this process are the radical cation of donor ($D^{\bullet+}$) and radical anion ($A^{\bullet-}$) of the acceptor. Upon shining light on the D/A pair, either D or A goes to an excited state and within the short excited-state lifetime ET occurs from donor to acceptor. This ET process is represented by Equation 4.1. The $D^{\bullet+}/A^{\bullet-}$ pair formed in the ET process is referred to as charge separated (CS) state and generally this is very short-lived because of the back electron transfer (BET) which regenerates the D/A system in its

ground state. A schematic representation of PET process is shown in Figure 4.1a. The BET process is the severe limitation of PET and close proximity of D and A favors both PET and BET and hence the CS states formed in such cases would be very short-lived.

$$D + A \xrightarrow{hv} D^{\bullet+} + A^{\bullet-} \qquad (4.1)$$

The water splitting reaction represented by Equations 4.2 and 4.3 is a multi-electron transfer process and requires 1.23 eV per electron transferred. Thus it is possible to split water if energy stored in CS state is more than 1.23 eV and if the CS state is sufficiently long-lived.

$$2H_2O \longrightarrow O_2 + 4H^+ + 4e^-, \quad E^0\,(pH = 7) = 0.82\ V\ vs\ NHE \qquad (4.2)$$

$$2H_2O + 2e^- \longrightarrow H_2 + 2OH^-, \quad E^0\,(pH = 7) = -0.41\ V\ vs\ NHE \qquad (4.3)$$

The $D^{\bullet+}$ formed in PET process in Equation 4.1 can take an electron from water to produce molecular oxygen if the oxidation potential (E_{ox}) of D is > 0.82 V and $A^{\bullet-}$ can utilise its electron to reduce water to molecular hydrogen, if the reduction potential (E_{red}) of A is more negative than -0.41 V. Thus, the reactions taking place in water splitting can be represented by Equations 4.4 - 4.6. It should be noted that, during the water splitting reaction the D and A are regenerated and the cycle can continue further.[5]

$$H_2O + 2D^{\bullet+} \longrightarrow \tfrac{1}{2}\,O_2 + 2H^+ + 2D \qquad (4.4)$$

$$2H^+ + 2A^{\bullet-} \longrightarrow H_2 + 2A \qquad (4.5)$$

$$H_2O + 2D^{\bullet+} + 2A^{\bullet-} \longrightarrow H_2 + \tfrac{1}{2}O_2 + 2D + 2A \qquad (4.6)$$

A detailed understanding of the ET processes taking place in natural photosynthetic reaction center can suggest several important ideas for designing artificial photosynthetic systems. It has been observed that a CS state with a quantum yield (Φ_{CS}) of near unity is obtained in the natural photosynthetic system with lifetime close to 1 s.[8] The purple bacterial reaction center remains as the best 'model system' for both natural and artificial photosynthetic complexes, which is schematically depicted in Figure 4.1b.

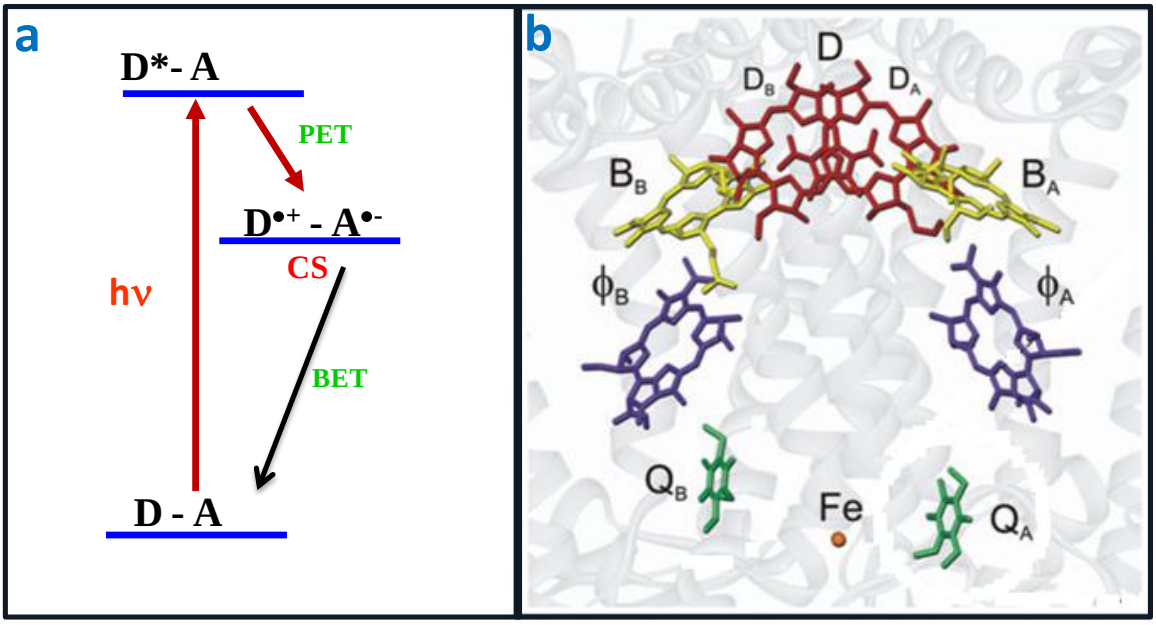

Figure 4.1. a) Schematic of PET and BET processes. b) Photosynthetic reaction center of purple bacteria.

The reason for high lifetime of CS state in the natural photosynthetic system can be attributed to the fact that the donors and acceptors are placed at specific distances and orientations relative to one another within a protein matrix. This rigidity in the system facilitates the ET process and hinders the BET process. In the end the $D^{\bullet+}$ and $A^{\bullet-}$ are separated by a lipid bilayer which prevents the stored energy getting wasted by BET.[9]

For the last several years, significant efforts have been devoted by researchers across the globe to design artificial systems to produce long-lived CS states. One of the important strategies adopted was to covalently link several donors and acceptors for

sequential ET to take place. Fukuzumi's group from Osaka University is one of the leading groups in this area and the group has prepared several dyads (D-A), triads (D-A_1-A_2 or D_1-D_2-A), and tetrads and studied PET processes in these systems. For example they have reported a tetrad system (Figure 4.2) which gave an extremely long-lived CS state with τ_{CS} = 380 ms in frozen benzonitrile.[10] Photo excitation (λ_{ex} = 532 nm) of this system initiated a cascade of energy transfer and multistep ET to finally produce a CS state comprising of ferricenium ion-C_{60} radical anion pair ($Fc^{\bullet+}/C_{60}^{\bullet-}$). This system represents one of the longest lived CS states whose lifetime is comparable to that of natural photosynthetic center even though the quantum yield of CS state is not very high (Φ_{CS} = 0.2).

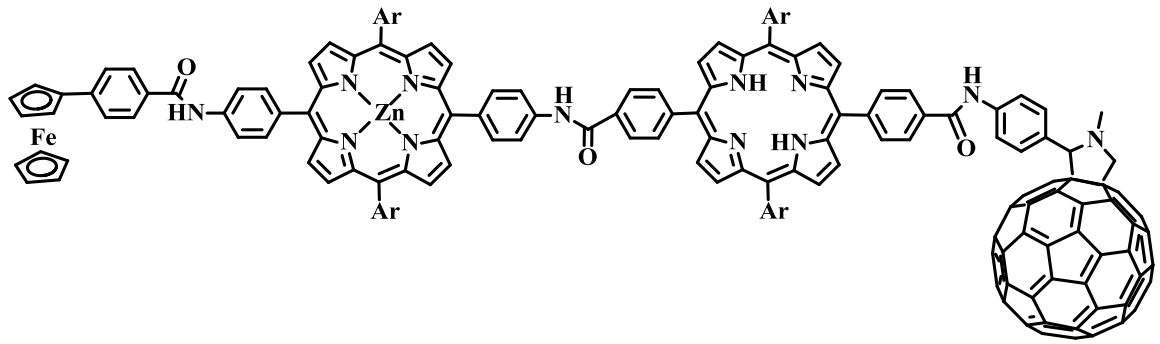

Figure 4.2. The molecular structure of a tetrad system which shows a lifetime of 0.38 s for the CS state.

In some of the polyads Φ_{CS} was found to be high but gave relatively low τ_{CS}. For example, Gust *et al.* in 1990 synthesized the pentad system shown in Figure 4.3, which exhibited τ_{CS} = 200 μs with overall quantum yield of 0.6.[11] Excitation of the free-base porphyrin of the pentad in dichloromethane solution initiated a series of ET within the molecule and finally gave a CS state with carotene radical cation and benzoquinone radical anion. The distance between radical cation and radical anion centers is very large which reduces the BET rate.

As is clear from the above examples it is necessary to connect multiple donors and acceptors covalently to obtain CS states with reasonably good lifetimes and quantum yields. However, the synthetic complexity involved in connecting multiple D and A moieties by covalent bonds must be taken into account. Further, purification of these large molecules can be a tedious job because PET reactions require compounds with utmost purity.

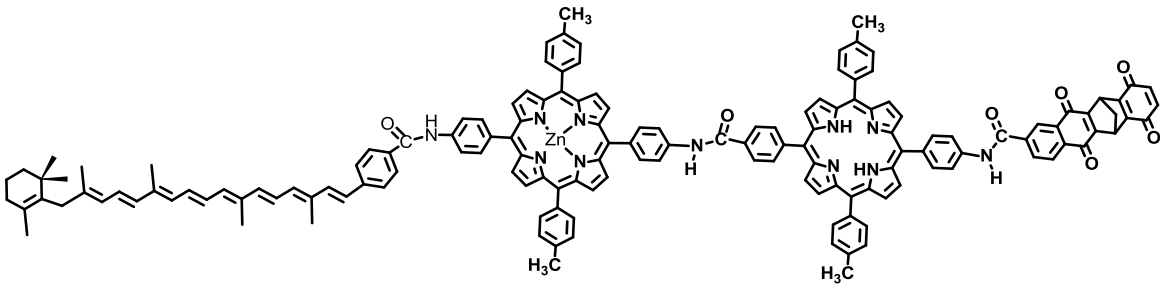

Figure 4.3. The molecular structure of pentad used in the study of PET.

Because of the recent developments in supramolecular chemistry, researchers started linking D and A by non-covalent interactions such as hydrogen-bonding, π–π stacking, hydrophobic/hydrophilic interactions etc. This idea is again borrowed from the natural photosynthetic center wherein the D and A are linked only by non-covalent interactions in the protein matrix. There are several reports in the literature in which D and A are connected by non-covalent interactions. For example, Harriman et al. as early in 1992 have reported a system in which porphyrin donor is attached to quinone acceptor by hydrogen bonding interactions and efficient PET has been observed between them.[12] Our group also reported PET between donor appended on Cyclodextrin (CD) and acceptor included in the CD cavity.[13,14] In almost all these systems a discrete self-assembled unit of D and A is formed and these did not exhibit any tendency to form ordered nano-structures.

In a recent report, Huber et al. studied PET between D and A systems embedded within a polymer.[15] A polymeric system having thiophene-linked fluorine as repeating units served as the donor and cationic fullerene served as acceptor (Figure 4.4) in this study. When mixed in water these molecules self-assembled to form a fiber network in which the D and A moieties are embedded. Upon photo-excitation the yellow color of the mixture turned to dark green because of the polaron formation which survived for nearly 2 weeks. The CS state formed with $\Phi_{CS} = 0.25$ was characterized by EPR and UV-Visible spectroscopy which showed characteristic absorption bands of donor radical cation and acceptor radical anion. In general, radical anions are not stable in water. In the present case the fullerene radical anion was highly stable most probably due to the protection afforded by the fibrous network which may be preventing it from coming into contact with water. A schematic representation of the molecular structures and PET process are shown in Figure 4.4.

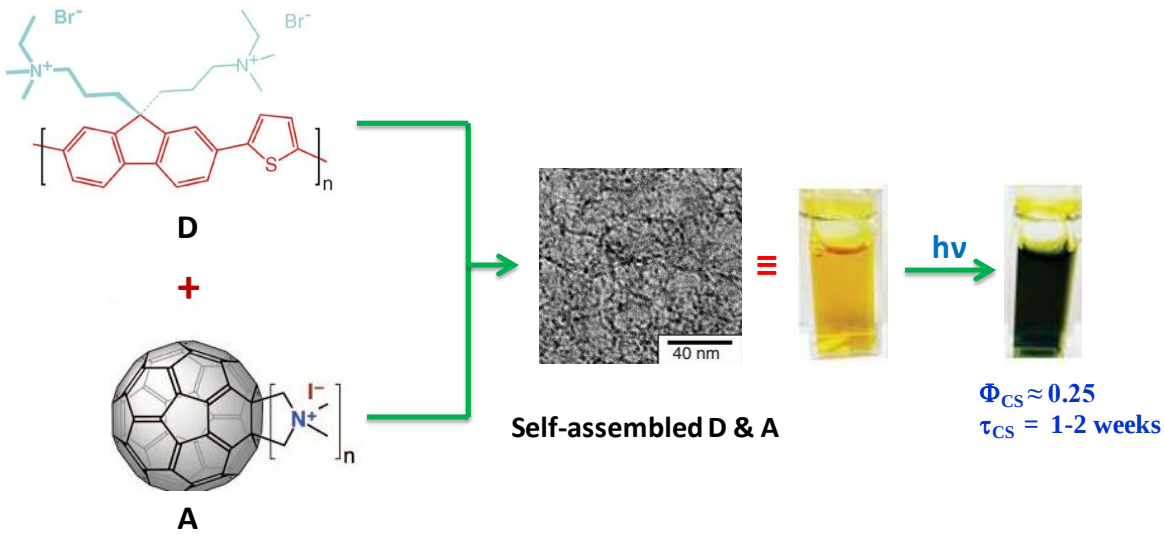

Figure 4.4. Schematic of the self-assembly of D and A leading to the formation of long-lived CS state.

The above publication has conveyed the idea that long-lived CS states may be attainable in water if D and A moieties are embedded within a fibrous network wherein

the D-A distances are fixed and D/A contacts which leads to facile BET are avoided. In Chapter 3 of this thesis we have described the formation of long fibers by joining together of vesicles. Our studies revealed that the fibrous system incorporated all the three components, namely β-CD, AD-AD and PI-PI. The PI-PI moiety is comprised of two pyromellitic diimide (PMDI) units and PMDI is known to be a good electron acceptor in PET reactions. If we can incorporate a donor moiety D in AD-AD to give, for example, AD-D-AD system, then integrative self-sorting in the three component system consisting of β-CD, AD-D-AD and PI-PI may lead to formation of fibrous networks. The fibrous system may have D and PMDI units at fixed distances apart and photo-excitation of D may lead to formation of a long-lived CS state. Our work in this direction is presented in this chapter.

For this study we have designed the ditopic molecule AD-AN-AD having a central anthracene unit which is linked to adamantane units through the 9- and 10-positions (Scheme 4.1). We expected this molecule to form a bis-inclusion complex with β-CD as shown in Scheme 4.1. Formation of the bis-inclusion complex was studied by ITC, UV-visible spectroscopy, fluorescence spectroscopy, fluorescence life-time studies and NMR titration experiments. Because of its amphiphilic nature, the bis-inclusion complex underwent further ordering which resulted in the formation of a supramolecular polymer as confirmed by atomic force microscopy (AFM), transmission electron microscopy (TEM) and wide-angle X-ray scattering (WAXS) experiments. The addition of one equivalent of PI-PI to this solution resulted in the formation of discrete nano-fibers as confirmed by ICD, TEM, WAXS and AFM experiments. We observed that the nano-fibers formed in this case were different to those formed in AD-AN-AD/β-CD case. Nanosecond laser excitation of the above three component system generated a CS state which survived for microseconds in the aqueous medium. The microsecond stability of

PMDI radical anion, which is otherwise unstable in water, could be attributed to the protection afforded to the anionic species by the supramolecular polymer.

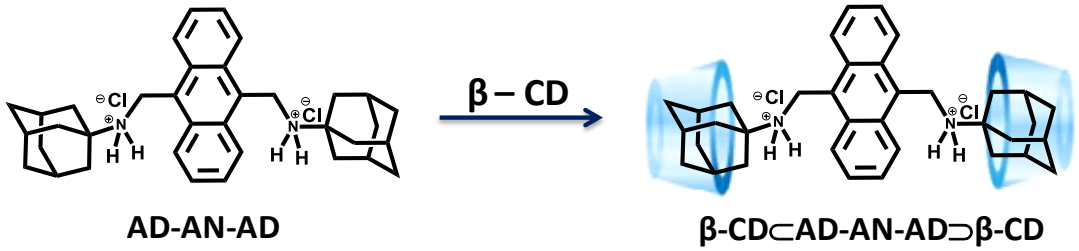

Scheme 4. 1. Structure of AD-AN-AD and its β-CD complex.

4.3. Results and discussions

4.3.1. Synthesis and characterization of molecules

Chemical modification of anthracene at the 9- and 10- positions is well reported in the literature. For the synthesis of AD-AN-AD we adopted a reported procedure[16] with necessary modifications which is shown in Scheme 4.2.

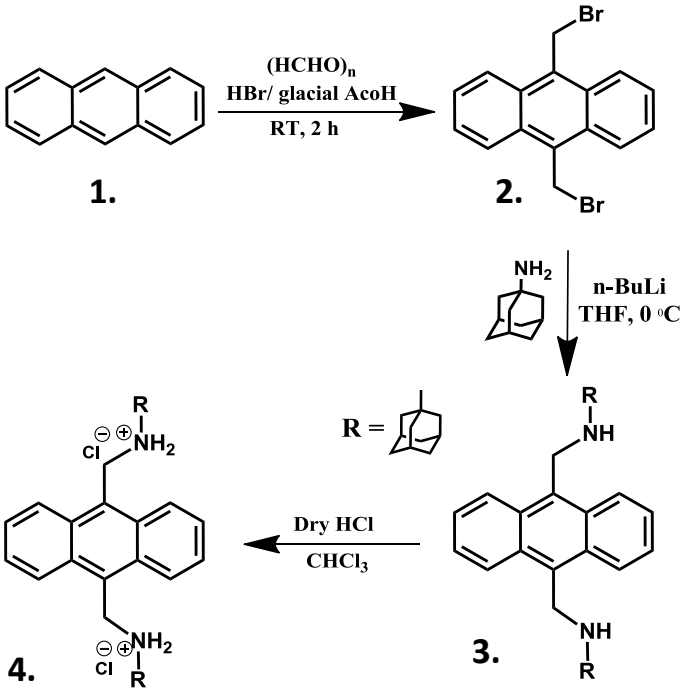

Scheme 4.2. Scheme showing steps involved in the synthesis of AD-AN-AD.

The procedure involved reaction of anthracene (**1**) with Paraformaldehyde in the presence of HBr in acetic acid to give 9,10-bis(bromomethyl)anthracene (**2**) which was purified by recrystallization from toluene. **2** was then treated with a solution of 1-adamantylamine and n-butylithium in dry THF to obtain compound **3** in 61% yield. **3** was converted to the water-soluble bis-hydrochloride salt (**4**) by treating with dry HCl in $CHCl_3$. **4** was purified by repeatedly washing with dry $CHCl_3$. All the intermediates and final product were thoroughly characterized by ^{1}H and ^{13}C NMR, HRMS and FTIR techniques.

Synthesis and characterization of PI-PI used in this study was described in Chapter 3(section 3.3) of this thesis.

4.3.2. Host-guest complexation studies of AD-AN-AD and β-CD

The AD-AN-AD was found to be moderately soluble in water and solutions of millimolar concentration could be easily prepared. When two equivalents of β-CD were added to AD-AN-AD solution in water, a supramolecular host-guest complex β-CD⊂AD-AN-AD⊃β-CD was formed in which the adamantane moieties of AD-AN-AD were encapsulated into β-CD cavity as shown in Scheme 4.1. This host-guest interaction was confirmed by ITC titration, UV-Visible spectroscopy, fluorescence spectroscopy and NMR titration and details are given in following sections.

4.3.2.1. Isothermal titration calorimetry studies

To measure the heat released during the interaction between AD-AN-AD and β-CD we have carried out ITC studies and the titration curve for the experiment is shown in Figure 4.5. ITC experiment was carried out by taking β-CD (10 mM, 40 µL) in the syringe and AD-AN-AD (0.1 mM, 200 µL) in the cell. Heat changes observed for AD-

AN-AD/β-CD complexation was moderately high and fitting of titration curve yielded values of K_a = 6.07 × 10^3 M^{-1}, ΔH = -24.4 kJ mol^{-1} and ΔS = -9.61 J mol^{-1} deg^{-1} and n = 1.93. The value of n (~ 2) indicates that AD-AN-AD has two binding sites for β-CD. Thus ITC studies confirmed that a 1:2 host-guest complex is formed between the two as shown in Scheme 4.1, which we designate here as β-CD⊂AD-AN-AD⊃β-CD.

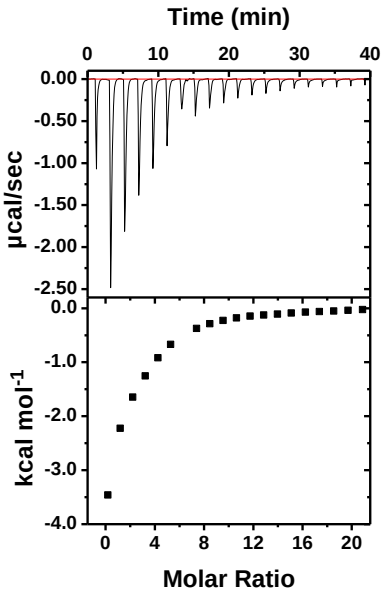

In cell (AD-AN-AD)	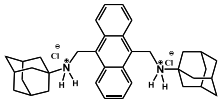	0.1 mM, 200 µL
In syringe (β-CD)		10 mM, 40 µL

Number of binding sites	1.93
Binding constant M^{-1}	6.07E3
ΔH kJ/mol	-24.4
ΔS J/mol/deg	-9.61

Figure 4.5. The ITC titration curve and fit parameters obtained for the titration of β-CD with AD-AN-AD.

In Chapter 2 of this thesis we described the β-CD⊂AD-AD⊃β-CD bis-inclusion complex, where ITC experiments gave values of K_a = 6.4 × 10^4 M^{-1}, ΔH = -81.9 kJ mol^{-1}, ΔS = -178 J mol^{-1} deg^{-1} and n = 1.9. A comparison would show that the K_a value obtained in the present case is one order lower. Further, the magnitudes of ΔH and ΔS also have decreased considerably. The reason for the low values in the present case can be attributed to the presence of positively charged sites near the adamantane moieties in AD-AN-AD. These charges are highly hydrated and more stable in water compared to the CD cavity and hence prefer to stay outside the cavity. Penetration of the adamantane groups

into the cavity in this case would be shallow compared to the β-CD⊂AD-AD⊃β-CD case, which ultimately explains the lower stability of the bis-inclusion complex.[17]

4.3.2.2. UV-visible absorption spectroscopy studies

Absorption spectroscopy is widely used to confirm the interaction of chromophores with CDs and literature gives several such examples.[18] In the present case, we have recorded the absorption spectrum of AD-AN-AD in the absence and presence of β-CD. The anthracene chromophore has absorption in the 240-270 nm and 320-400 nm regions and both these absorptions are shown in Figure 4.6. In Figure 4.6 the blue trace represents the absorption profile of AD-AN-AD and the red trace represents that of AD-AN-AD in the presence of two equivalents of β-CD. We observe that the spectral profile is similar for AD-AN-AD in the absence and presence of β-CD, indicating that the AN chromophore is not included in the β-CD cavity and is completely exposed to water.

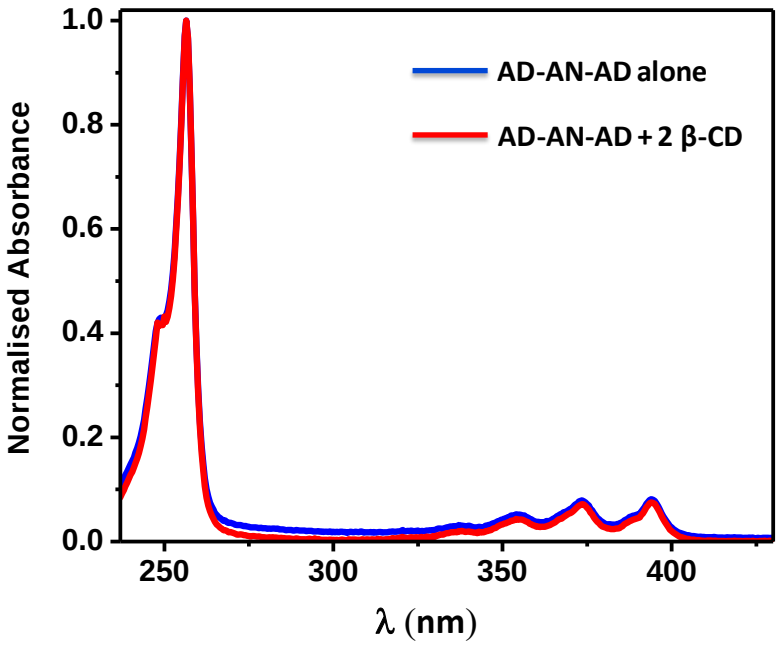

Figure 4.6. The absorption spectrum of AD-AN-AD in the absence (blue) and presence (red) of β-CD recorded in aqueous medium.

4.3.2.3. Fluorescence spectroscopy and fluorescence lifetime studies

It is widely reported in literature that, encapsulation of chromophore into CD cavity would affect the fluorescence spectra of compounds.[18,19] In order to confirm that the anthracene moiety of AD-AN-AD is not entering the cavity of β-CD, we have carried out fluorescence studies of AD-AN-AD in the absence and presence of β-CD (Figure 4.7a). It is evident from Figure 4.7a that there are no changes in the spectral profile of AD-AN-AD upon addition of β-CD which confirms that the anthracene moiety is not encapsulated in the CD cavity. Further, the fluorescence quantum yield of AD-AN-AD and AD-AN-AD/β-CD systems was found to be same (~71%) confirming our proposal. Along with fluorescence spectrum, we have also measured fluorescence lifetime of AD-AN-AD in the presence and absence of β-CD by time-correlated single photon counting (TCSPC) method. The fluorescence of AD-AN-AD showed a mono-exponential decay (Figure 4.7b) with a lifetime of 10.1 ns. The decay pattern as well as lifetime remained unaltered upon reaction with β-CD which supports the fluorescence spectroscopy experiments.

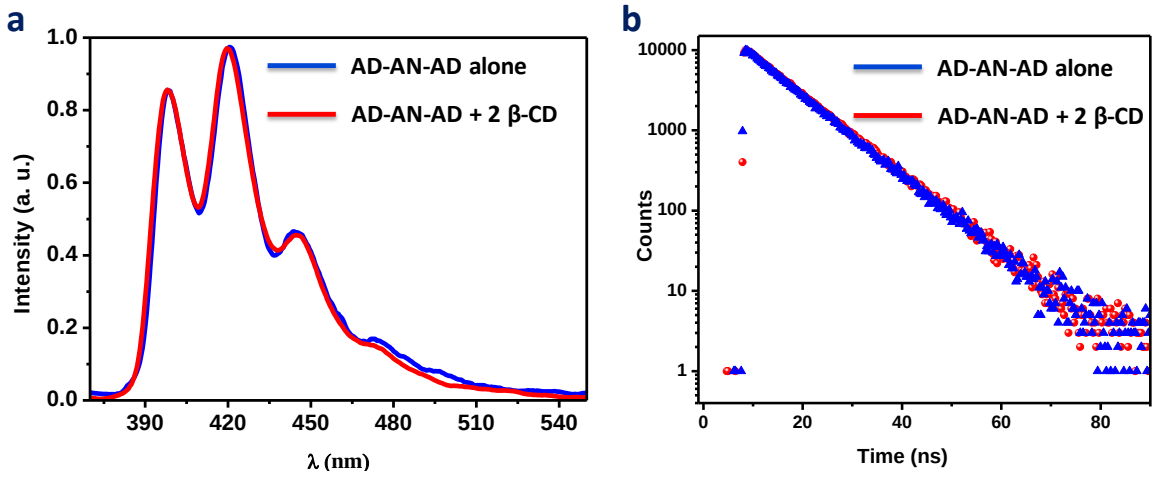

Figure 4.7. (a) The emission spectrum of AD-AN-AD in the absence (blue trace) and presence (red trace) of β-CD (2 eq.). (b) The fluorescence decay profiles of AD-AN-AD (blue trace) and AD-AN-AD/β-CD (red trace) system.

4.3.2.4. ^{1}H NMR titration studies

In order to get further details about the AD-AN-AD/β-CD inclusion complex, we carried out ^{1}H NMR titration experiments. Figure 4.8 shows the results of ^{1}H NMR titration experiment of AD-AN-AD (1 mM) with varying concentration of β-CD, where the concentration of β-CD is varied from 0 to 2 equivalents.

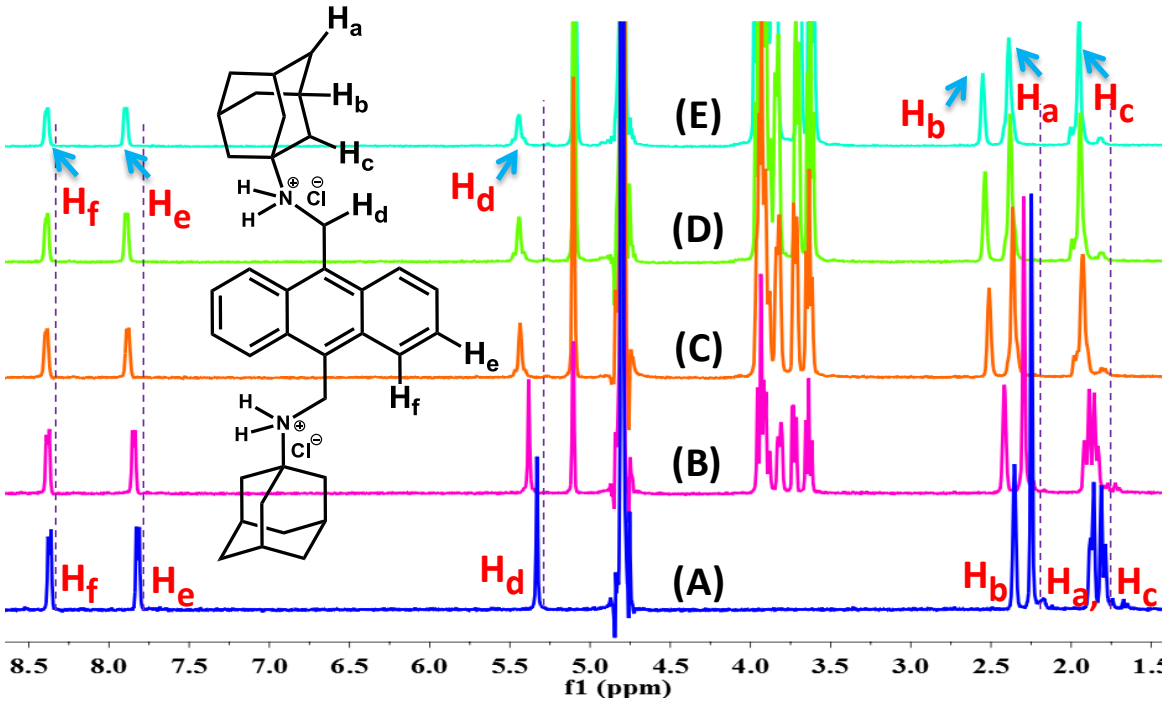

Figure 4.8. ^{1}H NMR titration spectra of AD-AN-AD (1 mM) in the absence (A) and presence (B-E) of β-CD (0.5 – 2 eq.) in D_2O.

In Figure 4.8, the lower panel shows the assignment of proton signals of AD-AN-AD and shift in the peak position is indicated by arrow in the top panel. The adamantane group of AD-AN-AD showed three clear signals between δ 1.4–2.5 ppm corresponding to H_a, H_b and H_c protons. With increase in the concentration of β-CD, these protons showed a downfield shift which is indicative of encapsulation of this moiety in the CD cavity (see Chapter 2 also). Apart from this phenomenon, with increase in the concentration of β-CD, we have seen the downfield shift of anthracene protons (H_e and H_f) along with a prominent shift in H_d protons. Because of the presence of positive charge near

adamantane, entry of H_d protons into β-CD cavity can be ruled out. Also, the molecular dimensions of β-CD and adamantane will not allow entry of H_d protons into β-CD cavity. Nevertheless the H_d protons showed large shift and peak broadening in the presence of β-CD. This suggests that interactions other than inclusion binding are also occurring in the AD-AN-AD/β-CD system. We believe that secondary interactions leading to formation of nano structures are taking place in the system. In order to probe such interactions and to see if any nano-structures are formed through these interactions, the AD-AN-AD/β-CD system was subjected to TEM, AFM and WAXS studies.

4.3.3. Self-assembly studies of AD-AN-AD and β-CD

The previous sections confirmed that AD-AN-AD interacts with two equivalents of β-CD in aqueous medium to get β-CD⊂AD-AN-AD⊃β-CD supramolecular complex. We observed an unexpected downfield shift in the aromatic and H_d protons of AD-AN-AD in the presence of β-CD (Figure 4.8) in ^{1}H NMR experiments. These shifts can be attributed only to the secondary interactions taking place in the β-CD⊂AD-AN-AD⊃β-CD bis-inclusion complex. In order to identify the supramolecular nano-structures formed by such interactions, we have carried out TEM, AFM and WAXS studies of this bis-inclusion complex which are discussed below.

4.3.3.1. High-resolution transmission electron microscopy studies

Figure 4.9 shows the HRTEM image of the fibrous structures obtained from an aqueous sample containing AD-AN-AD (10^{-5} M) and β-CD (2×10^{-5} M). The figure shows rigid nano-fibers with width ranging from 50-200 nm and several micrometers in length. Figure 4.9b shows the zoomed in portion of Figure 4.9a which shows that the nano-fibers do not have characteristic features of nano-tubes or twisted fibers. The TEM

image confirmed self-assembly of the β-CD⊂AD-AN-AD⊃β-CD bis-inclusion complex into supramolecular nano-fibers.

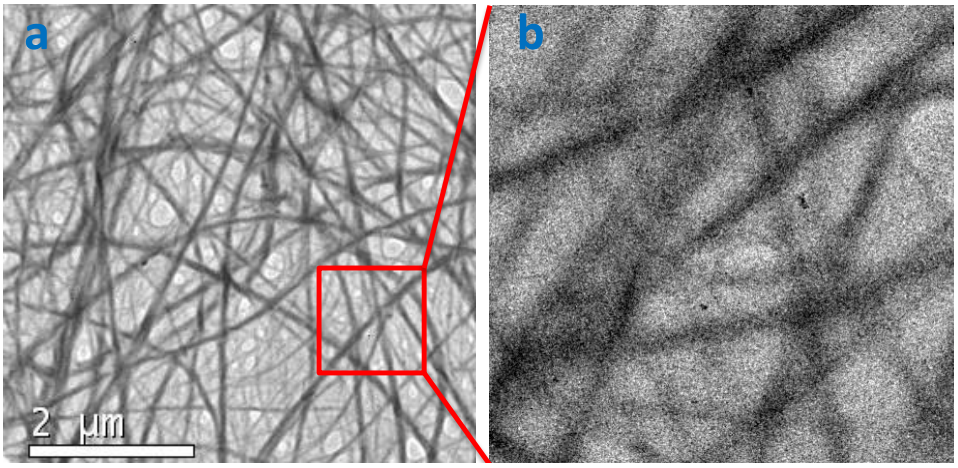

Figure 4.9. The HRTEM images of AD-AN-AD (10^{-5} M)/β-CD (2×10^{-5} M) system in water.

4.3.3.2. Atomic force microscopy studies

Figure 4.10a shows the AFM height image and Figure 4.10b shows the AFM 3D image obtained from an aqueous solution containing AD-AN-AD (10^{-5} M) and β-CD (2×10^{-5} M) cast on freshly cleaved mica surface.

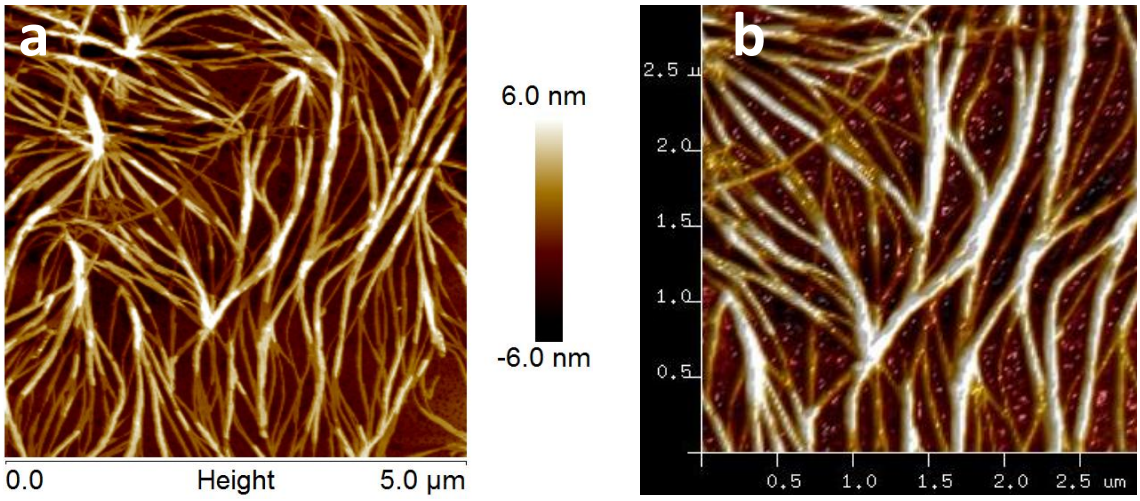

Figure 4.10. The AFM height image (a) and 3-D image (b) of AD-AN-AD (10^{-5} M)/β-CD (2×10^{-5} M) system in water.

The Figure 4.10 shows nano-fibers of several micrometers of length and 50-200 nm width with height varying in a small range of 4-8 nm. Thus the aspect ratio of these fibers (width/height ratio) is very high which is characteristic of nanotape-like structures. The results obtained in the AFM experiment are in good agreement with TEM results, and in both images the nano-fibers appeared as coiled structures with branching at some junctions.

4.3.3.3. 2D-Wide angle X-ray scattering studies

The TEM and AFM studies have revealed that the β-CD⊂AD-AN-AD⊃β-CD bis-inclusion complex got self-assembled into long fibrous or tape-like structures. In order to obtain molecular level information about the self-assembly WAXS studies were carried out on a dried film obtained from the aqueous β-CD⊂AD-AN-AD⊃β-CD solution. The concentration of AD-AN-AD (5×10^{-4} M) and β-CD (10^{-3} M) used was relatively higher so as to get good films.

Figure 4.11 shows the X-ray scattering pattern obtained for this film and the corresponding 2D plot is shown as its inset. In Figure 4.11, several distinct X-ray scattering peaks could be seen which confirmed a well ordered crystalline self-assembly for the β-CD⊂AD-AN-AD⊃β-CD bis-inclusion complex. We propose that scattering from different planes of self-assembled nano-fibers occurs to yield the observed multiple peaks in the spectrum. Of these peaks we could identify scattering peaks at 2θ of 5.83° and 11.02° which correspond, respectively, to *d* values of 15.14 Å and 7.89 Å which could be assigned to molecular dimensions of β-CD. Also sharp scattering occurred at a 2θ angle of 8.9° (*d* = 9.5 Å) which corresponds to the molecular length of anthracene unit. We also could identify a set of four peaks in the 2θ range of 23.5° – 26.07° which correspond to *d* values of 3.8 Å, 3.6 Å, 3.47 Å and 3.41 Å. It is reported in the literature

that the π-stacking of anthracene occurs at a distance of 3.3 Å to 3.87 Å depending on the type of packing of the anthracene core. The four peaks observed in Figure 4.11 are of relatively small intensity which suggests that there is a tendency for π-stacking for the anthracene chromophore in the β-CD⊂AD-AN-AD⊃β-CD self-assembled state. The effective π-stacking of anthracene unit is severely hindered because of larger molecular dimensions of β-CD (section 4.3.4). Thus the WAXS experiment further confirmed the TEM and AFM results which suggested a highly crystalline morphology for self-assembled β-CD⊂AD-AN-AD⊃β-CD bis-inclusion complex.

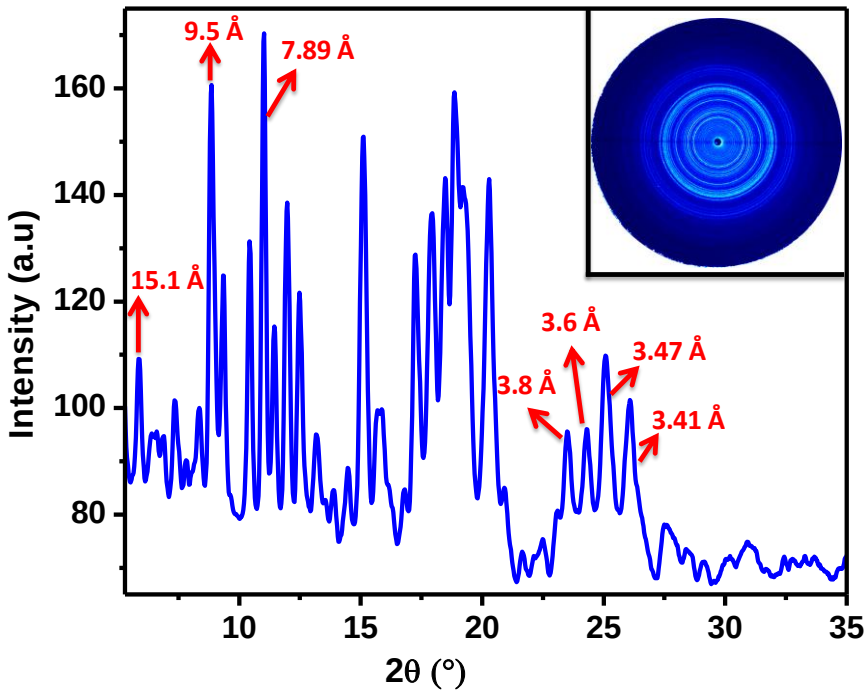

Figure 4.11. The WAXS spectrum obtained for AD-AN-AD (5×10^{-4} M)/β-CD (10^{-3} M) self-assembled system with inset showing the corresponding 2D plot.

4.3.3.4. Solvent dependent absorption spectroscopy studies

The absorption spectrum of anthracene has electronic transitions in the 320 to 400 nm and 240 to 265 nm regions. It is reported that the shape of the high energy electronic transition (240 to 265 nm) is strongly dependent on the degree of interaction between two

aromatic rings in self-assembled anthracene-containing systems.[20,21] This absorption consists of a major peak at 256 nm and a shoulder at 248 nm. The component around 256 nm corresponds to the absorption of a non-perturbed anthracene chromophore while the component near 248 nm represents electronically interacting anthracene units. Calculations showed that the intensity of the 248 nm peak increases as the interaction between anthracene units increases with a concomitant decrease in the intensity of 256 nm peak. Hence the intensities of these two peaks can indicate the strength of anthracene-anthracene interactions in self-assembled systems. In order to understand whether the anthracene moieties are really interacting with each other, we have recorded absorption spectra of AD-AN-AD/β-CD in different solvent compositions of DMSO and water and the results are shown in Figure 4.12.

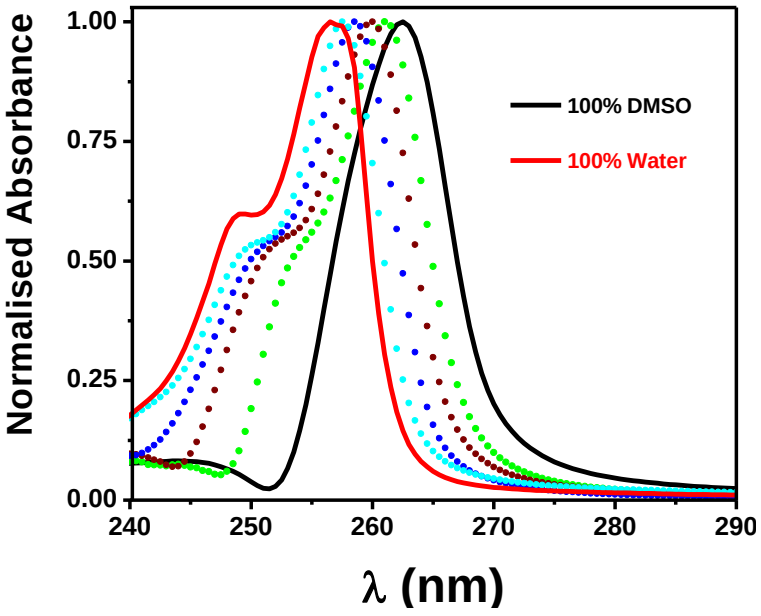

Figure 4.12. The absorption spectra of AD-AN-AD/β-CD in DMSO/water mixtures where the percentage of water increased from 0-100%.

In Figure 4.12, the traces in black and red respectively indicate the absorption of AD-AN-AD/β-CD system in 100% DMSO and 100% water while the broken lines are spectra recorded in DMSO/water mixtures of different compositions. We observed a

single peak centered around 260 nm in DMSO and upon adding water an additional shoulder peak started appearing near 250 nm. When the absorption was taken in 100% water the peaks at 248 and 256 nm are clearly seen. But the intensity of 248 nm peak was relatively smaller when compared to 256 nm peak in water suggesting that the electronic states of chromophore is largely non-perturbed. Thus we propose that for AD-AN-AD/β-CD system in water, anthracene chromophore is weakly interacting with each other.

4.3.4. Mechanism of self-assembly of AD-AN-AD/β-CD bis-inclusion complex

Previous experiments have confirmed that β-CD⊂AD-AN-AD⊃β-CD bis-inclusion complex was spontaneously self-assembled into supramolecular polymers. A schematic representation of most probable mechanism of this self-assembly process is shown in Scheme 4.3. In the molecule AD-AN-AD, the central anthracene moiety is highly hydrophobic and hydrophobic anthracene moieties have been employed successfully in the literature for the fabrication of functional materials. Also, the terminal adamantyl groups of AD-AN-AD are highly hydrophobic because of its hydrocarbon structure. But in β-CD⊂AD-AN-AD⊃β-CD bis-inclusion complex, both the adamantyl groups are encapsulated into the β-CD cavity which masks the hydrophobic character of adamantane. Thus in β-CD⊂AD-AN-AD⊃β-CD, the terminal β-CD along with adamantane with its amine hydrochloride part constitutes a hydrophilic group while the central π-electron rich anthracene is hydrophobic as shown in Scheme 4.3. Hence the β-CD⊂AD-AN-AD⊃β-CD bis-inclusion complex behaves like a typical bola-amphiphile formed by secondary interactions which can be called a ‘supramolecular amphiphile’ (SA).

The self-assembly of SA resulting in the formation of nano-structures is well documented in literature which is briefly discussed in Chapter 1 of this thesis. In some

cases, self-assembly of SA leading to formation of branched fibrous systems are also available.[22,23] After reviewing the literature, we propose a mechanism for the self-assembly of β-CD⊂AD-AN-AD⊃β-CD supramolecular complex which involves one-dimensional stacking of this complex as shown in Scheme 4.3.

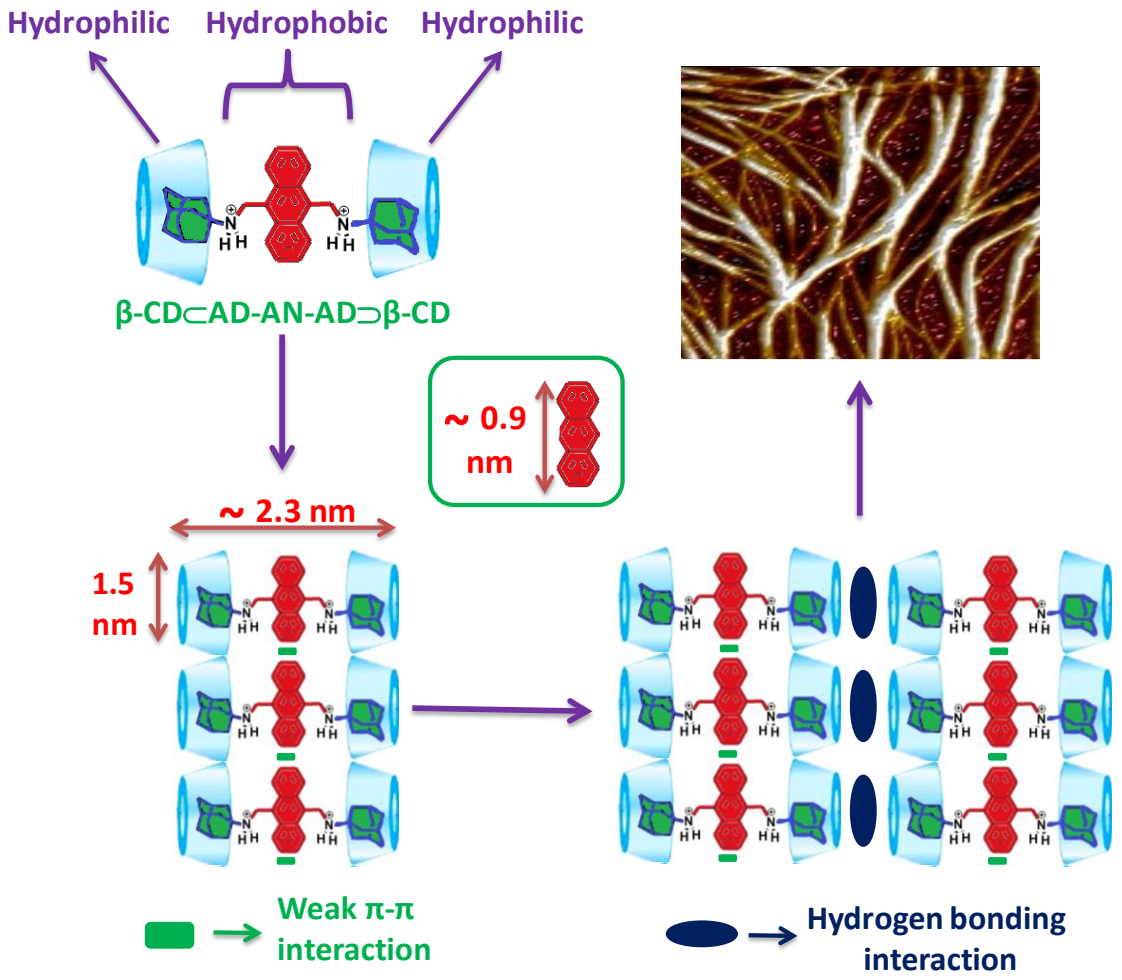

Scheme 4.3. Schematic representation of self-assembly process in AD-AN-AD/β-CD system.

The width of the outer-surface of the wider rim of β-CD is 1.5 nm and vertical length of anthracene chromophore is 0.9 nm (calculated from energy minimized structure) which are shown in Scheme 4.3. Thus anthracene cannot stack by its usual π-stacking fashion as the width of CD is larger compared to the dimensions of anthracene. Nevertheless the following observations support the formation of weak π-stacking of

anthracene moieties: (1) a weak shoulder band that appears at 248 nm in the absorption spectrum of AD-AN-AD/β-CD system, (2) shift and broadening of aromatic protons in the ^{1}H NMR titration and (3) weak scattering in the π-stacking region in the WAXS spectrum. Thus we propose that the ends of anthracene units may be involved in weak π-stacking interactions as shown in Scheme 4.3.

In Scheme 4.3 we also present linear structures resulting from hydrogen bonding interactions involving the narrow rims of β-CD. Seven hydroxyl groups are present at the primary rim of β-CD which are not involved in any intramolecular hydrogen bonding. When two rims of β-CD are very close to each other, H-bonding interactions can occur as shown in Scheme 4.3 and several of such reports are available in literature. As there are two β-CD units per amphiphile, both ends of the amphiphile may be involved in H-bonding interactions leading to the formation of the observed fibers.

4.3.5 Self-assembly of AD-AN-AD/β-CD system in the presence of PI-PI

In Chapter 3 of this thesis, we have reported the synthesis of PI-PI, which is a ditopic 1,4-bis(4-pyridyl)ethane derivative bearing *tert*-butyl PMDI derivatives at both ends. We have shown that this molecule has propensity to undergo rim-binding interaction with two equivalents of β-CD to give a bis-rim binding complex designated as β-CD⊱PI-PI⊰β-CD (see Chapter 3). β-CD has the capacity to simultaneously hold an adamantane group in inclusion binding mode and a *tert*-butylPMDI derivative in the rim-binding mode to give ternary complexes and this aspect was also discussed in Chapter 3. We observed that PI-PI could recognize the supramolecular vesicle surfaces which were decorated by the primary rims of β-CD by rim-binding interaction which led to the fusion of vesicles to give long fibrous structures. Herein we observed that the AD-AN-AD/β-CD system forms long fibrous structures the formation of which involved hydrogen bonding

interactions involving the narrow rim of β-CD as shown in Scheme 4.3. If the AD-AN-AD/β-CD system has to undergo rim-binding with PI-PI, the long fibrous structures must break in order to provide a pathway for PI-PI to insert itself in between two narrow rims. In fact we observed that the AD-AN-AD/β-CD fibrous system interacts with PI-PI and the details are given in the following sections.

4.3.5.1. ICD studies of AD-AN-AD/β-CD/PI-PI system

In order to confirm that the PI-PI interacts with AD-AN-AD/β-CD in the rim-binding mode, we have recorded ICD spectra of AD-AN-AD/β-CD and AD-AN-AD/β-CD/PI-PI systems and the results are shown in Figure 4.13.

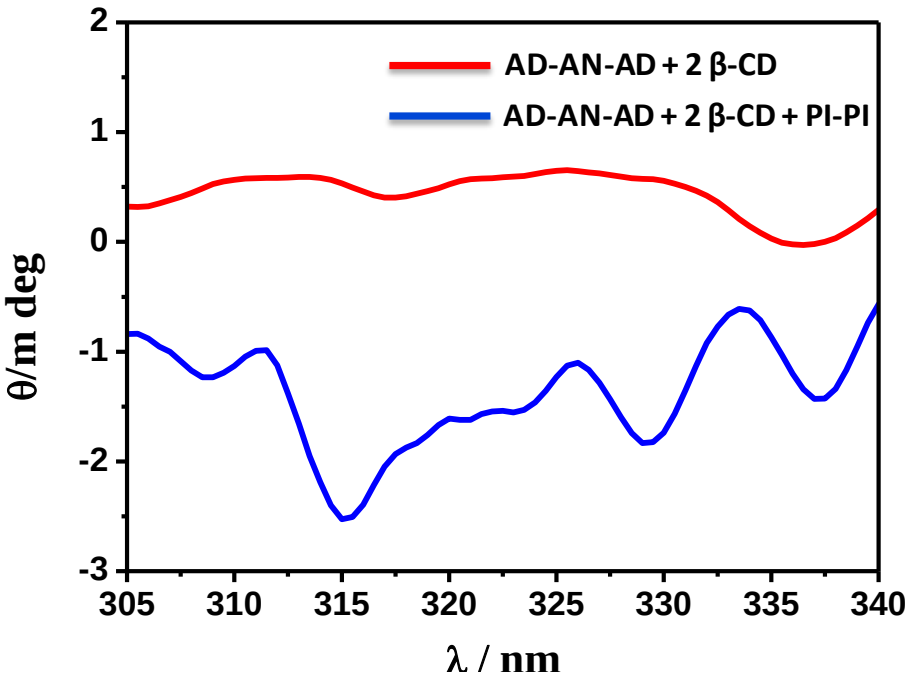

Figure 4.13. The ICD signals recorded for AD-AN-AD/β-CD (red trace) and AD-AN-AD /β-CD/PI-PI (blue trace).

Rim-binding interaction of PMDI with β-CD is characterized by the negative ICD signal around 320 nm. Figure 4.13 shows that AD-AN-AD/β-CD did not exhibit any CD signal. Upon adding one equivalent of PI-PI, negative CD signals develop around the

PMDI absorption (320 nm) indicative of the rim-binding interaction with PI-PI. Small negative absorptions develop in the absorption region of anthracene (> 330 nm) as well suggesting rearrangements of the AD-AN-AD/β-CD fibrous structure. The results suggest that PI-PI inserts itself into the AD-AN-AD/β-CD fibers through rim-binding interactions. The intensity of the ICD signal, however, is small suggesting that only a small fraction of PI-PI gets inserted into the fibrous structures.

4.3.5.2. TEM and AFM investigation of AD-AN-AD/β-CD/PI-PI system

Figure 4.14a shows the TEM image of AD-AN-AD (10^{-5} M)/ β-CD (2×10^{-5} M)/ PI-PI (10^{-5} M) system drop cast from an aqueous solution. Networked fibers could be seen in this image which confirms that the AD-AN-AD/β-CD/PI-PI three component system undergoes self-assembly in aqueous medium. The TEM image shows that, the morphology of nano-fibers obtained in this three component system (Figure 4.14a) is different compared with the morphology of the AD-AN-AD/β-CD system (Figure 4.9). In Figure 4.9 fibers of several micro meter lengths could be seen whereas in Figure 4.14a, the fibers were largely interwoven.

This argument is further confirmed by AFM studies. Figure 4.14b shows the AFM height image and Figure 4.14c shows the AFM 3D image of the three component system obtained by drop-casting an aqueous solution on freshly cleaved mica surface. In these figures the self-assembled networked fibers could be seen whose width and length are significantly shortened compared to the AD-AN-AD/β-CD system shown in Figure 4.10. Another significant difference of these fibers with AD-AN-AD/β-CD fibers is that, the fibers obtained in Figure 4.14b and c are highly interwoven while the fibers of AD-AN-AD/β-CD are rigid thus supporting the TEM results obtained. The TEM and AFM

experiments confirmed that the AD-AN-AD/β-CD/PI-PI system self-assembled in aqueous medium which resulted in the formation of nano-fibers.

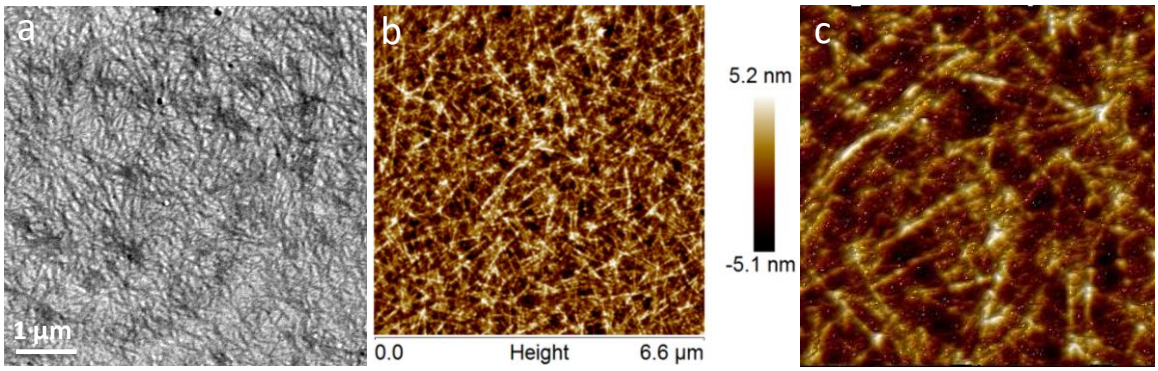

Figure 4.14. The TEM (a), AFM height (b) and AFM 3D image (c) of AD-AN-AD (10^{-5} M)/β-CD (2×10^{-5})/PI-PI (10^{-5} M) system.

4.3.5.3. 2D-WAXS studies of AD-AN-AD/β-CD/PI-PI system

Inorder to obtain the molecular level information of the self-assembly in AD-AN-AD/β-CD/PI-PI system, we have carried out WAXS studies of the three component system. For the studies, a dried film prepared from aqueous solution containing AD-AN-AD (5×10^{-4} M), PI-PI (5×10^{-4} M) and β-CD (10^{-3} M) was used. The resultant spectrum of X-ray scattering is shown in Figure 4.15 with the corresponding 2D plot shown in the inset. As observed in Figure 4.11 for the AD-AN-AD/β-CD system, scattering peaks corresponding to the molecular dimensions of β-CD and anthracene (15.1 Å and 7.57 Å for β-CD and 9.6 Å for anthracene moiety) were observed in Figure 4.15 also, suggesting that these moieties are part of ordered nano-assembly. One of the prominent differences in the WAXS spectrum of AD-AN-AD/β-CD/PI-PI system with AD-AN-AD/β-CD is that, the intensity of several of the peaks in the $2\theta = 10^{\circ}$ - 20° region and the π-stacking peaks in the region of $2\theta = 23^{\circ}$- 26° have dramatically decreased in intensity. This suggested that the nano-fibers obtained in the three component system are less ordered when compared to the crystalline fibers of the AD-AN-AD/β-CD system. Moreover, the

results shown in Figure 4.15 are in line with the results obtained in TEM and AFM experiments for three component system which showed highly networked fibers when compared to AD-AN-AD/β-CD crystalline nano-fibers.

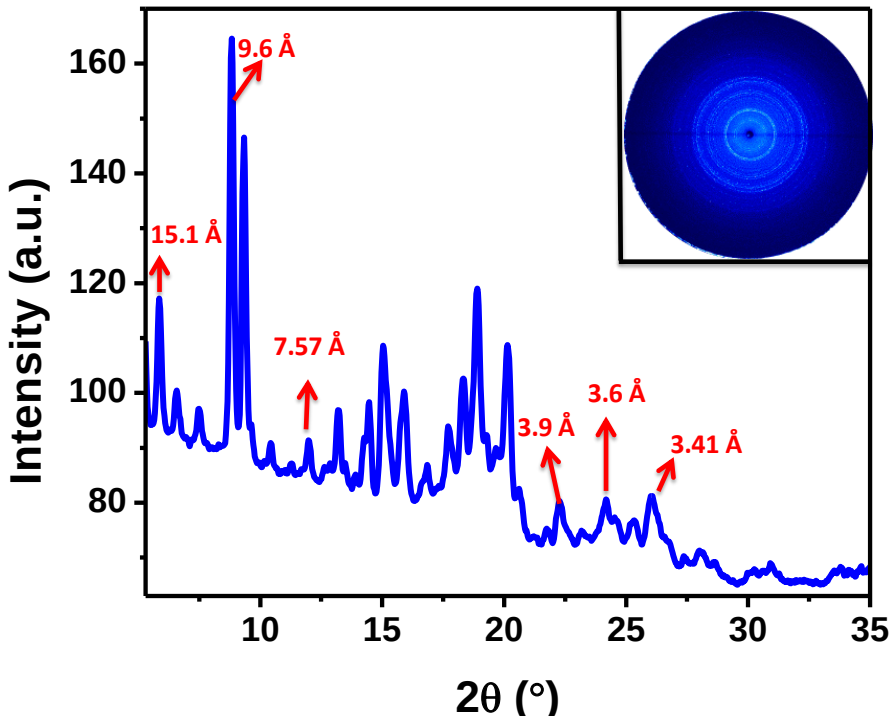

Figure 4.15. The WAXS spectrum obtained for AD-AN-AD (5×10^{-4} M)/β-CD (10^{-3} M)/ PI-PI (5×10^{-4} M) self-assembled system with inset showing the corresponding 2D plot.

4.3.6. Mechanism of self-assembly of AD-AN-AD/β-CD/PI-PI system.

When the three components AD-AN-AD/β-CD/PI-PI in the 1:2:1 ratio are mixed in aqueous medium, we observed the formation of nano-fibers which were characterized by microscopic and X-ray scattering experiments. A schematic representation of this process is shown in Scheme 4.4 (Step A). Both the end groups of AD-AN-AD and PI-PI can involve in host-guest interactions with native β-CD which can simultaneously hold adamantane and *tert*-butyl groups by inclusion and rim-binding modes, respectively. Thus, in the present case β-CD actually acts as a linker between AD-AN-AD and PI-PI. This iterative interaction in both directions lead to the formation of long supramolecular fibers in which AD-AN-AD and PI-PI are alternately placed.

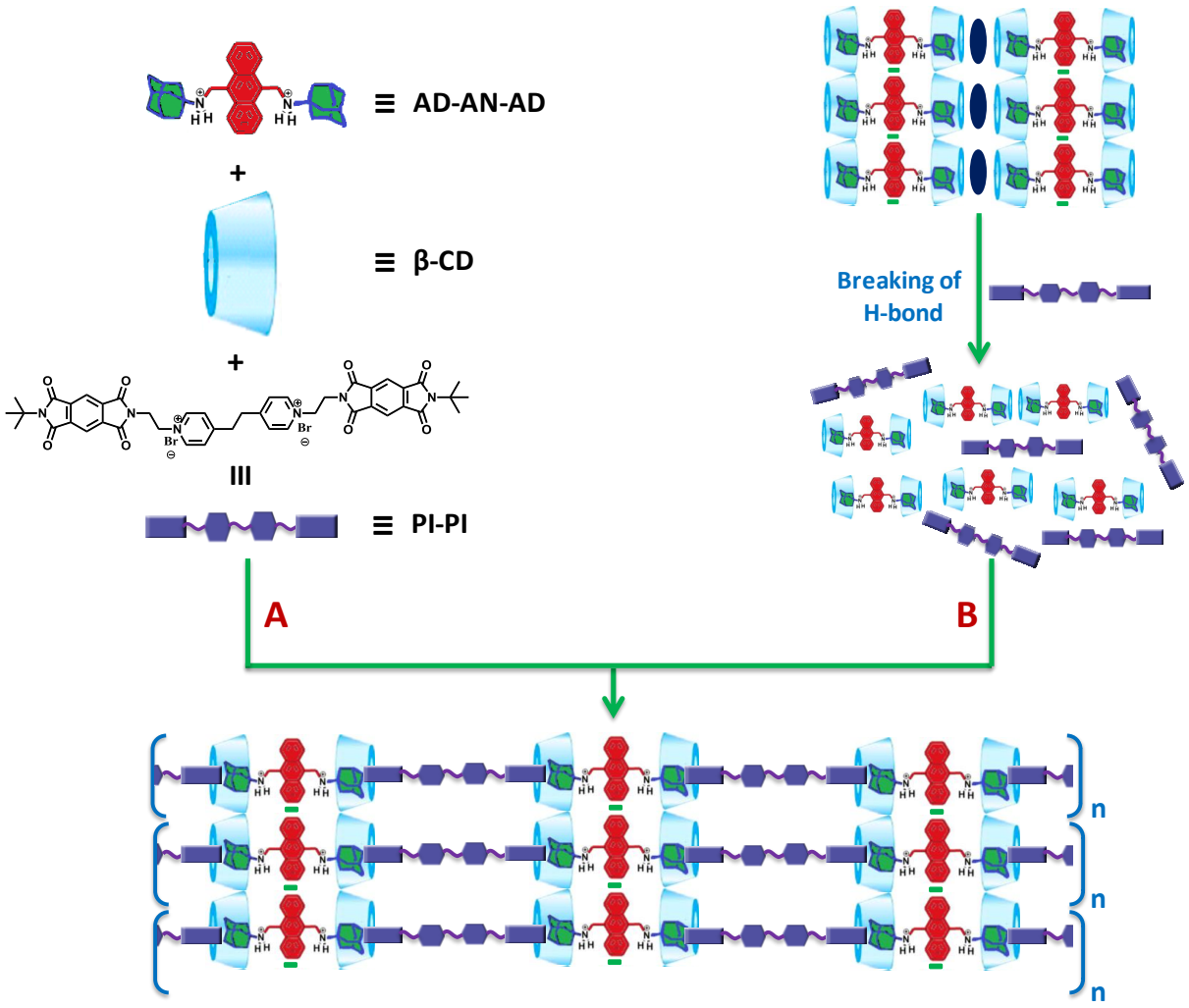

Scheme 4.4. Schematic representation of the self-assembly process in AD-AN-AD/β-CD/PI-PI system.

In Scheme 4.3, we have depicted that the β-CD⊂AD-AN-AD⊃β-CD system itself has propensity to undergo self-assembly which resulted in the formation of supramolecular polymers. Therein we proposed that the primary hydroxyl groups of β-CD are involved in intermolecular hydrogen bonding interactions which is the prominent interaction for the polymer formation. When one equivalent of PI-PI was added to the polymeric system, the resultant three-component system exhibited a different type of morphology (Figure 4.14). This suggested that the PI-PI reacts with primary rim of β-CD present in β-CD⊂AD-AN-AD⊃β-CD polymers.

For the rim-binding to occur, the fiber must first disassemble to give the bis-inclusion complex β-CD⊂AD-AN-AD⊃β-CD as shown in Scheme 4.4. The bis-inclusion complex then interacts with PI-PI in the rim-binding mode. As PI-PI is ditopic, the iterative reactions of β-CD⊂AD-AN-AD⊃β-CD with PI-PI at both the ends lead to the formation of nano-fibers which is illustrated as step B in Scheme 4.4. It is to be mentioned that only a small fraction of the PI-PI are incorporated into the fibrous network, as judged from the magnitude of the ICD signal. So the ····β-CD⊂AD-AN-AD⊃β-CD···PI-PI···· alternating structure shown in Scheme 4.4 need not be present throughout the length of the nano fiber. There may be large segments in the polymer where PI-PI is not present and the β-CD⊂AD-AN-AD⊃β-CD units are linked together by the hydrogen bonding interactions of the primary hydroxyl groups.

4.3.7. Photoinduced electron transfer studies in AD-AN-AD/β-CD/PI-PI system

Because of its suitable redox potentials anthracene has frequently been used as a donor in PET reactions.[14,24] As mentioned previously, PMDI is a good acceptor in PET reactions. The self-assembled AD-AN-AD/β-CD/PI-PI system has anthracene and PMDI present as part of a nano-fibrous assembly with AD-AN-AD and PI-PI are alternately placed. As per recent reports such self-assembled systems upon excitation can lead to generation of long-lived CS states.[15,25] This prompted us to undertake a detailed study of PET reactions in the self-assembled AD-AN-AD/β-CD/PI-PI system in aqueous solution. The PET reaction taking place in the system was studied by steady-state fluorescence quenching and laser flash photolysis studies.

4.3.7.1. Steady state fluorescence quenching studies

Figure 4.16a shows the fluorescence quenching of AD-AN-AD/β-CD system upon addition of increased equivalents of PI-PI. As can be seen from the spectra that the fluorescence of anthracene chromophore is quenched by PI-PI. In the presence of an acceptor, the fluorescence of donor can be quenched by two mechanisms, namely energy transfer and electron transfer. As the absorption of PMDI chromophore occurs at higher energy (below 330 nm) when compared to emission of anthracene chromophore (between 390-500 nm), emission quenching by energy transfer pathway can be ruled out. Thus it is safe to assume that the quenching of emission of AD-AN-AD occurs because of electron transfer mechanism. In this mechanism, upon light excitation the excited anthracene transfers an electron from its singlet state to PMDI's singlet state as shown in the equation 4.7.

$$\mathbf{AD\text{-}{}^{1}AN\text{-}AD + PMDI} \xrightarrow{h\nu} \mathbf{AD\text{-}AN^{\bullet+}\text{-}AD + PMDI^{\bullet-}} \qquad (4.7)$$

The electron transfer process results in the formation of radical cation of electron donor (AD-AN$^{\bullet+}$-AD) and radical anion of electron acceptor (PMDI$^{\bullet-}$) which is called CS state. The diffusion-mediated electron transfer can take place only if the donor and acceptors are colliding with each other (effective collisions). Since both AD-AN-AD and PI-PI are positively charged diffusion-mediated quenching will be slow because of charge repulsion. Hence the diffusion mediated fluorescence quenching would require very high concentration of PI-PI (>10^{-2} M to quench 50% emission of AD-AN-AD).[14] In the present case we observed 50% of emission quenching in the presence of 4×10^{-4} M PI-PI, suggesting that at least some of the quencher molecules are non-covalently associated with AD-AN-AD as shown in Scheme 4.4.

The free energy change (ΔG^0) for the PET process can be calculated using the Weller equation (Equation 4.8).

$$\mathbf{\Delta G^0 = E_{ox} - E_{red} - E_S - e^2/\varepsilon d} \quad \textbf{(4.8)}$$

In Equation 4.8, E_{ox} is the oxidation potential of AD-AN-AD, E_{red} is first reduction potential of PMDI, E_s is the singlet energy of AD-AN-AD, ε is the dielectric constant and d is the center to center distance between AD-AN-AD and PMDI. Since ε for water is very high, generally the last term in equation 4.8 is neglected while calculating ΔG^0 of PET reactions in water. We used the reported oxidation potential of dimethylanthracene (= 1.14 V vs. SCE) and reduction potential of PMDI (-0.58 V vs. SCE) for the calculation of ΔG^0. E_s of AD-AN-AD is assumed to be same as anthracene which is 3.2 eV. Substituting the values in equation 4.8 gave the value of ΔG^0 = -1.48 eV. A highly negative ΔG^0 indicates that the PET from singlet state of AD-AN-AD to PMDI occurs spontaneously upon light excitation of AD-AN-AD.

In order to examine the fluorescence quenching in detail, Stern-Völmer plot for the quenching was obtained which is shown in Figure 4.16b. The Stern Völmer plot is almost linear at lower concentration of PI-PI and showed an upward curvature at higher PI-PI concentration. An upward curvature in the Stern-Völmer plot is characteristic of combined static and dynamic quenching taking place in the system. Static quenching would correspond to quenching occurring within the fibrous assembly between AD-AN-AD and PI-PI which are alternately placed as shown in Scheme 4.4. The dynamic quenching will arise from the quenching due to free PI-PI present in the aqueous solution which are not the part of nano-assembly.

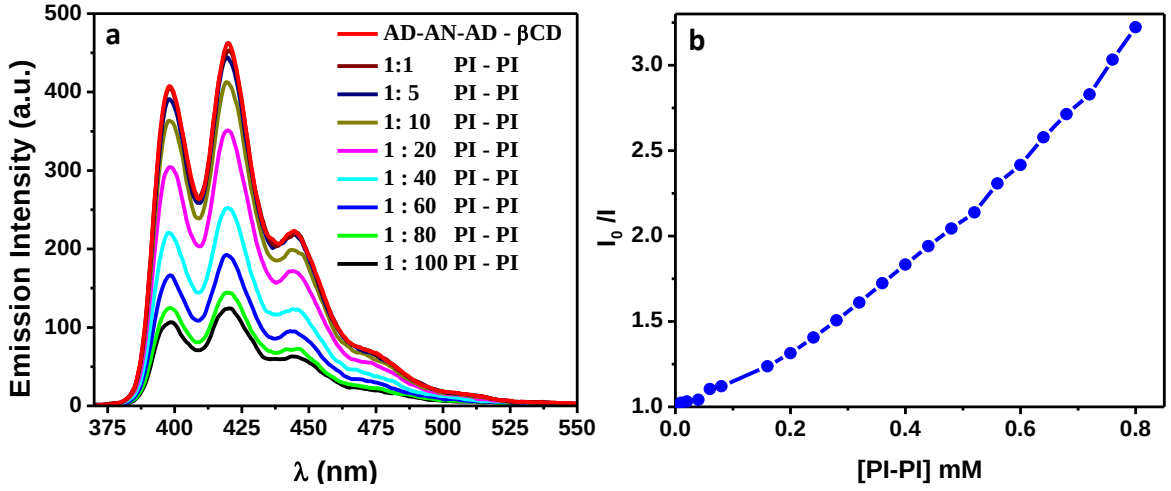

Figure 4.16. Fluorescence quenching of AD-AN-AD/β-CD (10^{-5} M) system upon increasing the [PI-PI] (a) and Stern-Völmer plot (b). The concentration of PI-PI was varied from 10^{-5} M to 10^{-3} M.

4.3.7.2. Nanosecond laser flash photolysis studies

Flash photolysis is a pump-probe technique in which the sample is first excited by a laser pulse and probed by variety of methods such as absorption spectroscopy, microwave conductivity etc. In nanosecond laser experiments, the pulse width of laser used for sample excitation is in the range of a few nanoseconds. The excited state species generated as a result of laser irradiation are probed by absorption spectroscopy using a fast detecting system comprising a fast digitizer and photomultiplier. In the present case, we have excited anthracene chromophore of AD-AN-AD by the 3rd harmonic (355 nm) of a Quanta Ray Nd:YAG laser. Figure 4.17a shows the transient absorption spectrum obtained in the laser flash photolysis of AD-AN-AD system at different time intervals following the laser excitation in de-aerated aqueous solution. The transient spectrum is characterized by an intense absorption around 420 nm and exhibited a decay time of 1.5 μs. The decay of the transient was enhanced in the presence of oxygen (inset in Figure 4.17a), which suggest that the transient spectrum is due to the $T_1 \rightarrow T_n$ absorption of anthracene chromophore.

Similarly, we have recorded the transient absorption spectra of AD-AN-AD in the presence of two equivalents of β-CD at different time intervals after laser excitation which is shown in Figure 4.17b. Inset of this figure shows the kinetic trace for the transient decay. The transient spectrum and lifetime were found to be similar to those of AD-AN-AD (Figure 4.17a) which suggests that formation of the bis-inclusion complex β-CD⊂AD-AN-AD⊃β-CD did not result in any changes in the triplet state properties of AD-AN-AD.

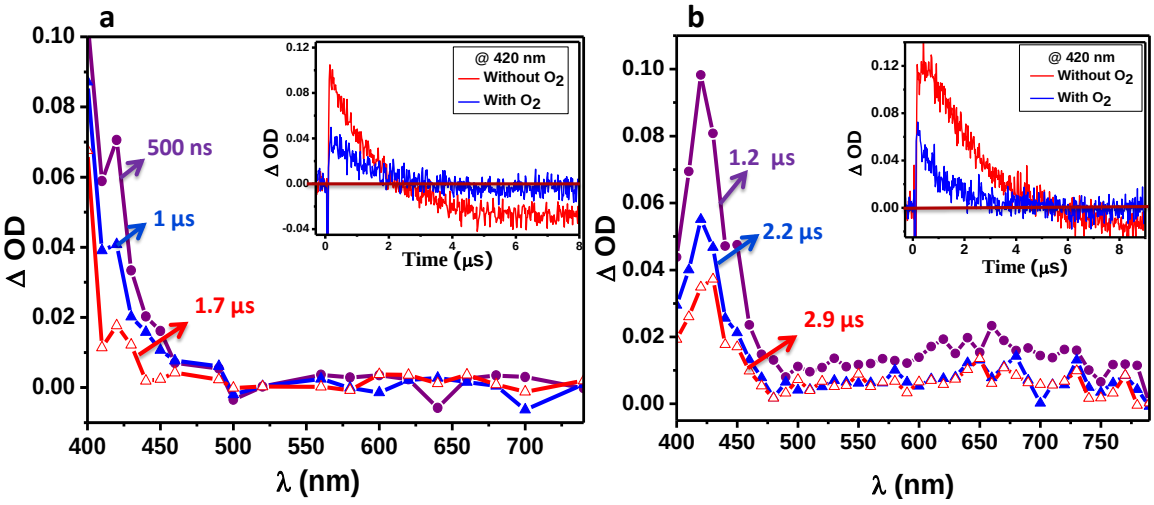

Figure 4.17. The laser flash photolysis experiments of AD-AN-AD (a) and AD-AN-AD/β-CD (b), recorded after indicated times following the laser flash. Insets show the decay profiles of the transients at 420 nm in the absence (red trace) and the presence (blue trace) of oxygen.

The kinetic traces obtained during the transient absorption experiments actually showed a negative absorption at longer time scales in the wavelength range of 400 – 500 nm. Negative absorption can occur because of sample bleaching or due to emission from the transient species. Sample bleaching will be observed only in its absorption region. In the present case, AD-AN-AD shows absorption below 400 nm only. Hence the negative absorption observed above 400 nm cannot be attributed to bleaching. We also have ruled out the possibility of sample decomposition during laser irradiation. AD-AN-AD was

irradiated in a photo reactor for 30 min. at 355 nm. ^{1}H NMR spectrum taken after irradiation was identical with the one taken before irradiation suggesting that AD-AN-AD is photo-stable. These experiments suggested that the negative absorption observed in the 400-500 nm regions arises from some sort of emission.

Analysis of the decay profiles in Figure 4.17 (see insets) suggests that the negative absorptions did not occur immediately after excitation. The insets in Figure 4.17 also suggest that the negative absorptions arise from the decay of the absorbing species, which is AD-^{3}AN*-AD. In other words we can assign this to delayed emission arising from triplet-triplet (T-T) annihilation as shown in Equation 4.9

$$\mathbf{AD\text{-}{}^{3}AN^{*}\text{-}AD + AD\text{-}{}^{3}AN^{*}\text{-}AD \longrightarrow AD\text{-}{}^{1}AN^{*}\text{-}AD + AD\text{-}AN\text{-}AD} \qquad \mathbf{(4.9)}$$

T-T annihilation can occur if $E_S < 2\ E_T$, which is satisfied in this case. In fact, delayed emission due to T-T annihilation is reported previously for 9,10-dimethylanthracene derivatives.[26]

In order to confirm that decay of the triplet absorption actually leads to delayed emission arising from T-T annihilation we recorded the transient spectrum at longer time scales for the AD-AN-AD and AD-AN-AD/β-CD systems. The transient spectra are shown in Figure 4.18a, b. The spectral profile in these figures has some similarity to the emission spectra of AD-AN-AD and AD-AN-AD/β-CD shown in Figure 4.7a which emitted in the 390 - 525 nm region. Also, the emission maxima shown in Figures 4.7a and Figure 4.18 are identical. Although the spectra did not show vibrational features of 9, 10-dimethylanthracene emission, we assigned this to emission from AD-^{1}AN*-AD, generated as a result of T-T annihilation. Delayed emission can also arise from a triplet state by the thermal activation method. But thermally activated delayed fluorescence (TADF) requires

very small singlet-triplet energy gap (ΔE_{ST}). Since the ΔE_{ST} is very high for anthracene derivatives, this TADF can be ruled out in the present case.

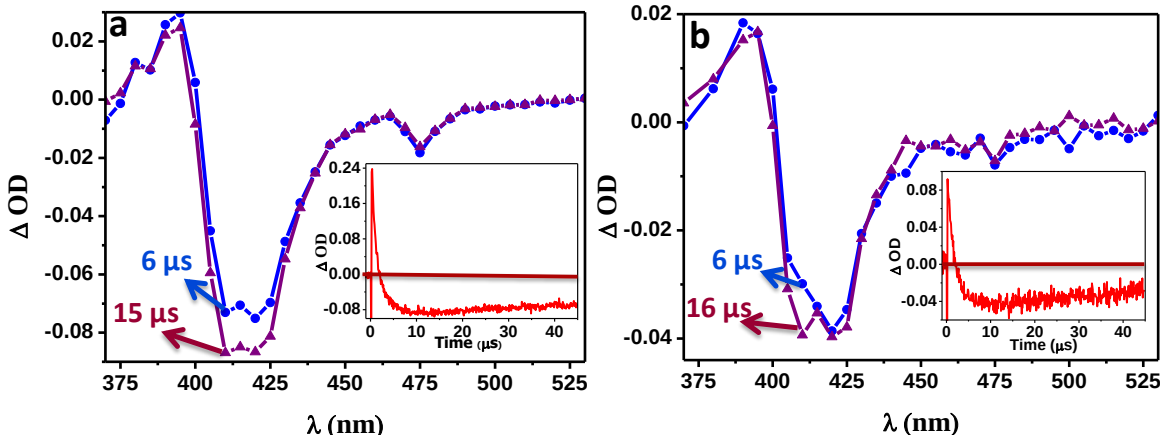

Figure 4.18. Transient spectra of (a) AD-AN-AD and (b) AD-AN-AD/β-CD recorded after indicated times following the laser flash. Insets show the decay profiles of the transients at 420 nm.

We have carried out laser flash photolysis studies of AD-AN-AD/β-CD/PI-PI system in aqueous medium inorder to study the triplet mediated electron transfer studies between anthracene and PMDI. The products formed in the reaction are the radical cation of AD-AN-AD and radical anion of PMDI as shown in Equation 4.10.

$$\text{AD-}^{3}\text{AN-AD} + \text{PMDI} \xrightarrow{h\nu} \text{AD-AN}^{\bullet+}\text{-AD} + \text{PMDI}^{\bullet-} \qquad (4.10)$$

We observed that the AD-^{3}AN*-AD triplet is quenched by PI-PI. Figure 4.19 shows the enhancement triplet decay rate upon increasing [PI-PI]. The triplet energy of AD-AN-AD can be assumed to be same as that of dimethyl anthracene (1.85 eV).[24] The triplet energy of PMDI is 2.45 eV[14] which is higher than that of AD-AN-AD. Thus the quenching of AD-AN-AD triplet observed in Figure 4.19 is not due to triplet energy transfer from ^{3}AN* to ^{3}PMDI which would be endergonic and hence we attribute this quenching to an electron transfer reaction as given in equation 4.10. The ΔG^{0} for the PET process from the triplet state can be calculated using Equation 4.8 by substituting triplet

energy (E_T) of AD-AN-AD instead of E_S. The E_T of AD-AN-AD is assumed to be same as that of dimethyl anthracene and value was taken from literature which is 1.85 eV. Substituting the values in equation 4.8 gave the value of ΔG^0 = -0.13 eV, which suggests that PET from AD-^{3}AN*-AD to PMDI is thermodynamically feasible.

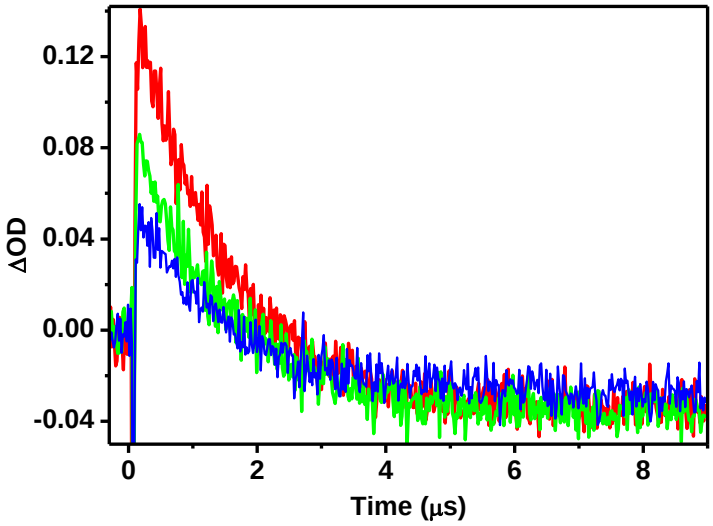

Figure 4.19. The decay of AD-AN-AD triplet in the absence (red trace) and presence (green – one eq. and blue – 5 eq.) of PI-PI.

Figure 4.20 shows the transient absorption spectra obtained for the AD-AN-AD/β-CD/PI-PI systems at two different concentrations of PI-PI. The transient spectra are characterized by absorptions in the 440 and 720 nm regions. PMDI$^{\bullet-}$ is known to absorb around 720 nm and AN$^{\bullet+}$ is known to absorb with maxima at 440 and 720 nm, with the 440 nm peak much more intense than the 720 nm peak. The kinetic traces obtained at different time scales are presented in Figure 4.21a-c. The 420 nm decay (Figure 4.21a) in this case showed slight leaching attributable to delayed emission, suggesting that AD-^{3}AN*-AD also contributes to the absorption at 420 nm. Thus we assign the 420 nm absorption to both AD-^{3}AN*-AD and AD-AN$^{\bullet+}$-AD and the 720 nm absorption to both AD-AN$^{\bullet+}$-AD and PMDI$^{\bullet-}$.

An inspection of the transient absorption spectra in Figures 4.20a, b and the decay traces Figures 4.21a-c reveals that the 420 nm transient is decaying much faster than the 720 nm transient in the longer time scales (>400 ns). Since the 420 nm absorption is composed of absorptions due to AD-^{3}AN*-AD and AD-AN$^{\bullet+}$-AD, one or both of these species may be decaying faster than the 720 nm component. If AD-AN$^{\bullet+}$-AD is decaying fast that would have reflected in the decay of the 720 nm species because the radical cation contributes to the 720 nm absorption also. Thus we attribute the faster decay of the 420 nm component to the faster decay of the triplet AD-^{3}AN*-AD.

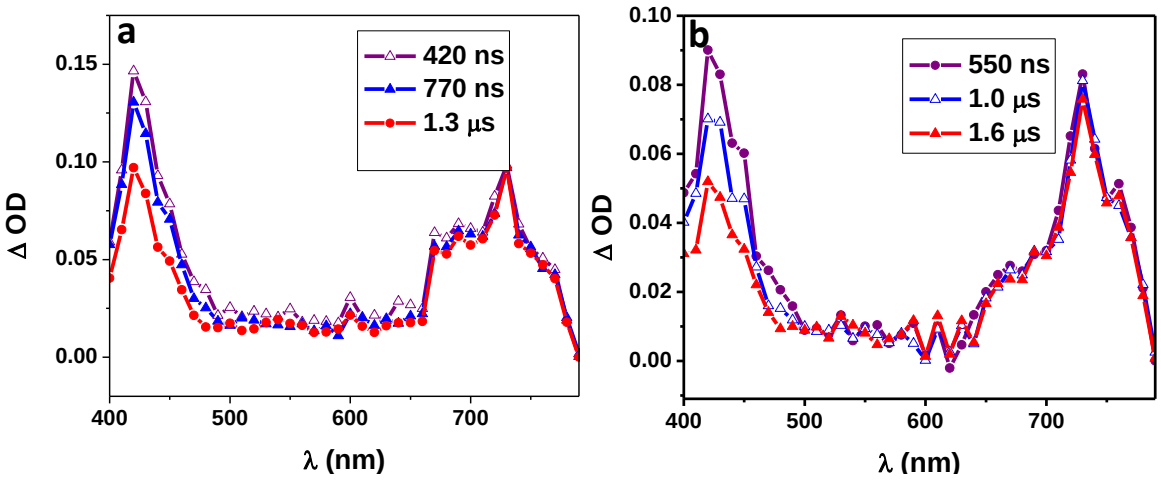

Figure 4.20. The transient absorption spectra of AD-AN-AD/β-CD/PI-PI nano-fibers in the presence of 1 equivalent of PI-PI (a) and the presence of 5 equivalent of PI-PI (b).

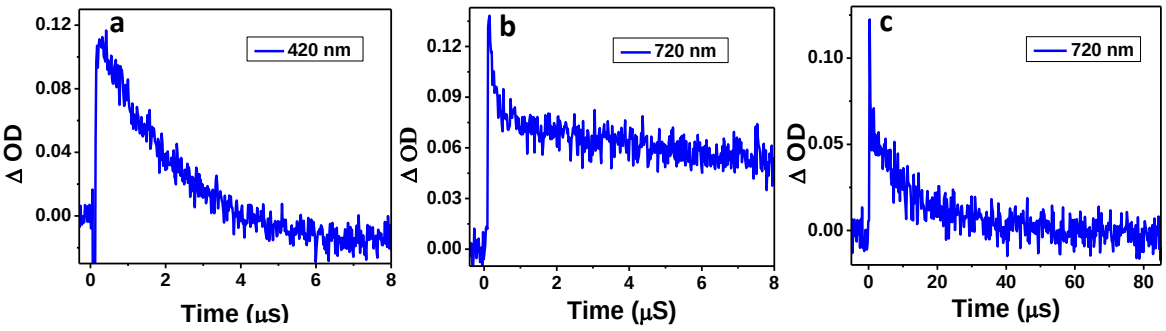

Figure 4.21. The kinetic traces at 420 nm in 1 µs window (a) 720 nm in 1 µs (b) and 720 nm in 10 µs window (c).

In order to confirm that $PMDI^{\bullet-}$ contributed to the absorption at 720 nm, transient absorption spectra of the AD-AN-AD/β-CD/PI-PI system in the presence of oxygen was recorded. It is well-known that oxygen quenches radical anions very efficiently, but generally radical cations are less affected. Figure 4.22 shows the transient absorption spectra of AD-AN-AD/β-CD/PI-PI in the presence of oxygen. It can be seen from the figure that the absorption in the 720 nm region got reduced considerably in comparison to the 420 nm absorption, which confirmed that $PMDI^{\bullet-}$ had contributed significantly to the 720 nm absorption in Figure 4.20. Oxygen also quenches the triplets faster than the radical cations. In Figure 4.22, we still see the decay of the triplet species. These triplets may correspond to β-CD⊂AD-^{3}AN*-AD⊃β-CD which are generated deep inside the fibrous network and not accessible to oxygen for the quenching to occur. These triplets also may not be accessible to PI-PI for electron transfer quenching.

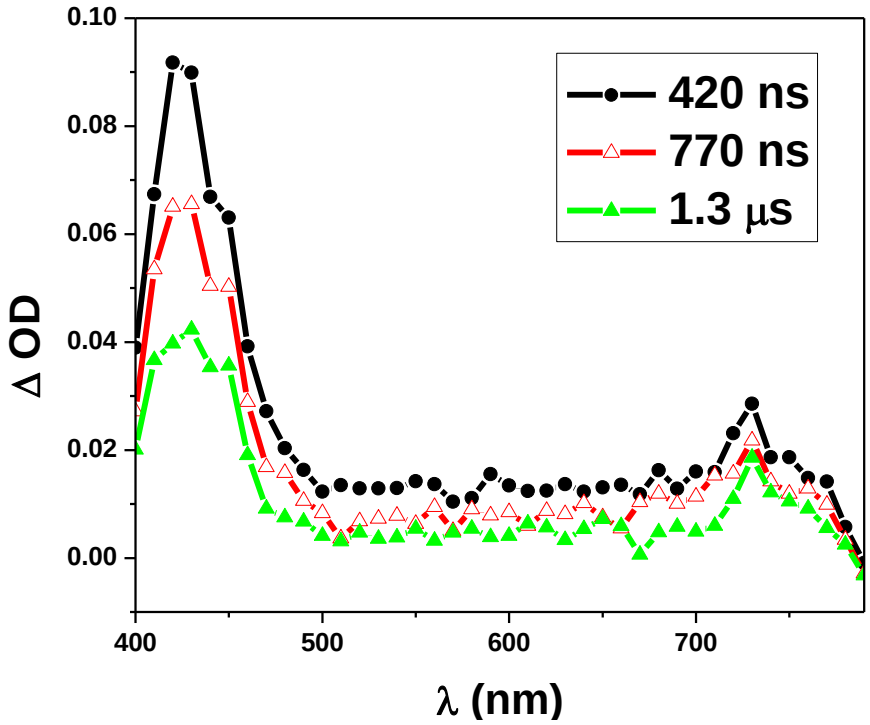

Figure 4.22. The transient absorption spectra of AD-AN-AD/β-CD/PI-PI with oxygen saturation.

The decay traces obtained for the transients at 420 and 720 nm in the absence and presence of oxygen for the AD-AN-AD/β-CD/PI-PI system are shown in Figure 4.23. The predominant decay of the 720 nm species in comparison to the 420 nm species can be clearly seen from these traces.

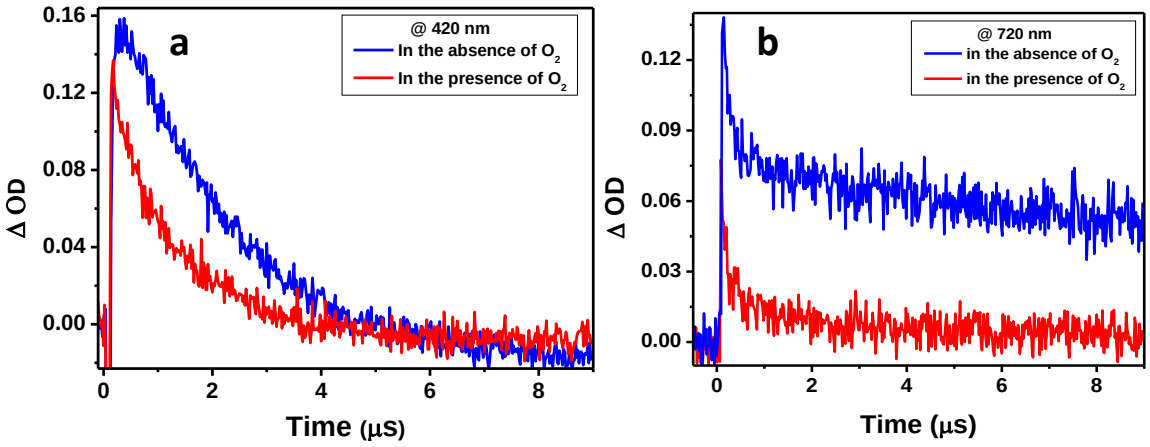

Figure 4.23. The kinetic traces recorded at 420 nm (a) and 720 nm (b) in the presence (red trace) and absence (blue trace) of oxygen.

The kinetic trace in Figure 4.21b for the 720 nm species shows a very fast decay followed by a slow decay. The fast component is attributed to decay of $PMDI^{\bullet-}$ which is present in solution or those present on the outside of the nano structure which is accessible to water. The fast decay corresponds to the protonation of $PMDI^{\bullet-}$ by water. Figure 4.21c shows the decay of the 720 nm species at a longer time scale. Complete decay of the transient was observed within 80 μs which suggest that no permanent products are formed in the reaction and that decay occurs by BET process. The fit of the decay data gave a lifetime of 59 μs for the 720 nm species.

The laser flash photolysis experiments thus confirmed that there is PET from AD-AN-AD to PMDI of PI-PI in the self-assembled nano-fibers of AD-AN-AD/β-CD/PI-PI system. An important finding from this experiment is that the fraction of CS state which survived for nearly 59 μs in aqueous medium exhibited a quantum yield (Φ_{CS}) of 0.08.

Since the extinction coefficient of $PMDI^{\bullet-}$ absorption is much larger than that of $AN^{\bullet+}$, most of the 720 nm absorption is due to the former.

The $PMDI^{\bullet-}$ longevity observed in the flash photolysis experiment was very surprising because radical anions are known to undergo efficient protonation in water.[27,28] In this case, we see a very fast initial reaction of the 720 nm transient (Figure 4.21b) which can be attributed to the protonation reaction. But nearly 10% of the radical anions escaped this protonation. We attribute this to the $PMDI^{\bullet-}$ which are placed in the interior or the fibrous structure. These are protected from protonation by water molecules because water cannot penetrate into the interior of the fiber. The proposal was further confirmed by laser flash photolysis studies of AD-AN-AD/PI-PI system in the absence of β-CD in the aqueous medium. The transient absorption spectra obtained at different times are shown in Figure 4.24.

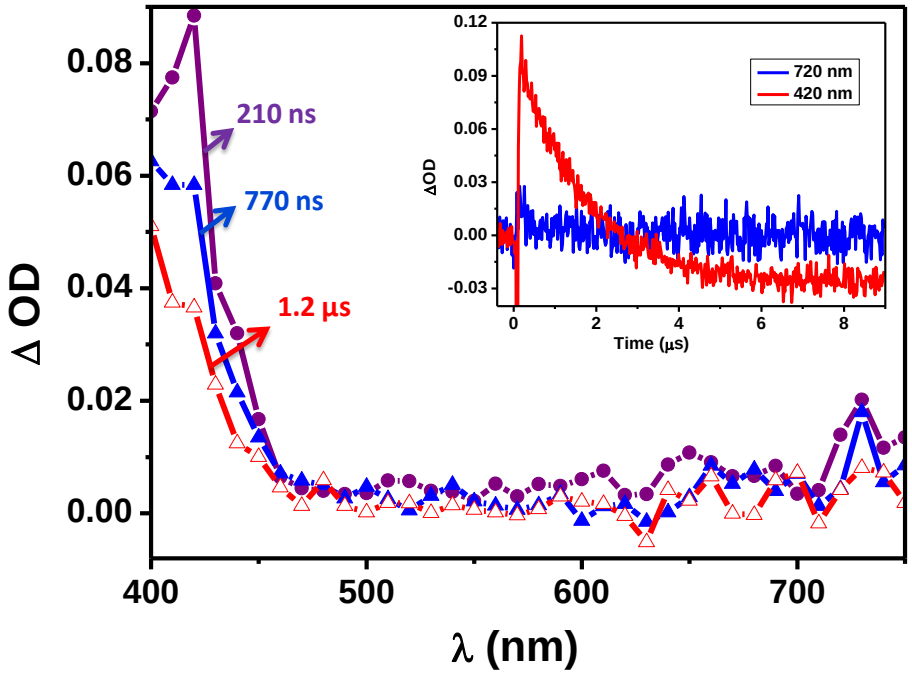

Figure 4.24. The transient absorption spectra of AD-AN-AD/PI-PI with insets showing kinetic traces at 420 nm (red trace) and 720 nm (blue trace).

The intense absorption in the 720 nm region seen in Figure 4.20a,b are absent in Figure 4.24. The absorption due to the triplet and radical cation at 420 nm can be seen clearly as these species are not sensitive to the aqueous environment. The kinetic traces shown as insets in Figure 4.24 (720 nm blue trace and 420 nm red trace) also supports our argument as 720 nm transient quenched almost immediately after its formation.

4.3.7.3. Electron paramagnetic resonance spectroscopy

Electron paramagnetic resonance (EPR) is routinely used for studying materials with unpaired electrons. This technique is similar to NMR spectroscopy, but the major difference is in EPR the spins of electrons are excited where as in NMR the spins of atoms are excited. In the presence of an external magnetic field, the energy levels of free electrons will split into multiple levels. This is exposed to microwaves of fixed frequency, which stimulates the electronic transition of an unpaired electron between these levels. By varying the magnetic field strength, the separation between electronic energy levels can be tuned. Thus the value of applied magnetic field strength (B_0) at which electronic transition occurs will be measured by EPR spectroscopy. EPR spectra can be interpreted by plotting the value of B_0 as such or another parameter namely g-factor (Landé g-factor) which is mathematically obtained from B_0. For a free electron, the value of g-factor is found to be 2.0023 units.

In the present case of AD-AN-AD/β-CD/PI-PI self-assembled nano-fibers, we have observed the formation of AD-AN$^{\bullet+}$-AD and PMDI$^{\bullet-}$ radicals upon light excitation in nano second laser flash photolysis experiments. In order to firmly confirm that there is a formation of such CS state by PET reactions, we have carried out EPR spectroscopy of AD-AN-AD/β-CD/PI-PI system. The AD-AN-AD/β-CD/PI-PI self-assembled system was irradiated by xenon lamp and simultaneously EPR of the system was recorded. The

result of the experiment is presented in Figure 4.25a, which shows a single sharp peak centered at a g value of 2.02 units. The presence of a sharp signal in EPR experiment confirms that there is the formation of radical cation and radical anions in the system upon light excitation.[29] Figure 4.25b shows the EPR spectrum of AD-AN-AD/β-CD/PI-PI system without light irradiation which confirms that no radicals are formed in the absence of light.

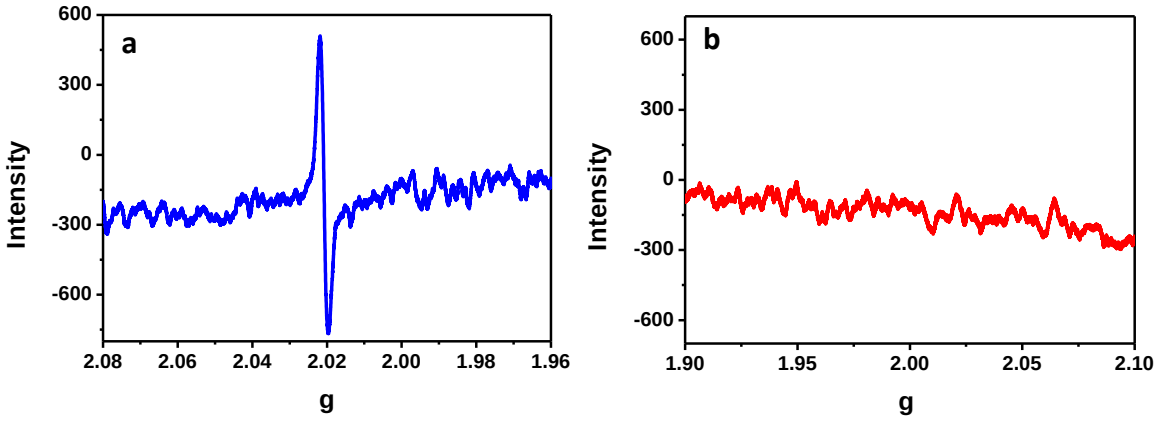

Figure 4.25. The EPR spectrum of AD-AN-AD/β-CD/PI-PI system with (a) and without (b) light irradiation.

4.4. Conclusions

In the present chapter, we have studied supramolecular interactions between β-CD and an anthracene derivative (AD-AN-AD) containing two adamantane units at its 9- and 10- positions. The supramolecular interactions between them led to the formation of rigid supramolecular polymers in the aqueous medium which was explicitly studied. We have also prepared a bis-PMDI derivative PI-PI which showed a propensity for rim binding with β-CD. Thus, the addition of PI-PI to AD-AN-AD/β-CD system resulted in the formation of nano-fibers which were different from AD-AN-AD/β-CD fibers. We showed that the anthracene and PMDI are arranged in a regular order in these nano-fibers which led to efficient PET reactions between them. The formed CS state in PET was found to

survive for more than 59 μs in the aqueous medium. The observed higher stability of radicals, particularly $PMDI^{\bullet-}$ which is unstable in water was attributed to protection of the radical anions within the supramolecular nano-fibers.

4.5. Experimental section

4.5.1. General methods

ITC data were obtained using microcal iTC 200. The raw data obtained were fitted and analyzed using origin 7.0 software provided along with the instrument. All NMR data were recorded in D_2O purchased from Aldrich, using a 500 MHz Bruker Avance DPX spectrometer. High-resolution mass spectra were obtained by using a JOEL JMS600 mass spectrometer. AFM measurements were carried out using Bruker multimode 8-HR instrument using micro fabricated TiN cantilever tips (NSG-10) with a resonating frequency of 299 kHz and a spring constant of 20-80 Nm^{-1} using tapping mode techniques. The samples for AFM were prepared by drop casting the solution on freshly cleaved mica surface and evaporating the excess solvent. TEM analyses were performed using FEI-TECNAI T30 G^2S-TWIN, 300 kV HRTEM microscope with an accelerating voltage of 100 kV and the samples were prepared by drop casting the solution on a formvar-coated copper grid (400 mesh) and evaporating excess solvent. The 2D X-ray measurements were carried out with Xeuss SAXS/WAXS system using a dried film of compound cast on aluminium foil.

The electronic absorption spectra were recorded using either Shimadzu UV-3101 or 2401PC UV-VIS-NIR scanning spectrophotometer. ICD spectra were obtained on a JASCO-J-810 Circular Dichroism Spectropolarimeter. Steady-state fluorescence experiments were performed with a SPEX Fluorolog F112X spectrofluorimeter by using

optically dilute solutions. The fluorescence quantum yield (Φ_{em}) of AD-AN-AD was obtained by recording the emission from optically matching solutions of AD-AN-AD in water and anthracene in ethanol as reference by using equation 4.11.

$$\Phi_{em} = \Phi_R \frac{A \ OD_R \ n^2}{A_R \ OD \ n_R^2} \quad \textbf{(4.11)}$$

In Equation 4.11, 'R' is the reference compound (anthracene), 'A' is the area under the emission spectrum; 'OD' is the optical density of the compound and 'n' is the refractive index of the solvent.

Nanosecond laser flash photolysis experiments were performed by using an Applied Photophysics Model LKS-20 laser kinetic spectrometer by using the third harmonic (355 nm) from a GCR-12 series Quanta Ray Nd: YAG laser. The analyzing and laser beams were fixed at right angles to each other. The probing light source was a 150 W xenon arc lamp. The light of the probe transmitted through a 1 cm sample quartz cuvette was dispersed by a mono-chromator and detected by a photomultiplier coupled to a digital oscilloscope (Agilent Infiniium DSO8064A, 600 MHz, 4 $GSas^{-1}$). Solutions for laser flash photolysis studies were de-aerated by purging with argon for 20 min before experiments. Φ_{CS} was determined by relative actinometry using equation 4.12 employing optically matching solution of AD-AN-AD in water as reference.

$$\Phi_{PMDI^{\bullet-}} = \Phi_R \frac{\Delta OD_{PMDI^{\bullet-}} \ \varepsilon_R}{\Delta OD_R \ \varepsilon_{PMDI^{\bullet-}}} \quad \textbf{(4.12)}$$

In Equation 4.12, 'R' is the reference compound (AD-AN-AD), 'ΔOD' is optical density, $\boldsymbol{\varepsilon_R}$ is extinction co-efficient of anthracene triplet (45,500 M^{-1}) and $\boldsymbol{\varepsilon}_{PMDI^{\bullet-}}$ is the extinction co-efficient of $PMDI^{\bullet-}$ (41,700).

4.5.2. Molecules and materials

β-CD, anthracene and 1,2-bis(4-pyridyl)ethane were purchased from Aldrich and used as received. The solvents and reagents were dried and purified by standard methods prior to use. Double distilled water was used for all the studies which were done in aqueous medium. The procedure for the synthesis of PI-PI is described in Chapter 3. The procedure for synthesis of AD-AN-AD is described below.

Synthesis of 2:

Anthracene (**1**) (5 g, 28 mmol) was dissolved in glacial acetic acid (30 ml) and to this 48% HBr in acetic acid (7 ml) and Paraformaldehyde (2.75 g) were added. The mixture was stirred at RT for 12 h. The yellow precipitate formed was filtered in Buchner funnel and washed several times with water. The dried compound was repeatedly recrystallized in toluene to get pure **2** (7.3 g, 71%).

^{1}H NMR (500 MHz, $CDCl_3$) δ [ppm]: 5.50 (s, 4 H), 7.68 (dd, 4 H), 8.38 (dd, 4 H); ^{13}C NMR (125 MHz, $CDCl_3$) δ [ppm]: 26.6, 124.4, 125.4, 126.7, 127.7; Mass m/z (FAB): 365.07 $(M + H)^+$.

A) Synthesis of 3:

To a stirred solution of 1-adamantalamine (1 g, 6.61mmol) in 50 ml of dry THF at 0° C, n-BuLi (2.64 ml, 2.5 M, 6.6 mmol) was added in a drop wise manner under Ar atmosphere. The mixture was allowed to stir at 0° C for 30 minutes and after that compound **2** (0.5 g, 1.37 mmol) was added. Then the mixture was allowed to stir at lab temperature for overnight. The reaction was quenched initially with little ethyl acetate and later with water and extracted with DCM. The organic layer was then separated, dried over anhydrous sodium sulphate and concentrated to get a yellow residue. This was

further purified by column chromatography over Al_2O_3. Elution of column with 15% ethyl acetate gave compound 3 as a yellow solid. Yield: 0.43 g (61 %).

^{1}H NMR (500 MHz, $CDCl_3$) δ [ppm]: 8.3 (q, 4H), 7.5 (q, 4 H), 4.7 (s, 4H), 2.1 (s, 6H), 1.9 (m, 12H) and 1.6 (m, 12H). ^{13}C NMR (125 MHz, $CDCl_3$) δ [ppm]: 130.7, 129.4, 126.2, 125, 50.8, 46.6, 41.6, 36.5 and 29.7.

HRMS (ESI): *m/z* calculated for $[C_{36}H_{44}N_2 + H]^+$ is 505.35 and found is 505.35.

B) Synthesis of 4:

Compound **3** (1 g, 1.98 mmol) was dissolved in dry chloroform (20 ml) in a 100 ml round bottomed flask. To this solution freshly prepared HCl gas (by mixing H_2SO_4 and NaCl) was passed under pressure for 10-15 minutes. The yellow precipitate formed was filtered and repeatedly washed with chloroform to get pure final compound **4**. Yield: 1.08 g. (95 %). Melting point: decomposes > 285° C.

^{1}H NMR (500 MHz, D_2O) δ [ppm]: 8.3 (q, 4H), 7.8(q, 4H), 5.2 (s, 4H), 2.3 (s, 6H), 2.2 (s, 12H) and 1.8 (m, 12H). ^{13}C NMR (125 MHz, D_2O) δ [ppm]: 130.0, 127.4, 123.9, 99.9, 59.4, 38.1, 34.9 and 29.0.

HRMS (ESI): *m/z* calculated for $[C_{36}H_{46}N_2^{2+} + H^+]$ is 507.37 and found is 507.36.

4.6. References

(1) Jia, J.; Seitz, L. C.; Benck, J. D.; Huo, Y.; Chen, Y.; Ng, J. W. D.; Bilir, T.; Harris, J. S.; Jaramillo, T. F.: Solar water splitting by photovoltaic-electrolysis with a solar-to-hydrogen efficiency over 30%. *Nat. Commun.* **2016**, *7*, 13237.

(2) Walter, M. G.; Warren, E. L.; McKone, J. R.; Boettcher, S. W.; Mi, Q.; Santori, E. A.; Lewis, N. S.: Solar water splitting cells. *Chem. Rev.* **2010**, *110*, 6446.

(3) Muhich, C. L.; Ehrhart, B. D.; Al-Shankiti, I.; Ward, B. J.; Musgrave, C. B.; Weimer, A. W.: A review and perspective of efficient hydrogen generation via solar thermal water splitting. *Wiley Interdisciplinary Reviews: Energy and Environment* **2016**, *5*, 261.

(4) Tachibana, Y.; Vayssieres, L.; Durrant, J. R.: Artificial photosynthesis for solar water-splitting. *Nat. Photon.* **2012**, *6*, 511.

(5) Kärkäs, M. D.; Verho, O.; Johnston, E. V.; Åkermark, B.: Artificial photosynthesis: Molecular systems for catalytic water oxidation. *Chem. Rev.* **2014**, *114*, 11863.

(6) Dadashi-Silab, S.; Doran, S.; Yagci, Y.: Photoinduced electron transfer reactions for macromolecular syntheses. *Chem. Rev.* **2016**, *116*, 10212.

(7) Wasielewski, M. R.: Photoinduced electron transfer in supramolecular systems for artificial photosynthesis. *Chem. Rev.* **1992**, *92*, 435.

(8) Cogdell, R. J.; Isaacs, N. W.; Howard, T. D.; McLuskey, K.; Fraser, N. J.; Prince, S. M.: How photosynthetic bacteria harvest solar energy. *J. Bacteriol.* **1999**, *181*, 3869.

(9) Cardona, T.; Sedoud, A.; Cox, N.; Rutherford, A. W.: Charge separation in photosystem ii: A comparative and evolutionary overview. *Biochimica et Biophysica Acta (BBA) - Bioenergetics* **2012**, *1817*, 26.

(10) Imahori, H.; Guldi, D. M.; Tamaki, K.; Yoshida, Y.; Luo, C.; Sakata, Y.; Fukuzumi, S.: Charge separation in a novel artificial photosynthetic reaction center lives 380 ms. *J. Am. Chem. Soc.* **2001**, *123*, 6617.

(11) Gust, D.; Moore, T. A.; Moore, A. L.; Lee, S.-J.; Bittersmann, E.; Luttrull, D. K.; Rehms, A. A.; DeGraziano, J. M.; Ma, X. C.; Gao, F.; Belford, R. E.; Trier, T. T.: Efficient multistep photoinitiated electron transfer in a molecular pentad. *Science* **1990**, *248*, 199.

(12) Harriman, A.; Kubo, Y.; Sessler, J. L.: Molecular recognition via base pairing: Photoinduced electron transfer in hydrogen-bonded zinc porphyrin-benzoquinone conjugates. *J. Am. Chem. Soc.* **1992**, *114*, 388.

(13) Balan, B.; Gopidas, K. R.: Photoinduced electron transfer in α-cyclodextrin-based supramolecular dyads: A free-energy-dependence study. *Chem. Eur. J.* **2006**, *12*, 6701.

(14) Balan, B.; Gopidas, K. R.: An anthracene-appended β-cyclodextrin-based dyad: Study of self-assembly and photoinduced electron-transfer processes. *Chem. Eur. J.* **2007**, *13*, 5173.

(15) Huber, R. C.; Ferreira, A. S.; Thompson, R.; Kilbride, D.; Knutson, N. S.; Devi, L. S.; Toso, D. B.; Challa, J. R.; Zhou, Z. H.; Rubin, Y.; Schwartz, B. J.; Tolbert, S. H.: Long-lived photoinduced polaron formation in conjugated polyelectrolyte-fullerene assemblies. *Science* **2015**, *348*, 1340.

(16) Sanju, K. S.; Ramaiah, D.: White photoluminescence and electroluminescence from a ternary system in solution and a polymer matrix. *Chem. Commun.* **2013**, *49*, 11626.

(17) Rakhi, A. M.; Gopidas, K. R.: Generation of long-lived methylviologen radical cation in the triplet-state mediated electron transfer in a β-cyclodextrin based supramolecular triad. *Chem. Phys. Lett.* **2015**, *618*, 192.

(18) Bohne, C.: Supramolecular dynamics. *Chem. Soc. Rev.* **2014**, *43*, 4037.

(19) Yamashina, M.; Sartin, M. M.; Sei, Y.; Akita, M.; Takeuchi, S.; Tahara, T.; Yoshizawa, M.: Preparation of highly fluorescent host–guest complexes with tunable color upon encapsulation. *J. Am. Chem. Soc.* **2015**, *137*, 9266.

(20) Zhang, X.; Sasaki, K.; Kuroda, Y.: Syntheses and photophysical studies of cyclodextrin derivatives with two proximate anthracenyl groups. *J. Org. Chem.* **2006**, *71*, 4872.

(21) Chen, K.-H.; Yang, J.-S.; Hwang, C.-Y.; Fang, J.-M.: Phospholipid-induced aggregation and anthracene excimer formation. *Org. Lett.* **2008**, *10*, 4401.

(22) Kumar, M.; Venkata Rao, K.; George, S. J.: Supramolecular charge transfer nanostructures. *Phys. Chem. Chem. Phys.* **2014**, *16*, 1300.

(23) Shao, L.; Zhou, J.; Hua, B.; Yu, G.: A dual-responsive supra-amphiphile based on a water-soluble pillar[7]arene and a naphthalene diimide-containing guest. *Chem. Commun.* **2015**, *51*, 7215.

(24) Fukuzumi, S.; Nakanishi, I.; Tanaka, K.: Multielectron oxidation of anthracenes with a one-electron oxidant via water-accelerated electron-transfer disproportionation of the radical cations as the rate-determining step. *J. Phys. Chem. A* **1999**, *103*, 11212.

(25) Sanders, A. M.; Magnanelli, T. J.; Bragg, A. E.; Tovar, J. D.: Photoinduced electron transfer within supramolecular donor–acceptor peptide nanostructures under aqueous conditions. *J. Am. Chem. Soc.* **2016**, *138*, 3362.

(26) Parker, C. A.; Joyce, T. A.: Delayed fluorescence of anthracene and some substituted anthracenes. *Chem. Commun* **1967**, 744.

(27) Tsuchiya, T.; Wielopolski, M.; Sakuma, N.; Mizorogi, N.; Akasaka, T.; Kato, T.; Guldi, D. M.; Nagase, S.: Stable radical anions inside fullerene cages: Formation of reversible electron transfer systems. *J. Am. Chem. Soc.* **2011**, *133*, 13280.

(28) Jaworski, J. S.; Cembor, M.: Kinetics of protonation of the acridine radical anion in dmf by water and alcohols. *Tetrahedron Lett.* **2000**, *41*, 7267.

(29) Bramley, R.; Strach, S. J.: Electron paramagnetic resonance spectroscopy at zero magnetic field. *Chem. Rev.* **1983**, *83*, 49.

List of publications

1. Unusual self-assembly of a hydrophilic β-cyclodextrin inclusion complex into vesicles capable of drug encapsulation and release.
   Nagaraj Nayak and Karical R. Gopidas* *J. Mater. Chem. B*, **2015**, *3*, 3425-3428.

2. Integrative Self-sorting in a three component system leading to the formation of long fibrous structures.
   Nagaraj Nayak and Karical R. Gopidas* *ChemistrySelect* **2016**, *5*, 1028–1032

3. Donor-β-Cyclodextrin-Acceptor supramolecular nano-fibers: Study of self-assembly and photoinduced electron transfer process under aqueous conditions.
   Nagaraj Nayak and Karical R. Gopidas* (manuscript to be submitted)

List of posters presented at conferences

1. Self-assembly of a native β-cyclodextrin – adamantane bis-Inclusion complex into vesicles and their chemical stimuli-responsive aggregation and disassembly
   Nagaraj Nayak and Karical R. Gopidas*
   17th CRSI National Symposium in Chemistry, February 06-08, 2015, at CSIR - NCL, Pune.

2. Morphological transformation of vesicles into nano-fibers triggered by vesicle surface recognition: An example for integrative self-sorting
   Nagaraj Nayak and Karical R. Gopidas*
   18th CRSI National Symposium in Chemistry, February 05-07, 2016, at Punjab University, Punjab.